NAVAL POSTGRADUATE SCHOOL

MONTEREY, CALIFORNIA

THESIS

ASSESSING EVAPORATION DUCT VARIABILITY IN THE EASTERN MEDITERRANEAN SEA IN SUPPORT OF RADAR AND RADIO COMMUNICATIONS

by

Süleyman C. Gürbüz

December 2016

Thesis Advisor: Qing Wang
Second Reader: Wendell Nuss

Approved for public release. Distribution is unlimited.

THIS PAGE INTENTIONALLY LEFT BLANK

REPORT DOCUMENTATION PAGE	*Form Approved OMB No. 0704-0188*

1. AGENCY USE ONLY *(Leave blank)*	**2. REPORT DATE** December 2016	**3. REPORT TYPE AND DATES COVERED** Master's thesis

4. TITLE AND SUBTITLE ASSESSING EVAPORATION DUCT VARIABILITY IN THE EASTERN MEDITERRANEAN SEA IN SUPPORT OF RADAR AND RADIO COMMUNICATIONS	**5. FUNDING NUMBERS**
6. AUTHOR(S) Süleyman C. Gürbüz	
7. PERFORMING ORGANIZATION NAME(S) AND ADDRESS(ES) Naval Postgraduate School Monterey, CA 93943-5000	**8. PERFORMING ORGANIZATION REPORT NUMBER**
9. SPONSORING /MONITORING AGENCY NAME(S) AND ADDRESS(ES) N/A	**10. SPONSORING / MONITORING AGENCY REPORT NUMBER**

11. SUPPLEMENTARY NOTES The views expressed in this thesis are those of the author and do not reflect the official policy or position of the Department of Defense or the U.S. Government. IRB Protocol number ____N/A____.

12a. DISTRIBUTION / AVAILABILITY STATEMENT Approved for public release. Distribution is unlimited.	**12b. DISTRIBUTION CODE** A

13. ABSTRACT (maximum 200 words)

Electro-magnetic (EM) propagation is greatly affected by atmospheric conditions. Although this subject has been an active area of research, a comprehensive evaporation ducting study for the Eastern Mediterranean Sea does not exist. The main objective of this thesis is to make detailed analyses of evaporation ducts in the Eastern Mediterranean Sea in support of Navy and civilian activities in the region.

In this thesis, the European Center for Medium-Range Weather Forecasts (ECMWF) surface reanalysis data from 1990 to 2015 are used. The Coupled Ocean-Atmosphere Response Experiment (COARE) bulk surface flux algorithm is modified to output vertical profiles of temperature and humidity with input from the ECMWF reanalysis data. The vertical profiles are then used to derive the associated evaporation duct height (EDH) and evaporation duct strength (EDS). The temporal and spatial variations of EDH and EDS are analyzed to provide an evaporation ducting climatology for the Eastern Mediterranean Sea. The sensitivity of EDH and EDS to certain atmospheric factors is further analyzed to develop a more comprehensive understanding of atmospheric effects on EM propagation. The results show that EDHs are highest in summer, between 12 and 15 UTC (coordinated universal time), and EDHs are greatest in the Aegean Sea.

14. SUBJECT TERMS evaporation ducts, ducting, Mediterranean Sea, EM propagation, atmospheric effects on EM propagation	**15. NUMBER OF PAGES** 101
	16. PRICE CODE

17. SECURITY CLASSIFICATION OF REPORT	**18. SECURITY CLASSIFICATION OF THIS PAGE**	**19. SECURITY CLASSIFICATION OF ABSTRACT**	**20. LIMITATION OF ABSTRACT**
Unclassified	Unclassified	Unclassified	UU

NSN 7540-01-280-5500 Standard Form 298 (Rev. 2-89) Prescribed by ANSI Std. 239-18

THIS PAGE INTENTIONALLY LEFT BLANK

Approved for public release. Distribution is unlimited.

ASSESSING EVAPORATION DUCT VARIABILITY IN THE EASTERN MEDITERRANEAN SEA IN SUPPORT OF RADAR AND RADIO COMMUNICATIONS

Süleyman C. Gürbüz
Lieutenant Junior Grade, Turkish Navy
B.S., Turkish Naval Academy, 2010

Submitted in partial fulfillment of the
requirements for the degree of

MASTER OF SCIENCE IN METEOROLOGY AND PHYSICAL OCEANOGRAPHY

from the

NAVAL POSTGRADUATE SCHOOL
December 2016

Approved by: Qing Wang
Thesis Advisor

Wendell Nuss
Second Reader

Wendell Nuss
Chair, Department of Meteorology

THIS PAGE INTENTIONALLY LEFT BLANK

ABSTRACT

Electro-magnetic (EM) propagation is greatly affected by atmospheric conditions. Although this subject has been an active area of research, a comprehensive evaporation ducting study for the Eastern Mediterranean Sea does not exist. The main objective of this thesis is to make detailed analyses of evaporation ducts in the Eastern Mediterranean Sea in support of Navy and civilian activities in the region.

In this thesis, the European Center for Medium-Range Weather Forecasts (ECMWF) surface reanalysis data from 1990 to 2015 are used. The Coupled Ocean-Atmosphere Response Experiment (COARE) bulk surface flux algorithm is modified to output vertical profiles of temperature and humidity with input from the ECMWF reanalysis data. The vertical profiles are then used to derive the associated evaporation duct height (EDH) and evaporation duct strength (EDS). The temporal and spatial variations of EDH and EDS are analyzed to provide an evaporation ducting climatology for the Eastern Mediterranean Sea. The sensitivity of EDH and EDS to certain atmospheric factors is further analyzed to develop a more comprehensive understanding of atmospheric effects on EM propagation. The results show that EDHs are highest in summer, between 12 and 15 UTC (coordinated universal time), and EDHs are greatest in the Aegean Sea.

THIS PAGE INTENTIONALLY LEFT BLANK

TABLE OF CONTENTS

LIST OF FIGURES

THIS PAGE INTENTIONALLY LEFT BLANK

LIST OF TABLES

THIS PAGE INTENTIONALLY LEFT BLANK

LIST OF ACRONYMS AND ABBREVIATIONS

ABL	atmospheric boundary layer
ASTD	air-sea temperature difference
CASPER	Coupled Air-Sea Processes and Electromagnetic ducting Research
CP	continental polar air mass
CT	continental tropical air mass
ECMWF	European Center for Mid-Range Weather Forecast
EDH	evaporation duct height
EDS	evaporation duct strength
EM	electromagnetic
HPA	hectopascal
LTSM	long term seasonal means
MB	millibar
MP	maritime polar air mass
MT	maritime tropical air mass
NAVSLAM	Navy Atmospheric Vertical Surface Layer Model
RH	relative humidity
SA	sub-area
SLP	sea level pressure
SST	sea surface temperature
TOGA COARE	Tropical Ocean-Global Atmosphere Coupled Ocean-Atmosphere Response Experiment
UTC	coordinated universal time

THIS PAGE INTENTIONALLY LEFT BLANK

ACKNOWLEDGMENTS

First, I would like to thank my advisors, Professor Qing Wang and Professor Wendell Nuss, for their endless mentoring, guidance, support, and tolerance. They not only helped me complete my thesis, but they also taught me how to conduct a scientific study.

I would also like to thank Dr. Denny Alappattu and Ltjg. Mehmet Kahraman (Turkish Navy) for always being there for me. The road was long and difficult, but with them, I never felt alone.

I also thank my program officer, CDR Paula Travis, my professors, and my friends for making my time at NPS unforgettable.

Most importantly, I want to express my deepest appreciations to my father, Faruk Gurbuz; my mother, Gulay Gurbuz; and my brother, Kamil Gurbuz. There are not enough words to explain my feelings for them. I think I should simply say that I cannot imagine my life without them.

THIS PAGE INTENTIONALLY LEFT BLANK

I. INTRODUCTION

A. THESIS OBJECTIVES

The objective of this thesis research is to assess temporal and spatial variation of atmospheric parameters affecting radio communication and radar propagation in the Eastern Mediterranean Sea. The results from this study will provide insight into seasonal, diurnal, and spatial variability of the atmospheric refractive conditions in the Eastern Mediterranean Sea. These results support naval operations by providing guidance on the expected impact of the atmosphere on electromagnetic (EM) propagation that suits operational needs, specifically, to detect or not to be detected. The ultimate goal of this research is to provide sailors with information on current refractive conditions as well as future conditions well represented by the forecast models.

B. NAVY RELEVANCE

It is of vital importance for naval units to fully exploit the surrounding environment, including the current and future atmospheric conditions that affect the operation or performance of our ships, systems, sensors, and weapons. Inaccurate assessments of the atmospheric conditions may affect naval operations adversely and cause tactically unfavorable conditions with increased vulnerability. For this reason, taking atmospheric effects into consideration is a critical need rather than a mere tactical advantage.

EM wave propagation is greatly affected by atmospheric conditions. Ranges of different types of sensors, communication devices, radars, weapons, and other equipment are subject to changes in atmospheric conditions. In order to increase operational success and unit effectiveness, atmospheric effects on systems must be predicted early enough to be taken into consideration in the planning phase of operations. In this regard, we should precisely predict those effects and advise commanders on the impact of those effects to planned operational activities.

In the world of modern communications, prediction of the atmospheric effects on communication systems is extremely important to naval operations. Without effective

communication between units, it would be impossible to command, control, and effectively coordinate joint activities. In this case, the battlefield would become much more blurry with many uncertainties. Therefore, a complete knowledge of the battlespace environment is critical to the success of naval operations.

C. MOTIVATION

The Mediterranean Sea is the world's largest inland sea and very important for maritime security operations. It is a strategic region for both the United States and its allies. The strategic importance of the Mediterranean is increasing as the national security issues in the surrounding countries become intensified. The Mediterranean Sea is also very important for merchant shipping because it is estimated that almost one third of the merchant shipping in the world crosses through the Mediterranean Sea.

Maintaining effective radio communication and radar coverage is critical for all types of vessels, especially Navy ships as these capabilities directly affect the efficiency and success of naval operations. EM wave propagation conditions in the atmosphere have a vital importance on the performance of systems that depend on radio frequency. Accurate depiction of the refractive environment reduces vulnerability and increases combat effectiveness, and hence, increases the possibility of overall success in the operation. For this reason, EM wave propagation conditions in the atmosphere must be taken into consideration in both the planning and execution phases of naval operations.

The atmospheric influence on EM propagation has been an active area of research for decades. Figure 1 shows an early study by Anderson (1944) illustrating the correlation of the low inversion base and enhanced signal level due to surface-based ducts. Research in this area has continued over the past 70 years, incorporating a much broader range of frequencies, particularly into the high frequency bands. Hermann et al. (2002) studied the horizontal variability of refractivity in Australia. Their study showed that EM waves from a transmitter in a duct can encounter signal loss of magnitude 20 decibels (dB) or greater to receivers above the duct, although there were signal enhancements in the duct. Mason (2010) studied "atmospheric effects on radio frequency wave propagation in a humid near-surface environment". Mason's study confirmed the strong correlation between the

propagation loss in the surface layer and the antenna height. The most recent extended effort on EM propagation study is the ongoing Coupled Air-Sea Processes and Electromagnetic ducting Research (CASPER), a comprehensive multi-university project supported by the Office of Naval Research. Results from CASPER should help enhance our current understanding of the atmospheric effects on EM propagation and provide guidance on new approaches to better predict such effects.

Figure 1. Low Inversion Base and Enhanced Signal Level Due to Surface-based Ducts. Source: Anderson (1944).

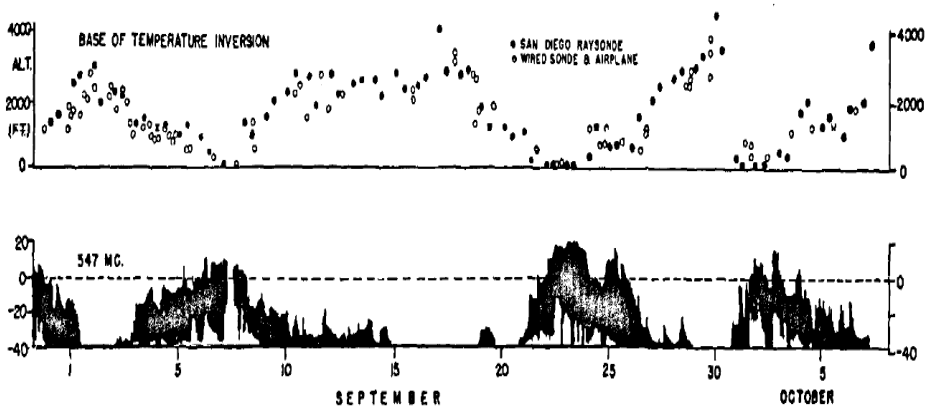

There are also similar studies that have focused on the Aegean Sea and inland Turkey. Two of those studies were conducted by K. Raptis (2012) and S. Turk (2010). Raptis (2012) examined "climatological factors affecting EM surface ducting in the Aegean Sea region" using rawinsonde measurements. A similar study by Turk (2010) analyzed "atmospheric effects on communication and electronic warfare systems within Turkey and surrounding areas" using a similar dataset.

Despite the previously mentioned and other earlier studies, ducting conditions in the Eastern Mediterranean Sea have not been well characterized in the past. Nevertheless, this area has significant Navy presence requiring accurate forecast and better understanding of the EM propagation conditions. This region is the focus of this thesis work.

THIS PAGE INTENTIONALLY LEFT BLANK

II. BACKGROUND

A. THE EASTERN MEDITERRANEAN SEA

In this section, geography and meteorological features of the Eastern Mediterranean Sea are briefly described.

1. Geography of the Eastern Mediterranean Sea

The name "Mediterranean" comes from Latin "Medius Terrae," meaning "in the middle of the land" (OCA/CNES 2015). The Mediterranean Sea deserves its name because it is in the middle of the Europa, Asia, and Africa continents.

"The Mediterranean Sea extends between the 30° and 46° North latitudes, 5°50′ West and 36° East longitudes. It is approximately 2,500 miles long in the east-west direction and 500 miles wide in the north-south direction" (HMSO 1962). It has an outlet to the Atlantic through the Strait of Gibraltar, which is only eight miles wide at its narrowest point. It also has connections with the Black Sea through the Aegean Sea and Turkish Straits and with the Red Sea through the Suez Canal. Except along the east coast of Tunisia in North Africa, it is mostly surrounded by mountains that are close to the coast (HMSO 1962). The average depth of the Mediterranean Sea is 1,500 meters (m), the deepest part being 5,121 m at the Matapan trench in the Ionian Sea (The Mediterranean Sea 2015). Figure 2a shows the geographical location and depths of the Mediterranean Sea together with the countries that surround it. (The landscape of the Eastern Mediterranean Sea is depicted in Figure 2b.)

The Mediterranean Sea can be geographically divided into the Western basin and the Eastern basin by Sicily Island. The Western basin covers an area of 0.85 million square kilometers and the Eastern basin covers an area of 1.65 million square kilometers (Soto-Navarro and Criado-Aldeanueva 2012). The Western Mediterranean is composed of the Alboran, Balearic, Tyrrhenian, and Ligurian Seas while the Eastern Mediterranean is composed of the Levantine, Adriatic, Ionian, and the Aegean Seas (The Mediterranean Sea 2015).

Figure 2. a) Mediterranean Sea and Surrounding Countries (Top),
b) Landscape of the Eastern Mediterranean Sea (Bottom).

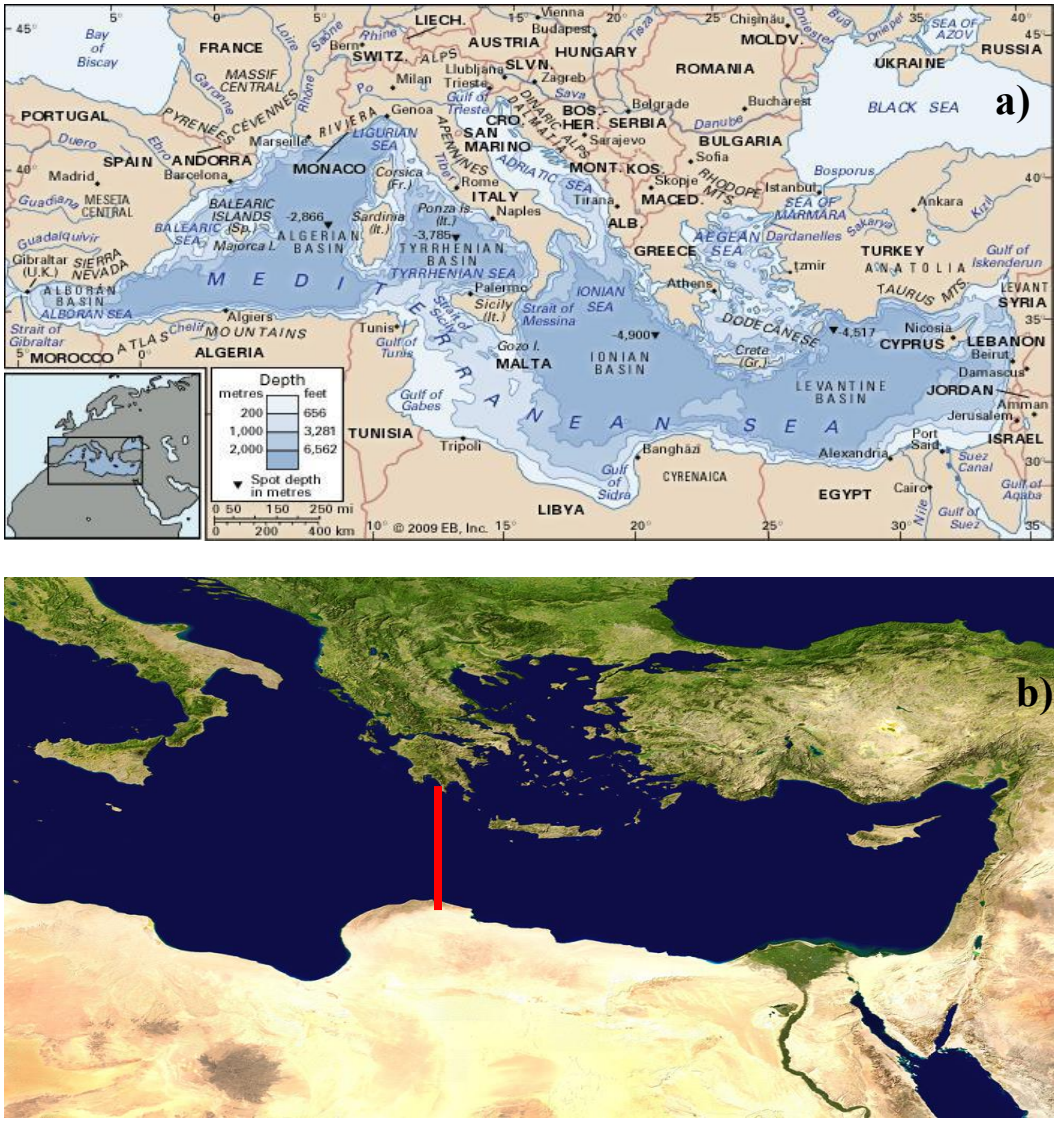

Source: *Encyclopedia Britannica* (2010) and National Geographic Society (2009)

The Eastern Mediterranean Sea is to the east of the Strait of Sicily and includes the Ionian and Levantine basins and the Adriatic and Aegean Seas (Rizzoli, Hecht 1988). The Levantine Basin is connected to the Ionian Basin through the Cretan passage, which is 300 kilometers (km) wide and 2000 m deep on average. In this study, the east part of the Eastern Mediterranean Sea, which is the part to the east of continental Greece (east of the red line in Figure 2b), is considered as the focus area and more detailed analyses are made for this area.

2. Meteorological Features of the Mediterranean Sea

The Mediterranean climate is known for its windy, wet, and mild winters and relatively calm, hot, and dry summers. The seasonal features are strongly associated with the strong pressure systems of the Atlantic Ocean, Eurasia, and Africa. These pressure systems include the Icelandic Low Pressure System, the Azorean High Pressure System, the Basra Low Pressure System, and the Siberian High Pressure System.

Four different types of air masses that are transported to the Mediterranean region with the main pressure systems previously mentioned are the Maritime Polar Air Masses (mP), Continental Polar Air Masses (cP), Maritime Tropical Air Masses (mT), and Continental Tropical Air Masses (cT). Polar air masses are prevalent in the winter, and tropical air masses are dominant in the summer (Sensoy 2004). These air masses are illustrated in Figure 3.

Figure 3. Air Masses Affecting the Mediterranean Region.
Source: Sensoy (2004).

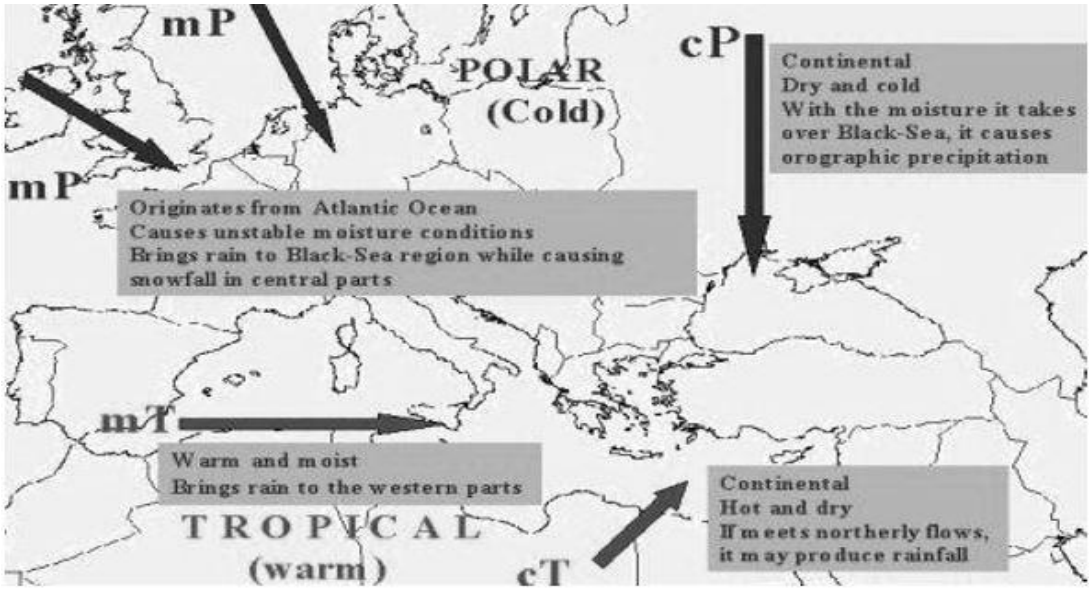

Mediterranean climate is highly seasonal because of the seasonal characteristics of high- and low-pressure systems in the region. For this reason, climatic conditions in the Mediterranean Sea will be explained on a seasonal basis and in the two groups of

"warm seasons" and "cool seasons." Warm seasons include the months from June to September, and cool seasons include the months from October to May. October and May are considered as transitional months (HMSO 1962).

a. Cool Seasons

During cool seasons, the Mediterranean climate is highly affected by the Azorean High, which is generally formed over the Atlantic Ocean or Western Europe. The Azorean High often brings a significant amount of moisture and rainfall to the Mediterranean Sea from the west.

The Azorean High also transports cold air mass from the northwest to the Mediterranean Sea in cool seasons. This cold air mass flowing over relatively warmer water causes vertical instability and pressure depressions in the Mediterranean region. The Siberian High sometimes extends to the west and also brings cold air from north to the Mediterranean Sea (Mentes and Kaymaz 2007). Typical January locations of the Azorean and Siberian High Pressure Systems and associated circulation patterns are shown in Figure 4a.

Another important aspect of the cool season climate in the Mediterranean Sea is its high relative humidity compared to the surrounding lands. Maritime air masses from the Atlantic Ocean bring humid air to the Mediterranean Sea. Figure 4b shows the long term (1981–2010) mean of specific humidity (in gram per kilogram (g/kg)) at 1000 millibar (mb) level from December to February. The difference in specific humidity between the Mediterranean Sea and the surrounding continents is about 2.5 g/kg.

Figure 4. a) Pressure Systems and Associated Circulation Patterns in January, b) 1000 mb Level Specific Humidity (g/kg) for Winters 1981–2010.

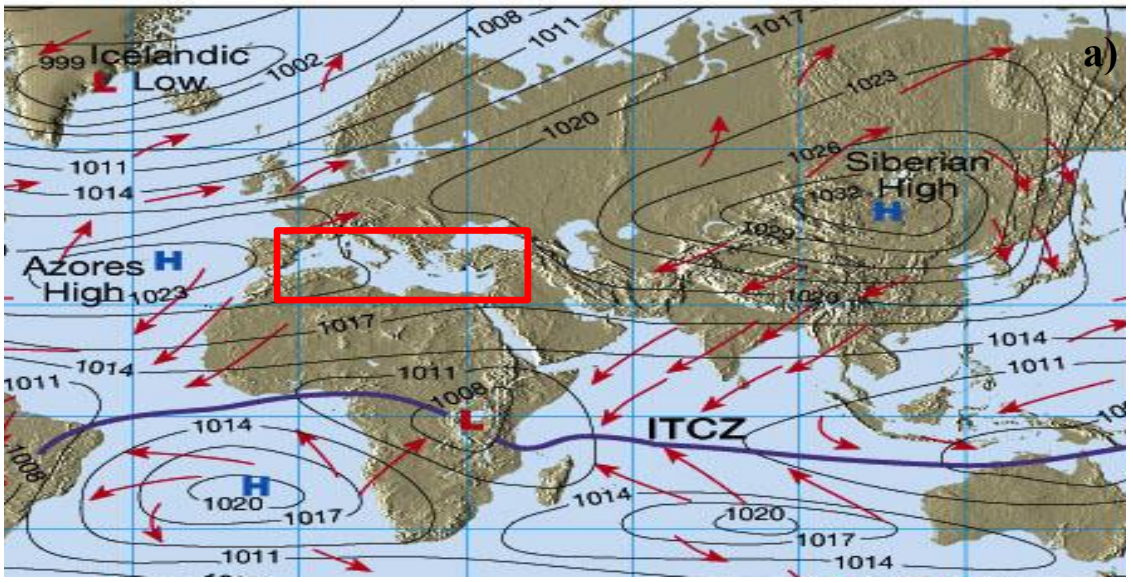

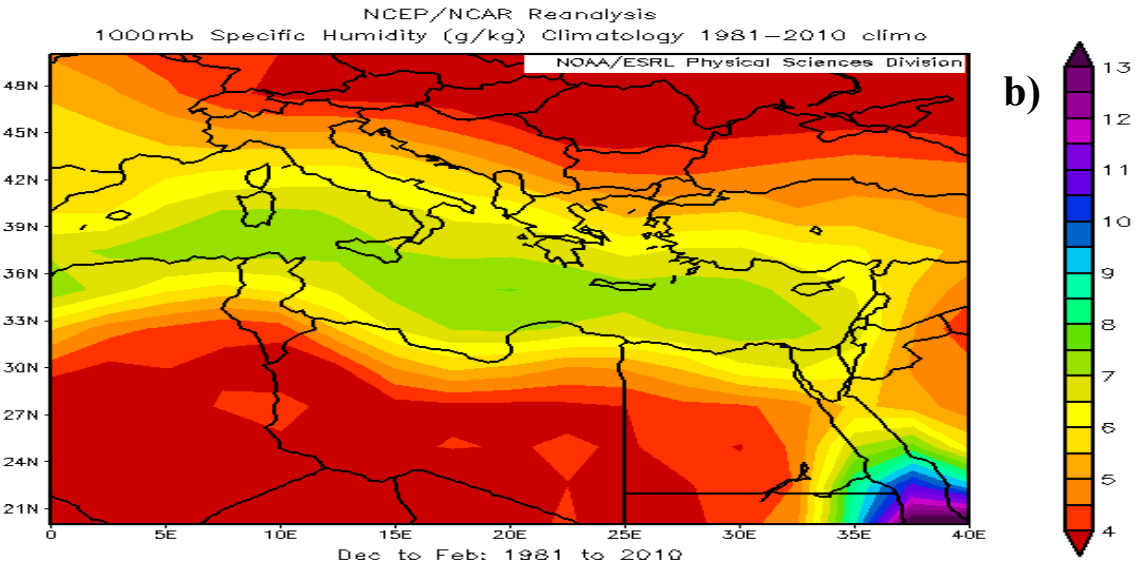

Adapted from EIU (2016) and NOAA (2016).

b. Warm Seasons

During the warm seasons, the Azorean High/Bermuda High formed in the central Atlantic and the Basra thermal Low formed in southwest Asia dominate Mediterranean weather. The Bermuda High extends eastward and causes northerly/northwesterly flow over the Mediterranean Sea. The Basra thermal Low also causes northerly/northeasterly flow and brings warm air from the east and northeast to the Eastern Mediterranean Sea (Aviation Meteorology 2012). Figure 5a depicts major pressure systems and associated circulation patterns in July.

Figure 5b shows that the Eastern Mediterranean Sea is significantly more humid compared to the Aegean Sea and the Western Mediterranean Sea. The highest specific humidity in July over the Eastern Mediterranean Sea is around 17.5 g/kg compared to 14 g/kg on the western side and ~7 g/kg over land to the south. The main reasons for the relatively humid air in the Eastern Mediterranean are warm waters and strong moisture fluxes from warm waters to the atmosphere (N. Skliris et al. 2011). Specific humidity in the Eastern Mediterranean Sea is almost twice as high in the warm season as it is in the cool season.

Figure 5. a) Pressure Systems and Associated Circulation Patterns in July, b) 1,000 mb Level Specific Humidity (g/kg) for Summer 1981–2010.

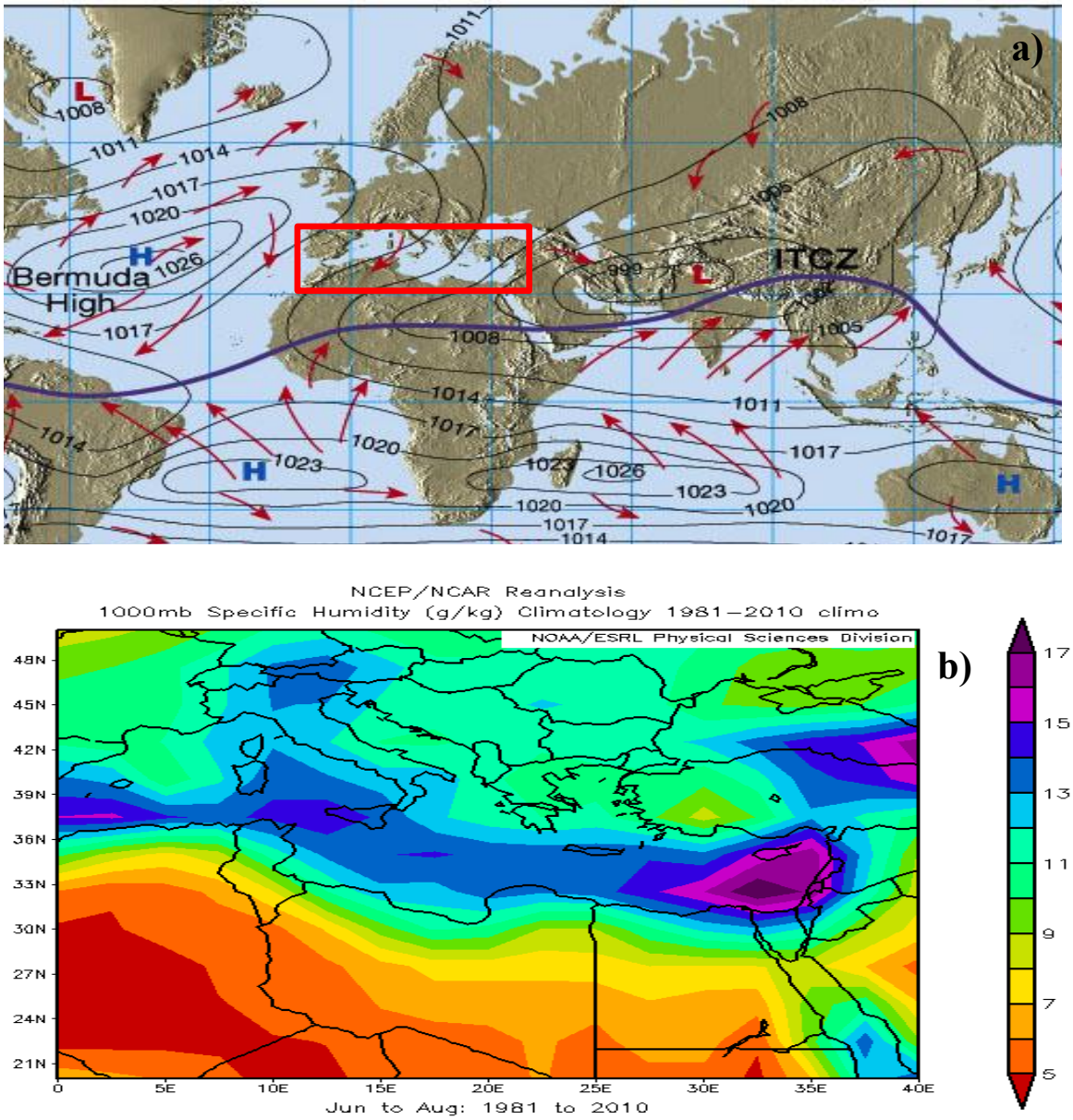

Adapted from EIU (2016) and NOAA (2016).

B. ATMOSPHERIC EFFECTS ON EM PROPAGATION

In this section, background information on anomalous EM propagation and refractivity, refraction categories, ducting and evaporation duct models are provided.

1. Anomalous EM Propagation and Refractivity

EM radiation is electromagnetic energy that propagates as waves. It has magnetic and electric fields that are perpendicular to each other and to the direction of propagation. EM waves propagate in straight paths in a vacuum or a homogeneous media. In a heterogeneous medium, such as the atmosphere, EM waves may deviate from the straight line path, a phenomenon usually referred to as refraction (Petty 2006). The variation in refractivity in the atmosphere is caused by complex variabilities in humidity, pressure, and temperature.

Propagation of EM radiation in the atmosphere is determined by the vertical and horizontal gradients of the refractive index of air, *n*, which is the ratio of the phase speed of the EM wave in a vacuum (*c*) to that in the air (*v*). Because the speeds of EM wave fronts in a vacuum and in the air are very close to each other, *n* is a quantity close to 1. To represent the differences of *n* better, refractivity (*N*) that describes the difference of *n* from 1 amplified by 10^6 is commonly used (Equation 1). The vertical gradient of *N* ($\partial N/\partial Z$) determines the change of the directions in EM wave propagation in the atmosphere.

$$N = (n - 1) \times 10^6 \tag{1}$$

For microwave frequencies and below, Equation (2) from Bean and Dutton (1968) relates *N* to the atmospheric variables of absolute temperature (T), partial pressure of water vapor (e), and total atmospheric pressure (P):

$$N = 77.6 \times \frac{P}{T} - 5.6 \times \frac{e}{T} + 3.73 \times 10^5 \times \frac{e}{T^2} \tag{2}$$

where *T* is in Kelvin (K), and *P* and *e* are in Hectopascal (hPa).

The modified refractivity (*M)* is also commonly used to describe refraction of waves relative to the earth's surface. *M* takes into account the Earth's curvature and is a

dimensionless quantity defined in Equation (3), where r_e is the radius of earth (≈ 6.378 × 10^6 m) and *z* is the height above the surface in meters (Turton et al. 1988).

$$M = N + \frac{z}{r_e \times 10^{-6}} = N + 0.1568 \times z \quad (3)$$

In a standard atmosphere, pressure and water vapor pressure slowly decrease with height and temperature decreases more significantly with height. The strongest vertical gradient of *M* occurs in the surface layer and at the top of the Atmospheric Boundary Layer (ABL) because of the strong gradients in humidity and temperature in these regions (Cherrett 2015). In a standard atmosphere, *N* decreases with height, whereas *M* increases with height.

2. Refraction Categories

The vertical gradient of *M* ($\partial M/\partial Z$), rather than its absolute value, determines how EM rays bend relative to the earth's surface. When ($\partial M/\partial Z$)=0, EM propagates in parallel with the earth's surface. When ($\partial M/\partial Z$)>0, EM rays curve away from the earth's surface and towards the surface when ($\partial M/\partial Z$)<0 (Turton et al. 1988). EM wave propagation paths in different refractivity conditions are schematically shown in Figure 6. Anomalous refractive conditions and a comparison of *N* and *M* gradients in these conditions are shown in Table 1.

Table 1. Comparison of *N* and *M* Gradients for Refractive Conditions. Adapted from Bean and Dutton (1968).

Refractive condition	dN/dz (N units/km)	dM/dz (M units/km)	Distance to Surface Horizon
Subrefraction	0 < N	157 < M	Reduced
Normal	-79 < N < 0	78 < M <157	Standard
Superrefraction	-157 < N < -79	0 < M < 78	Increased
Trapping	N < -157	M < 0	Greatly Increased

Figure 6. EM Wave Propagation Paths in Different Refractivity Conditions. Source: Murphy (2005).

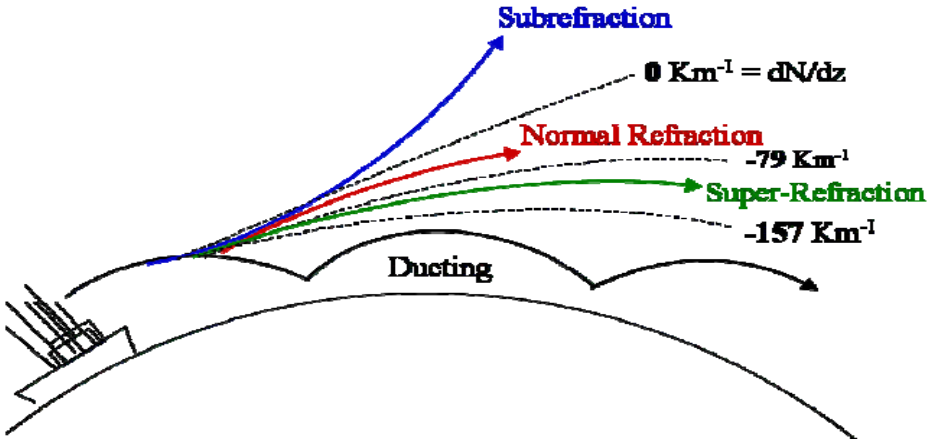

3. Ducting and Ducting Types

A duct is a "wave guide" where EM waves can travel to longer distances. Ducts occur only when there is a trapping layer, defined as the layer with negative *M* gradients. Figure 7 depicts the various types of atmospheric ducts, with the yellow regions indicating the vertical extents of the trapping layers. The height of a duct is related to the height of the trapping layer and the *M* profile itself. The top of the duct is the top of the trapping layer, while the bottom of the duct is either the surface or the level at which *M* is the same as that at the top of the trapping layer (Murphy 2005).

A significant decrease in humidity, which also means a significant decrease in water vapor pressure, is the main contributing factor for duct formation. Hence, any mechanism that creates vertical gradients profiles of temperature or moisture (i.e., warm and dry air over cool or moist air) is likely to result in a duct (Turton et al. 1988). With this perspective, sea breezes, convective processes, night-time radiative cooling, frontal formations, and advection all have potential to result in favorable conditions for formation of ducts of different types and strengths. The three types of ducts, surface ducts, surface-based ducts, and elevated ducts (Figure 7) are discussed in detail next.

Figure 7. M Profiles and Associated Ducting Types.
Adapted from Rogers (1998).

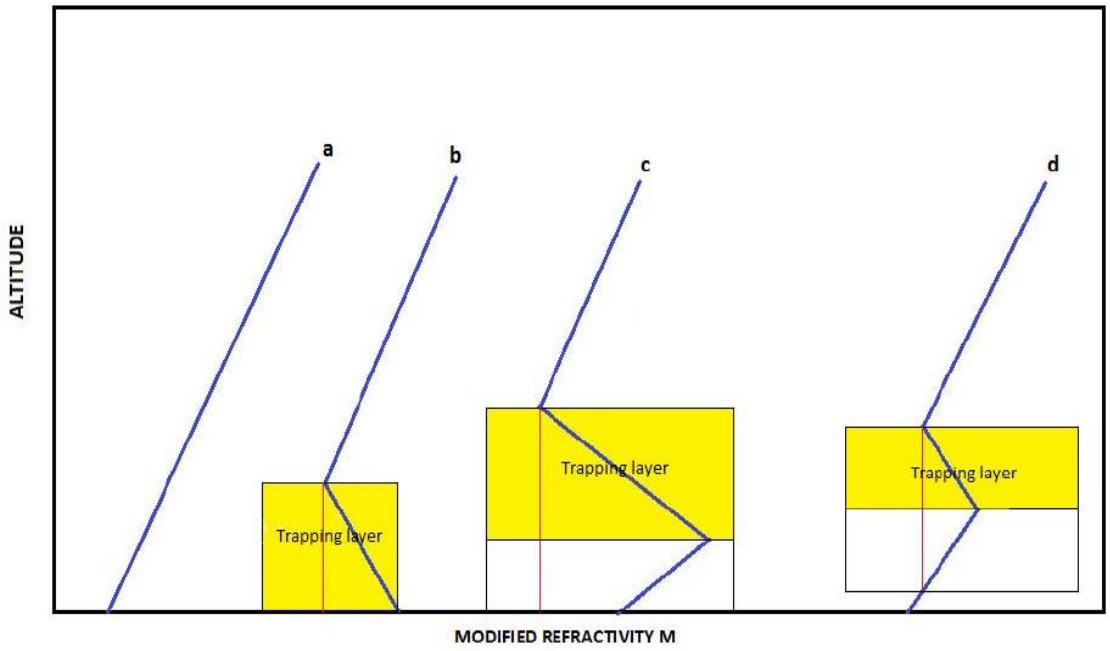

(a) standard atmosphere—no ducting, (b) surface duct, (c) surface-based duct, and (d) elevated duct. The red line indicates the vertical extent of the ducts.

Refraction and associated ducting conditions have important effects on the propagation of EM waves and thus on radar coverage and radio communication. Ducts trap EM waves and affect the propagation loss, which is the ratio of effective transmitted power to the received power between our sensors.

Longer wavelengths can be trapped by ducts with larger EDH and EDS. Maximum wavelength (minimum frequency) that can be trapped by ducts is given in Equation (4):

$$\lambda_{\max} = \frac{2}{3} CD(\Delta M)^{\frac{1}{2}} \tag{4}$$

where $\lambda_{\max}$ is the maximum trapped wavelength, D is the duct height (m), ΔM is the duct strength (M deficit), and $C=3.77x10^{-3}$ for a surface based duct, and C=5.66 $x10^{-5}$ for

an elevated duct (Turton et al. 1988). The typical values of maximum trapped wavelengths and minimum trapped frequencies are given in Table 2.

Table 2. Minimum EM Frequencies that Can Be Trapped by Ducts. Source: Guest (2010).

Minimum Trapped Frequency (MHz)	Maximum Trapped Wavelength	Radar (Radio) Band	Duct Thickness	
			feet	meters
150	2.0 m	A (VHF)	587	179.0
192	1.56 m	A (VHF)	499	152.0
220	1.36 m	A (TAC UHF)	453	138.0
425	70.6 cm	B (TAC UHF)	294	89.6
1000	30.0 cm	D	166	50.6
3000	10.0 cm	F	80	24.3
5800	5.2 cm	G	51	15.6
8500	3.5 cm	I	40	12.2
9600	3.1 cm	I	37	11.2
10250	2.9 cm	J	35	10.7
15000	2.0 cm	J	27	8.3
30000	1.0 cm	K	17	5.24

a. Surface Ducts

When the trapping layer base is at the surface, the associated duct is referred to as a surface duct. Evaporation ducts are a special type of surface duct and the most frequently occurring duct, particularly over the ocean. The evaporation duct height (EDH) is the height at which *M* has its minimum value (Martin 2007). Evaporation duct strength (EDS) is the difference of *M* at the surface and minimum *M*. EDH usually ranges from a few meters to 30–40 m.

Evaporation ducts are formed by a strong gradient of humidity close to the surface due to evaporation of water at the surface, over land, and at sea. For this reason, they often occur over warm water where there is often a strong humidity gradient just above

the sea surface. EM waves are trapped in evaporative ducts and their propagation ranges become longer than their free space range (Babin 1996).

b. Surface-Based Ducts

Surface-based ducts occur when a strong elevated trapping layer creates a duct that extends to the surface. For surface-based duct formation, the air temperature must increase or the vapor pressure must decrease with height rapidly. Because these conditions usually occur over oceans or other types of large water masses, surface-based ducts are common over those places (Newton 2003).

c. Elevated Ducts

Unlike surface and surface-based ducts, the elevated ducts do not extend to the surface. They are associated with the elevated trapping layers. A subsiding air with strong inversions of moisture and temperature aloft creates the best atmospheric conditions for the formation of elevated ducts. Elevated ducts can form up to a height of 4 km in the atmosphere, but are usually below 2 km (Murphy 2005).

It is worth noting that different combinations of ducts can be found at the same location at different heights in the atmosphere. With complicated *M* profiles, multiple elevated ducts commonly occur together with surface and surface-based ducts (Cherrett 2015).

4. Evaporation Duct Models

In order to understand and predict variabilities in EM wave propagation, we need to calculate the *M* profiles in the atmosphere, for which evaporation duct models are needed. Air temperature, sea surface temperature, relative humidity, and wind speed are required inputs to these models, and *M* profiles are the outputs.

For this calculation, evaporation duct models use bulk atmospheric measurements at a single altitude and relate vertical profiles of momentum and heat fluxes at different altitudes. With that approach, evaporation duct models calculate vertical profiles of temperature, humidity, and pressure from the measured quantities at a single level. The *M*

profiles and associated EDH and EDS are then easily computed using the output vertical profiles from evaporation duct models. The Paulus-Jeske (PJ) model (Jeske 1973; Paulus 1985), Babin-Young-Carton (BYC) model (Babin et al. 1997), and the Coupled Ocean-Atmosphere Response Experiment (COARE) (Fairall et al. 1996) are some of the evaporation duct models that are most commonly used.

In this study, the COARE surface flux algorithm (Fairall et al. 1996) is modified to output temperature and humidity profiles in the surface layer. These profiles can be used to compute the *M*-profile for EM propagation. The COARE surface flux algorithm is thus an evaporation duct model.

The COARE algorithm started by Fairall et al. (1996) is based on the Liu-Katsaros-Businger (LKB) surface layer model (Liu et al. 1979) parameterizations. These parameterizations (which were also used by the BYC model) use data from the Tropical Ocean and Global Atmosphere Coupled Ocean-Atmosphere Response Experiment (TOGA COARE). COARE parameterizations, as well as LKB parameterizations, depend on the Monin-Obukhov similarity theory of Monin and Obukhov (1954), which states that vertical gradients of temperature and specific humidity can be calculated using scaling parameters that are in correlation with vertical fluxes of momentum, sensible heat, and latent heat. The Naval Postgraduate School (NPS) evaporation duct model (Frederickson et al. 2000) also uses formulations similar to those in COARE parameterizations and is now known as NAVSLAM (Navy Atmospheric Vertical Surface Layer Model) (Cherett 2015).

The COARE evaporation duct model version 3.0 was published by Fairall et al. (2003). Updates and verifications for COARE have been included in that paper by Fairall et al. (2003). According to Fairall et al. (2003), COARE 3.0 was found to be accurate within 5 percent for wind speeds of 5–10 meter per second (m/s) and 10 percent for wind speeds of 10–20 m/s.

III. DATA AND METHODOLOGY

A. DATA

In this study, data from the ERA-Interim dataset produced by the European Center for Mid-range Weather Forecast (ECMWF) were used. This dataset is the latest atmospheric reanalysis dataset produced by ECMWF. The reanalysis field, available from 1979, is continuously updated in real time. The dataset can be accessed online at http://apps.ecmwf.int/datasets/data/interim-full-mnth/levtype=sfc/.

The ERA-Interim dataset was first created in 2006, and became available in real time in 2009. It has been updated on a monthly basis since then with a delay of one to two months. The data from the ERA-Interim dataset are relatively high-resolution with reanalysis data. Horizontal resolution of the data is approximately 80 km and the data have 60 vertical levels. Model level 60 is at 1012.05 mb pressure level (10 m) and model level 1 is at 0.1 mb pressure level (64560 m). Available resolution on the latitude/longitude grid is between $0.125^{o}\times0.125^{o}$ and $3^{o}\times3^{o}$ (Dee et al. 2011). In this study, data with a grid resolution of $0.125^{o}\times0.125^{o}$ are used.

The ERA-Interim dataset conducts four analyses per day, at 00, 06, 12, and 18 UTC (coordinated universal time). From those analyses, 6-hour estimates of three-dimensional meteorological parameters and 3-hour estimates of surface parameters and other two-dimensional parameters as well as two 10-day forecasts are produced. An analysis makes use of observations taken from 9 hours earlier and 3 hours after the analysis. For instance, an analysis at 12 UTC uses observations between 03 UTC and 15 UTC (Berrisford et al. 2011).

Throughout this study, the monthly mean data from 1990 to 2015 were used. These are referred to as synoptic monthly mean data because they are monthly means of variables for synoptic hours of 00, 06, 12, and 18 UTC. Synoptic monthly mean data are produced from 6-hour and 12-hour forecasts initiated at 00 UTC or 12 UTC. For surface parameters, 3-hour and 9-hour forecasts are also used in order to have 3-hour data

(Berrisford et al. 2011). In this study, 3-hour surface data and 6-hour model level data were used. Data used in this study are summarized in Table 3.

Table 3. Information on the Data Variables Used in This Study.

Data	**Height(m)**	**Model Level**	**Units**	**Symbols**
Dew Point Temperature	2	Surface	K	DpT
Air Temperature	2	Surface	K	Ta2
Air Temperature	10	Model (Level 60)	K	Ta10
Sea Level Pressure	Surface	Surface	Pa	SLP
Sea Surface Temperature	Surface	Surface	K	SST
u component of Wind	10	Surface	m/s	u
v component of Wind	10	Surface	m/s	v
Wind Speed	10	Surface	m/s	WS

ERA-Interim data are available in GRIB and NetCDF formats. In this study, data in NetCDF format were used. Analyses and graphical results were made in the MATLAB environment. A sample plot of 1990–2015 July monthly mean of wind speed data for the study area is depicted in Figure 8.

Figure 8. Mean Wind Speed (in m/s) in July between 1990 and 2015.

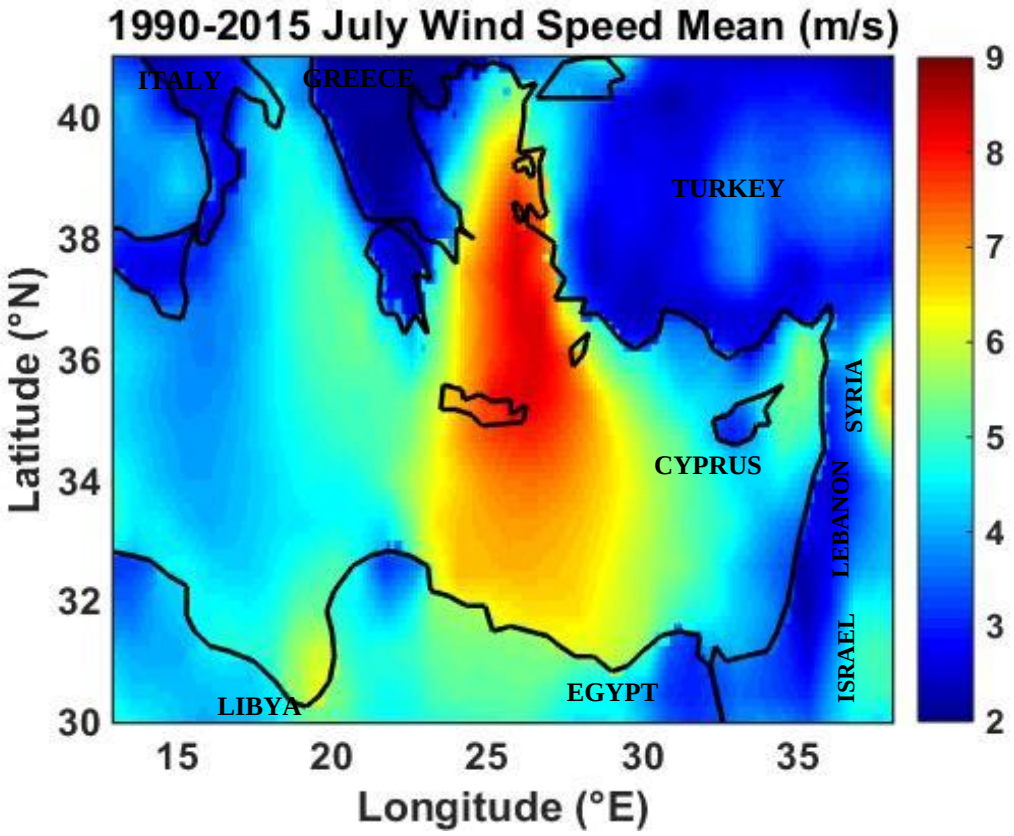

B. METHODOLOGY

In this section, general information about the calculations made in the study and four atmospheric factors, which were used to assess the atmospheric impacts on EM ducting, are described.

1. M-Profile Calculations

Three-hourly values of Sea Level Pressure (SLP), *Ta2*, *DpT*, *u*, *v*, and Sea Surface Temperature (SST) were used to calculate *M* Profiles in the study region. Relative Humidity (RH) at 2 m height was calculated using *DpT* and *Ta2*. The SLP, RH, *Ta2*, *u*, *v*, and SST were input into MATLAB version of the COARE bulk profile algorithm modified to output vertical profiles by John Kalagiros at the National Observatory of Athens, Greece. Vertical profiles of mean wind (U), vapor pressure (e), temperature (T),

and pressure (P) were generated from the COARE algorithm for 0–50 m at 0.1 m vertical resolution. These profiles were used to calculate *M* based on Equation (3), resulting in the corresponding *M* profiles in the surface layer. Example plots of *e*, *T*, and the associated *M* profile are shown in Figure 9.

Figure 9. Examples of e, T, and Associated M Profiles.

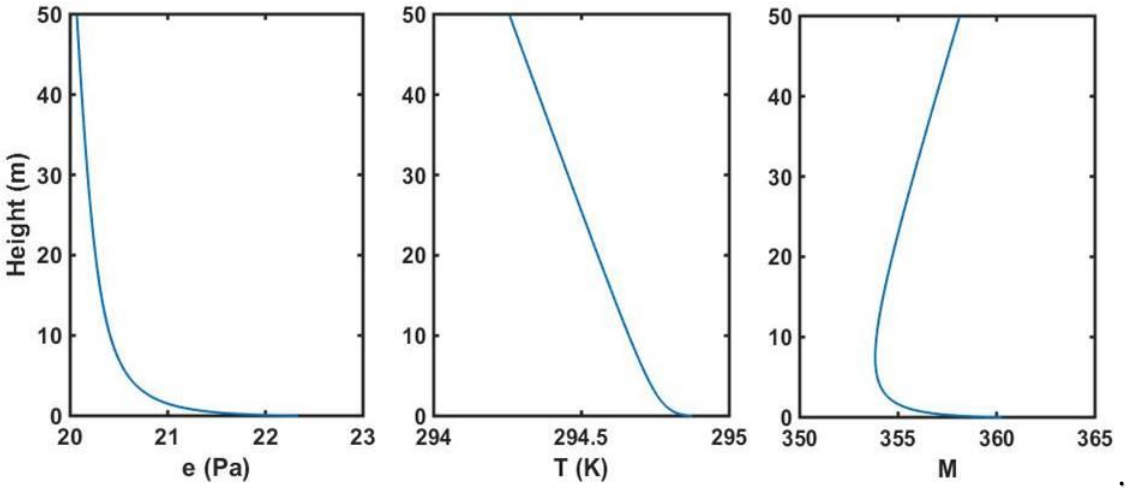

2. EDH and EDS Calculations

After acquiring *M* profiles, 3-hour EDH and EDS values were calculated and plotted using MATLAB. EDHs were defined by finding the heights at which *M* is at its minimum. Similarly, EDSs were computed by subtracting minimum *M* values from the *M* values at the surface. EDH is in m whereas EDS has no units.

For assessing the temporal and diurnal variations of EDH and EDS, monthly and seasonal means of EDH and EDS were generated every three hours. In this study "UTC" (0) time was used to represent the diurnal variations. It should be noted that the region of interest for this study includes four time zones: "UTC" (0), "A" (+1), "B" (+2), and "C" (+3).

In addition to the analysis made for the entire study region, the Aegean Sea and the eastern part of the Eastern Mediterranean Sea were selected as the focus area for more

in-depth analyses. The focus area was divided into five sub-areas (shown in Figure 14 in Chapter IV, Section B), and monthly and 3-hour means and standard deviations of EDH and EDS were calculated for each sub-area. The results for each sub-area are presented in the next chapter.

Throughout the study, the months of December, January, and February were grouped as the winter season; March, April, and May as the spring season; June, July, and August as the summer season; and September, October, and November were considered as the fall season. The EDH and EDS in the fall season of the Eastern Mediterranean Sea averaged between 1990 and 2015 are shown in Figure 10 as examples.

Figure 10. 1990–2015 Fall Means of a) EDH (in m) and b) EDS (No Units).

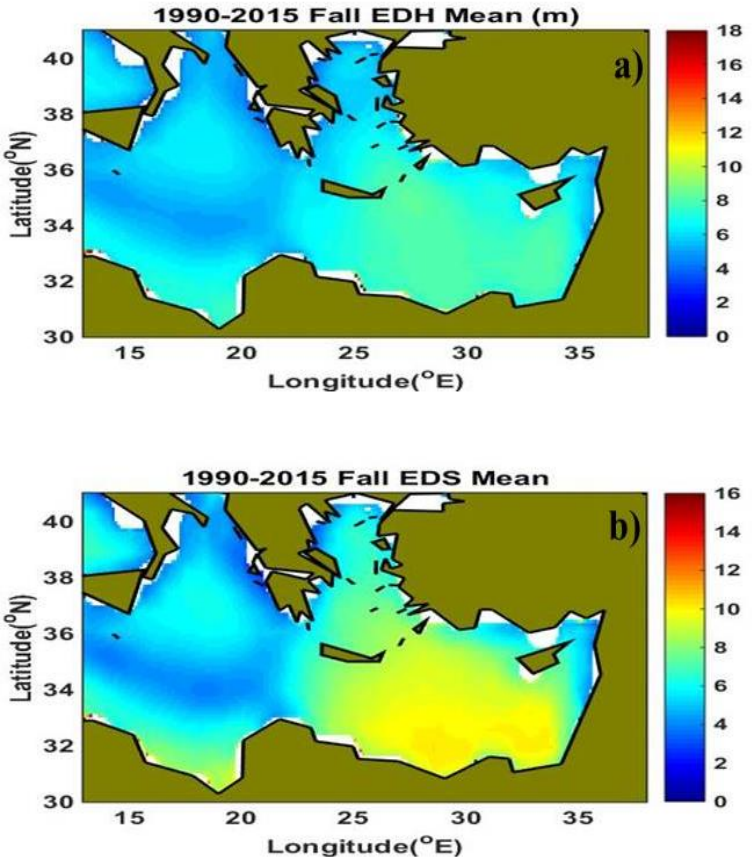

3. Assessing Effects of Atmospheric Factors on EDH and EDS

After analyzing the spatial and temporal variabilities in EDH and EDS, effects of atmospheric factors on these variabilities are assessed. Four atmospheric factors were selected for analyses since they are directly related to factors significantly affecting EDH and EDS. These atmospheric factors are air-sea temperature difference (ASTD), specific humidity depression (*Dq*), wind speed, and bulk Richardson number (*Rb*).

ASTD is defined as T_{air}-*SST*, which is the difference between the air temperature at the 2 m height and the SST. When ASTD is positive, the atmosphere is stable and when ASTD is negative, the atmosphere is unstable.

Dq is the difference in specific humidity between the 2 m height (calculated from *Ta2*, *P* and RH) and the surface (calculated from SST assuming 98% RH). *Dq* is essentially a representation of the near surface moisture gradient.

Rb represents the relative magnitude of buoyancy and shear driven turbulence. When buoyancy is negative (i.e., buoyancy as a sink of turbulent kinetic energy), *Rb* can be used as an indicator of the turbulence stability of the atmosphere. *Rb* was computed by the following formula:

$$Rb = \frac{g\Delta T / T}{\Delta u^2 / \Delta z} \tag{5}$$

where g is gravity, ΔT is the difference between the temperature at the 10 m height and SST, T is the average of these temperatures, Δu is the difference between wind values at the 10 m height and the surface (winds at the surface were assumed zero), and Δz is 10 m. All variables are available from the ECMWF reanalyses dataset.

Cherrett (2015) identified that *Dq* and *Rb* are two key parameters in determining EDH and EDS. Similar analyses are made in this thesis using the reanalysis data. To this end, monthly, seasonal, and diurnal variations of the four variables were calculated and analyzed for the study area. Additionally, EDH and EDS were plotted against different combinations of these four variables in order to assess the effects of these factors on EDH and EDS. Results of these analyses are presented in the next chapter.

Throughout the study, EDH and EDS were calculated and shown only for regions over the water. Although there are no missing data in the input variables, there are areas (white regions) in the EDH and EDS spatial distribution plots where evaporation ducts cannot be identified.

Figure 11 shows profiles of *q*, *T*, and *M* from the Aegean Sea in the summer season. In this example, *M* decreases monotonically with height beyond the lowest 50 m without the presence of a minimum. A meaningful evaporation duct thus does not exist. This *M* profile was caused by strong specific humidity decrease and temperature increase in the first 50 m, which are not realistic.

Figure 11. q (g/kg), T (K) and M Profiles (Generated by COARE) Where EDH Is Defined above 50 m.

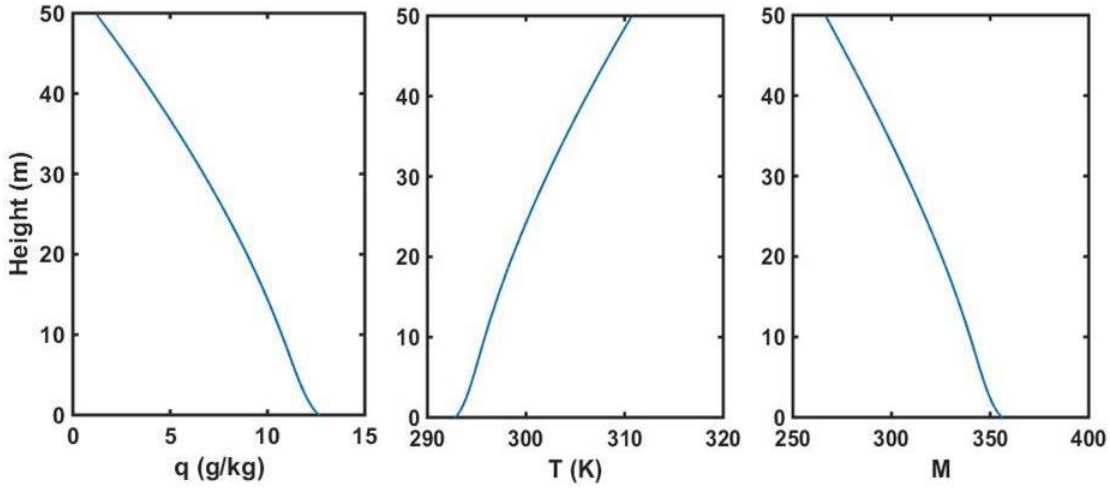

These unrealistic *q* and *T* profiles result when the surface layer is strongly stable. In the summer season, horizontal advection may bring warm and dry air over the study area. The example in Figure 11 has an ASTD of 0.6 K, indicating slightly stable stratification. However, the significant decrease in specific humidity within the lowest 50 m is not reasonable. This is likely a result of the model difficulties in dealing with a stable and weak wind surface layer (Cherrett 2015). It was found that most of the white regions are along the coast. A large number of profiles similar to those in Figure 11 were analyzed. Most of such profiles are associated with stable thermal stratifications (positive ASTD).

THIS PAGE INTENTIONALLY LEFT BLANK

IV. RESULTS

Results of the study are presented in this chapter. In Section A, long-term seasonal means (LTSM) of EDH and EDS across the study region are presented. Plots of monthly means of EDH and EDS values are given in the Appendix. In Section B of this chapter, monthly means and standard deviations of EDH and EDS for the focus area are analyzed. Each of the five sub-areas in the focus area (shown on the map in Section B) is examined separately. In Section C, diurnal variations of EDH and EDS values in the focus area are summarized for each season.

Section D and Section E focus on the analysis of ASTD, WS, *Dq*, and *Rb*, which are four atmospheric factors that affect the EDH and EDS the most. In Section D, seasonal variations of the atmospheric factors are illustrated. In Section E, the sensitivity of EDH and EDS to the atmospheric factors is analyzed across the focus area.

A. EDH AND EDS LTSM

In this section, long-term seasonal means of EDH and EDS in the Eastern Mediterranean Sea are presented.

1. EDH LTSM

Long term seasonal means of EDHs over the eastern part of the Mediterranean Sea are illustrated in Figure 12. We can see from Figure 12 that EDHs are lowest in the spring, although they are very close to those in the winter. EDHs are generally in the range of 4–6 m in the spring and 5–8 m in the winter. EDHs increase significantly after the spring and reach their maximum in the summer. This increase can be considered as the strongest temporal variation in EDHs. The summer mean of EDHs ranges between 11 m and 18 m in the Aegean Sea and 9 m and 12 m in the north of Crete Island. The strongest spatial variation of EDHs also occurs in the summer.

Figure 12. EDH Long Term Seasonal Means (1990-2015) in the Eastern Mediterranean Sea for a) Winter, b) Spring, c) Summer, and d) Fall. (Colors represent EDH in meters).

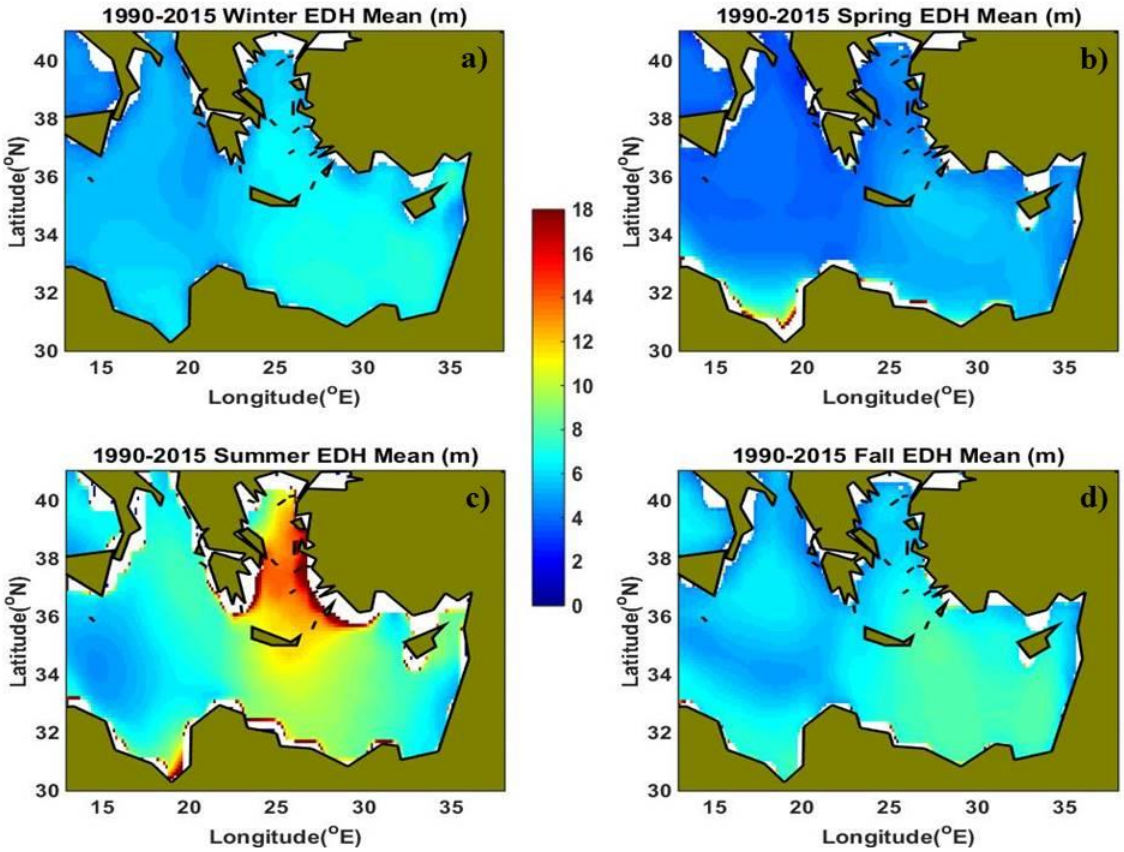

2. EDS LSTM

Long term seasonal means of EDSs over the Eastern Mediterranean Sea are illustrated in Figure 13. It is clear from the figure that EDSs are the lowest in the spring when they are between 4 and 7. EDSs are highest in the fall. Spatial variation in EDSs is also the largest in the fall. EDSs are between 7 and 11 in the east part of the Eastern Mediterranean Sea and between 5 and 7 in the west part of it in the fall. EDSs in the eastern part of the Eastern Mediterranean Sea are higher than those in the western part of it in all seasons. The strongest temporal variation in EDS occurs between the spring and the summer.

Figure 13. EDS Long Term Seasonal Means (1990-2015) in the Eastern Mediterranean Sea for a) Winter, b) Spring, c) Summer, and d) Fall. (Colors represent EDS (No Units)).

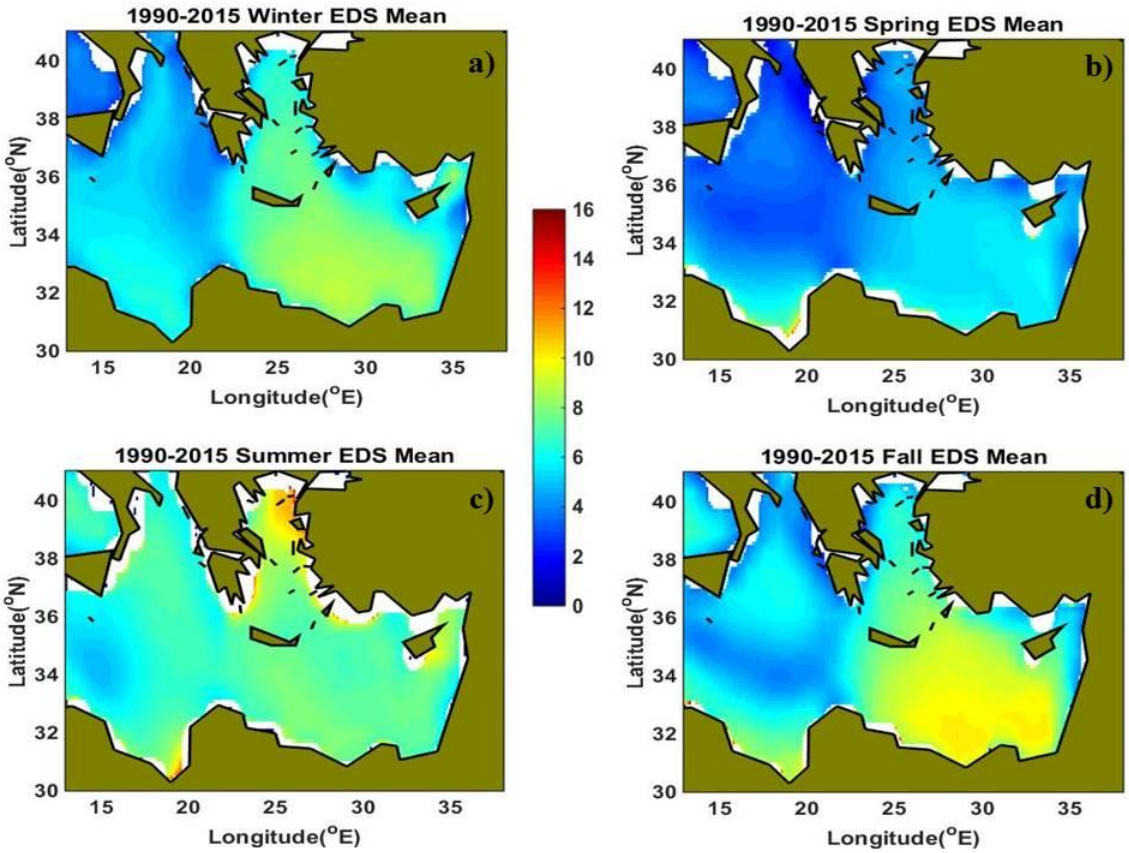

It is noted that the eastern Mediterranean region is separated into two main areas with rather distinct differences in both EDH and EDS. The area in the west of continental Greece (west of the red line in Figure 2b) in general has a weak evaporation duct with lower duct height and weaker duct strength, while greater variability is seen in the area to the east of continental Greece (east of the red line in Figure 2b). The eastern part of the eastern Mediterranean is referred to as the 'focus area'.

B. MONTHLY MEANS AND STANDARD DEVIATIONS OF EDH AND EDS FOR THE FOCUS AREA

In this section, monthly variations of EDH and EDS in the focus area are examined in detail. The focus area is divided into five sub-areas as shown in Figure 14. Sub-area 1 (SA-1) extends between 36° N and 40° N in latitude, 23°30′ E and 27° E in longitude; sub-area 2 (SA-2) extends between 33°30′ N and 36° N, 22° E and 29° E; sub-area 3 (SA-3) is between 33°30′ N and 36° N, 29° E and 36° E; sub-area4 (SA-4) extends between 31° N and 33°30′ N, 29° E and 36° E; and finally sub-area 5 (SA-5) covers 31° N to 33°30′ N and 22° E to 29° E.

Figure 14. Five Sub-Areas in the Focus Area (Latitude and Longitude Range for Each Sub-area Are Given in the Text).

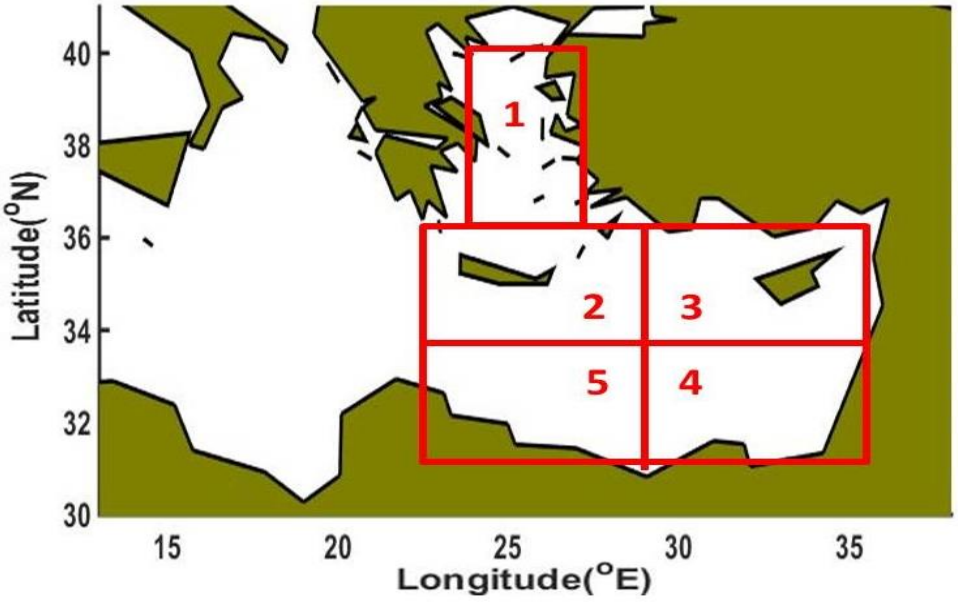

1. Monthly Values of EDH for Each Sub-Area

Monthly means of EDH in each sub-area are calculated and presented in Table 4.

Table 4. Monthly Values of EDH for Each Sub-area (Mean ± Standard Deviation in m).

Month	SA-1	SA-2	SA-3	SA-4	SA-5
January	6.65 ± 0.49	6.67 ± 0.34	6.88 ± 0.69	6.76 ± 0.64	6.60 ± 0.54
February	5.88 ± 0.47	6.53 ± 0.44	6.01 ± 0.47	6.57 ± 0.44	7.08 ± 0.45
March	5.24 ± 0.33	5.06 ± 0.38	4.82 ± 0.45	5.38 ± 1.15	6.05 ± 1.21
April	3.79 ± 0.32	4.37 ± 0.30	5.43 ± 2.17	5.88 ± 2.26	5.99 ± 2.55
May	6.38 ± 2.33	6.27 ± 1.06	6.60 ± 2.21	6.38 ± 1.33	7.18 ± 3.67
June	10.43 ± 5.84	9.61 ± 2.33	8.20 ± 3.80	7.36 ± 1.95	9.84 ± 3.43
July	16.14 ± 5.03	11.49 ± 2.19	9.12 ± 3.12	7.81 ± 3.06	10.79 ± 4.11
August	15.78 ± 4.26	11.00 ± 0.93	8.71 ± 2.58	7.91 ± 2.68	11.61 ± 5.46
September	9.90 ± 1.99	10.50 ± 1.42	9.06 ± 2.30	8.98 ± 2.10	10.37 ± 2.14
October	5.37 ± 0.39	6.14 ± 0.50	6.67 ± 0.87	6.96 ± 1.32	6.76 ± 0.79
November	4.87 ± 0.59	6.41 ± 0.52	6.79 ± 1.50	7.40 ± 0.74	7.23 ± 0.65
December	6.18 ± 0.28	6.72 ± 0.44	6.52 ± 0.88	7.45 ± 0.58	7.32 ± 0.57

a. SA-1

The highest EDHs of the entire Mediterranean Sea occur in SA-1 in the summer months when the peak EDH value reaches 16.14 m in July. In the non-summer months, EDH values in SA-1 are similar to those in other regions. Standard deviations also have the largest values in the focus area during summer months, which indicate the strongest spatial variability of the region in SA-1. The greatest temporal variabilities also occur in SA-1, especially from May to June and from August to September.

b. SA-2

EDHs do not change very much from January to May in SA-2, but they increase substantially in June and reach their peak in July. SA-2 has the second highest mean EDH in the summer, after SA-1. After August, EDH gradually decreases and has similar spatial variability to that in SA-1. Spatial and temporal variabilities in EDH are less strong compared to SA-1.

c. SA-3

EDHs in SA-3 are highest in the summer months (also in September). However, yearly temporal variabilities, especially before and after the summer transition, are weaker than those in SA-1 and SA-2. Monthly means of EDH in SA-3 are very close to those in other regions except for the summer months. EDH in SA-3 has the typical monthly variability in the general area.

d. SA-4

Unlike the regions previously discussed, EDHs in SA-4 are the highest in September. EDHs in November and December in SA-4 are higher than those in other regions. EDHs in this region show the least annual variability compared to any other region.

e. SA-5

SA-5 also shows the typical monthly variability and considerable similarity with EDHs in SA-2. As in SA-2, spatial variabilities of EDH in SA-5 are high in the summer months, as indicated by high standard deviation values.

2. Monthly Values of EDS for Each Sub-Area

Monthly means of EDS in each sub-area are calculated and presented in Table 5.

Table 5. Monthly Values of EDS for Each Sub-Area (Mean ± Standard Deviation (No Units)).

Months	SA-1	SA-2	SA-3	SA-4	SA-5
January	7.24 ± 0.56	7.69 ± 0.57	7.16 ± 1.17	7.49 ± 1.23	7.74 ± 0.96
February	6.39 ± 0.60	7.25 ± 0.57	6.00 ± 1.05	7.58 ± 0.72	7.94 ± 0.58
March	5.27 ± 0.31	5.12 ± 0.41	4.58 ± 0.81	5.52 ± 0.55	5.97 ± 0.60
April	3.30 ± 0.55	4.28 ± 0.34	5.16 ± 0.47	5.37 ± 0.52	5.39 ± 0.81
May	5.46 ± 0.43	5.25 ± 0.54	5.77 ± 0.52	5.86 ± 0.33	5.72 ± 0.52
June	6.37 ± 0.86	6.19 ± 0.52	6.17 ± 0.87	5.89 ± 0.75	6.56 ± 0.51
July	9.78 ± 1.27	7.78 ± 0.45	7.69 ± 1.33	7.32 ± 1.45	7.68 ± 1.28
August	9.90 ± 1.46	8.25 ± 0.57	8.48 ± 1.41	7.91 ± 1.63	8.32 ± 1.47
September	9.79 ± 0.60	10.12 ± 0.55	10.21 ± 1.22	10.49 ± 1.91	10.67 ± 1.10
October	5.61 ± 0.63	6.62 ± 1.04	7.24 ± 1.23	8.26 ± 1.36	7.80 ± 0.91
November	4.10 ± 0.84	6.65 ± 1.09	6.86 ± 1.32	8.37 ± 1.20	8.16 ± 1.14
December	6.82 ± 0.53	7.40 ± 0.97	6.44 ± 1.49	8.53 ± 1.03	8.58 ± 1.00

a. SA-1

EDSs in SA-1 are highest in July, August, and September. But summer EDSs in SA-1 are only slightly higher than those in other regions. An EDS of 3.30, which occurs in April in the region, is the lowest EDS occurring in the entire Eastern Mediterranean Sea.

b. SA-2

EDSs in SA-2 are lowest in the spring. Winter, summer, and fall means of EDSs in the region are very close to each other. EDSs reach their peak in September. Temporal and spatial variations are limited in SA-2.

c. SA-3

EDSs in SA-3 have the typical monthly variability of the general region. They reach their peak in September. Temporal and spatial variations are limited also in SA-3.

d. SA-4

Highest EDSs in the entire Mediterranean Sea occur in SA-4 in the fall. The greatest temporal variability of EDS in SA-4 occurs from July to August and August to September. Spatial variability in SA-4 is higher than that in any other region as seen in the standard deviation in Table 5.

e. SA-5

EDSs in the winter are higher in SA-5 than those in any other region. EDSs in SA-5 reach their peak in September. Seasonal means of EDSs in the region are highest in the winter. Temporal and spatial variations are very limited also in SA-5.

C. DIURNAL VARIATIONS IN THE FOCUS AREA

In this section, 3-hour EDH and EDS values in all seasons are examined and presented separately for each sub-area to assess the diurnal variations in the sub-areas. Mean values are referred to as averaging over the corresponding sub-area.

1. Diurnal Variations in SA-1

Plots of 3-hour means of EDHs and EDSs in SA-1 are shown in Figure 15. It is clear from Figure 15a that the diurnal variation of EDH in SA-1 is not strong except in the summer. The summer season has the strongest diurnal variation in the entire Mediterranean Sea, with the minimum EDH occurring at 6 UTC and the maximum at 21 UTC. The reason for this extremely strong diurnal variation of EDH in the summer is the stable conditions (positive ASTDs) in the region. The strong correlation between diurnal variations of ASTD and EDH in SA-1 for the summer and winter is shown in Figure 23 in Section D.

Figure 15. Composite Diurnal Variation from 3-hour Means of a) EDH and b) EDS in SA-1 for Each Season from 1990 to 2015.

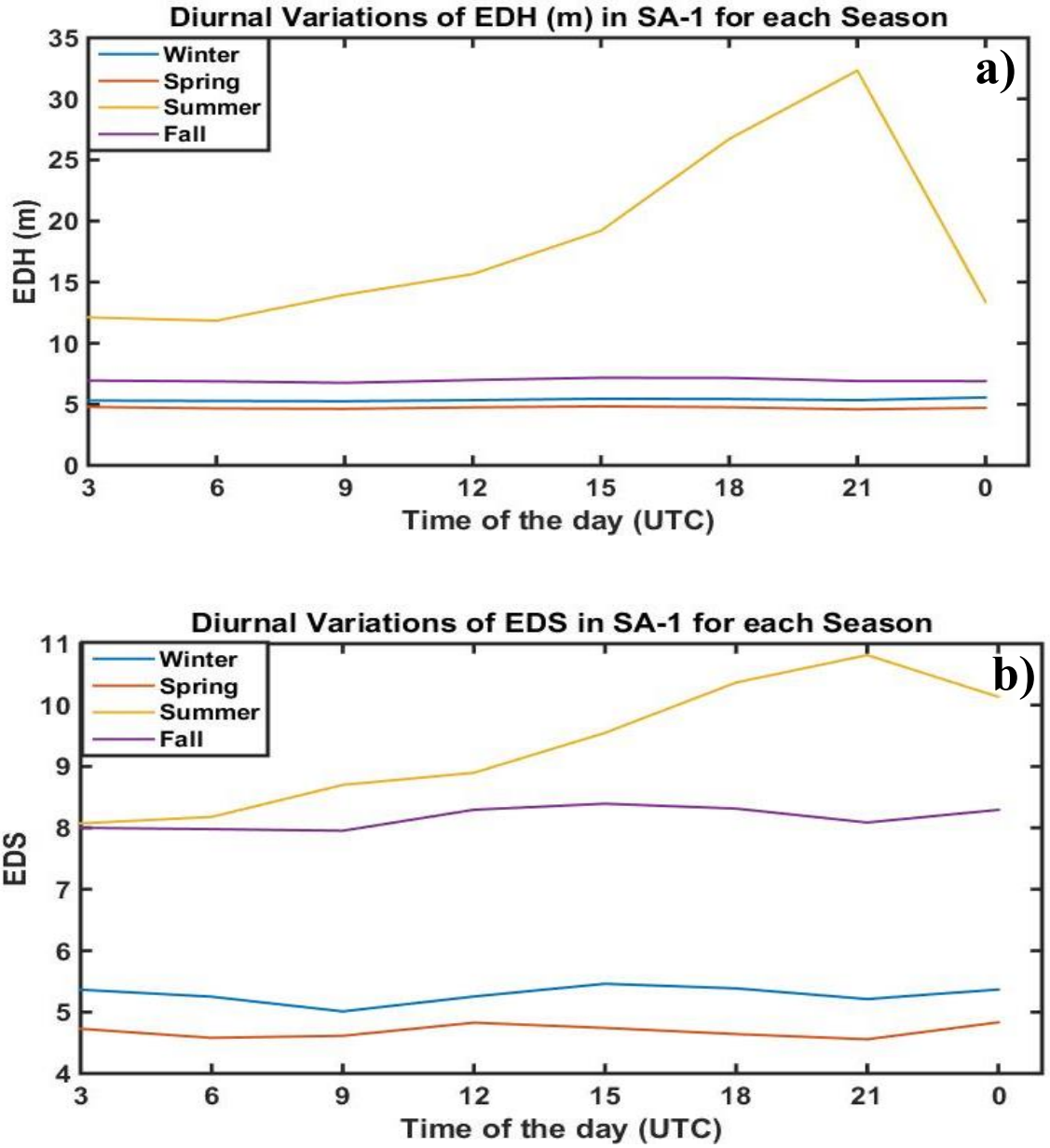

Diurnal variation of EDS in SA-1 (Figure 15b) is also stronger in the summer compared to other seasons. In the summer, EDSs are at a minimum at 3 UTC and then increase throughout the day, reaching a maximum at 21 UTC. Diurnal variations of EDSs in the winter, spring, and fall are so small that they are almost negligible.

2. Diurnal Variations in SA-2

Plots of three-hourly means of EDHs and EDSs in SA-2 are shown in Figures 16a and 16b, respectively.

Figure 16. Composite Diurnal Variation from 3-hour Means of a) EDH and b) EDS in SA-2 for Each Season from 1990 to 2015.

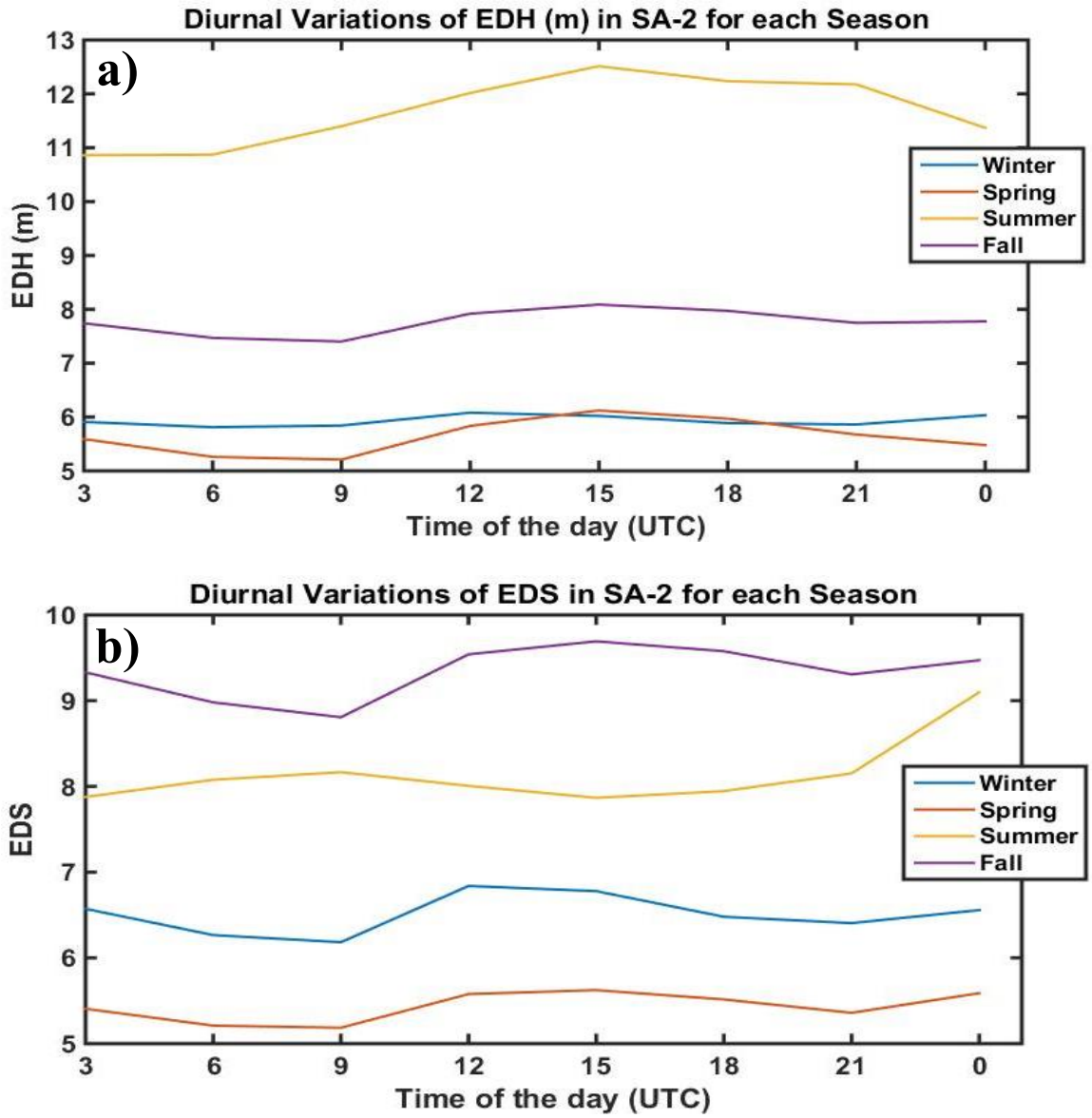

As shown in Figure 16a, diurnal variation of EDH in SA-2 is strongest in the summer and least strong in the winter. Diurnal variation of EDH is around 1.5 m in the summer and less than 1 m in other seasons. EDHs are at a minimum around 9 UTC and a maximum around 15 UTC. As shown in Figure 16b, diurnal variation of EDS in SA-2 is strongest in fall. EDSs are lowest around 9 UTC and highest between 12 and 15 UTC in winter, spring, and fall. In summer, EDSs are at a maximum at 0 UTC, and at a minimum at 3 UTC.

3. Diurnal Variations in SA-3

Plots of 3-hour means of EDHs and EDSs in SA-3 are shown in Figure 17. Diurnal variation of EDHs in SA-3 is strongest in the summer. Minimum EDH in the summer is 8 m at 6 UTC, and maximum EDH is about 11.8 m at 15 UTC. Diurnal variations of EDHs are similar also in the fall and spring with smaller magnitudes of EDHs. Diurnal variation of EDH is almost negligible in the winter.

Figure 17. Composite Diurnal Variation from 3-hour Means of a) EDH and b) EDS in SA-3 for Each Season from 1990 to 2015.

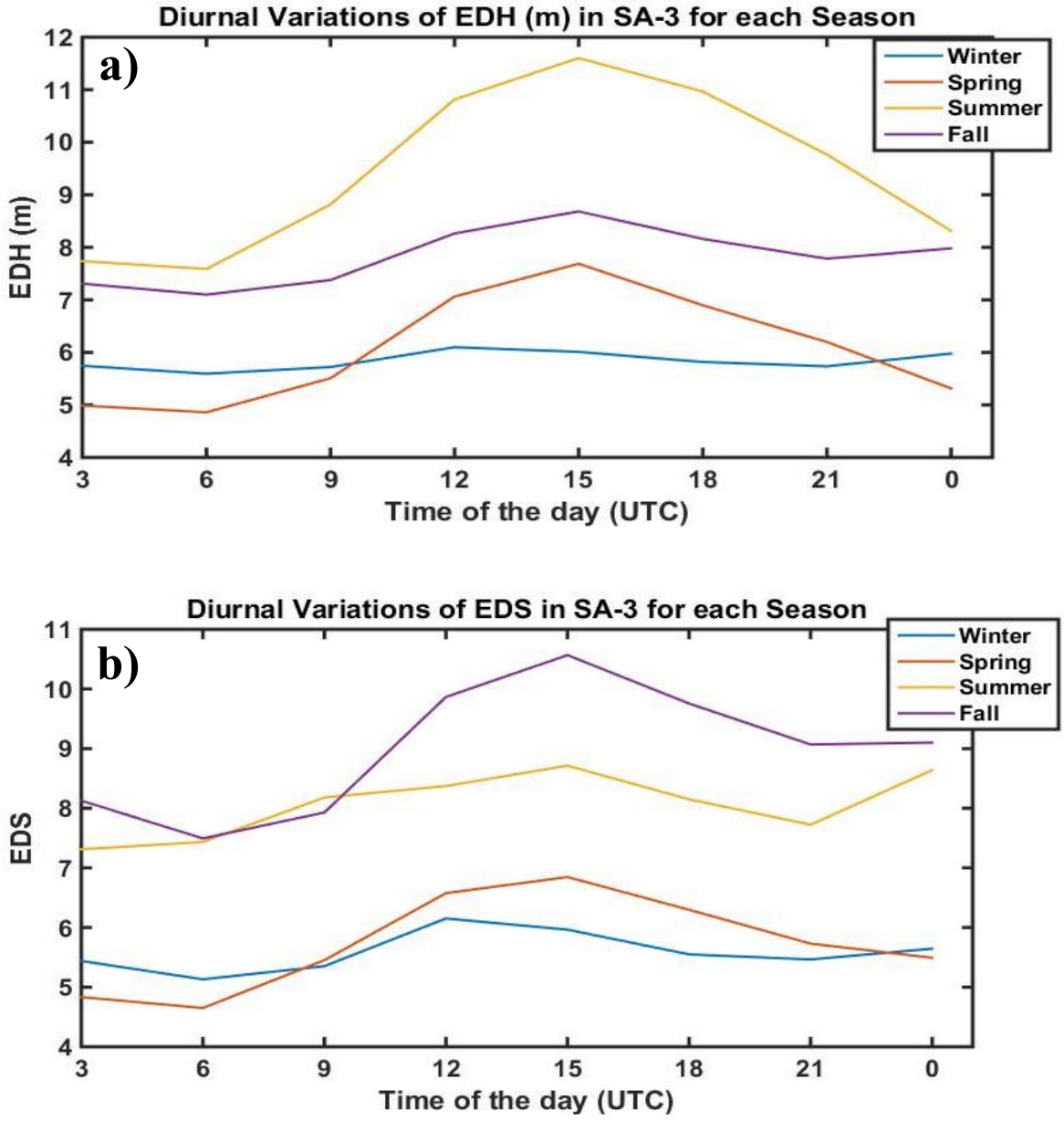

Minimum EDS in SA-3 occurs between 3 and 6 UTC, and maximum EDS occurs between 12 and 15 UTC as in other regions. Diurnal variation of EDS is strongest in the fall, with a minimum EDS of about 7.6 at 6 UTC and a maximum EDS of about 10.7 at 15 UTC. Diurnal variation of EDS is least strong in the winter.

4. Diurnal Variations in SA-4

Plots of 3-hour means of EDHs and EDSs in SA-4 are shown in Figure 18. Diurnal variation of EDH in SA-4 is strongest in the summer. It is also strong in spring, with smaller magnitudes of EDHs than in summer. Diurnal variation of EDH is smallest in the winter.

Diurnal variation of EDS is strongest in the fall, with a minimum EDS of about 9.5 at 6 UTC and maximum EDS of about 12.5 at 15 UTC. The diurnal variation of EDS in the fall is the strongest diurnal variation of the entire Eastern Mediterranean Sea. Diurnal variation of EDS in SA-4 is small in the summer and winter. It is greater in the spring than in summer and winter although EDSs in the spring are smaller in magnitude.

Figure 18. Composite Diurnal Variation from 3-hour Means of a) EDH and b) EDS in SA-4 for Each Season from 1990 to 2015.

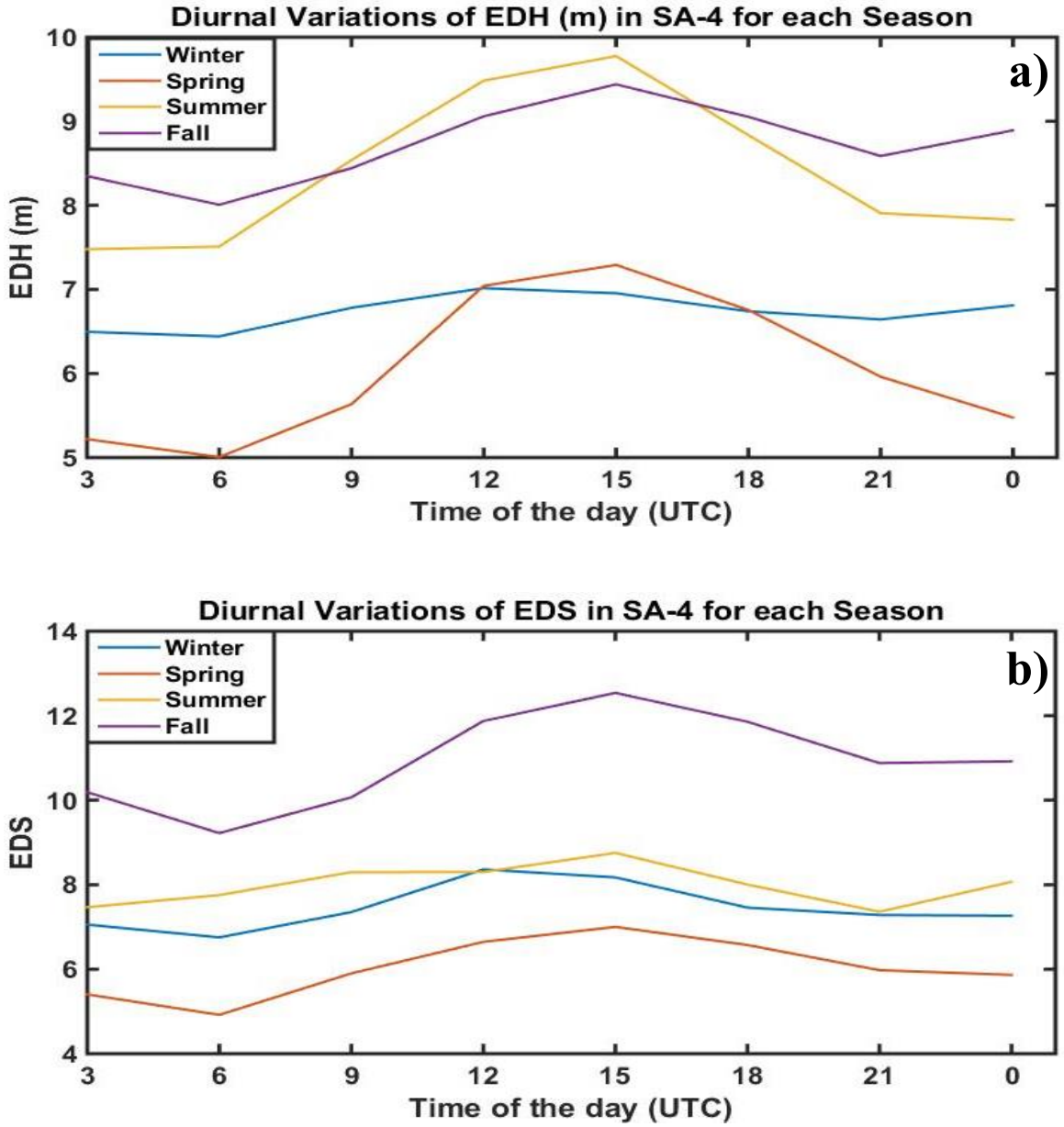

5. Diurnal Variations in SA-5

Plots of the 3-hour means of EDHs and EDSs in SA-5 are shown in Figure 19.

Figure 19. Composite Diurnal Variation from 3-hour Means of a) EDH and b) EDS in SA-5 for Each Season from 1990 to 2015.

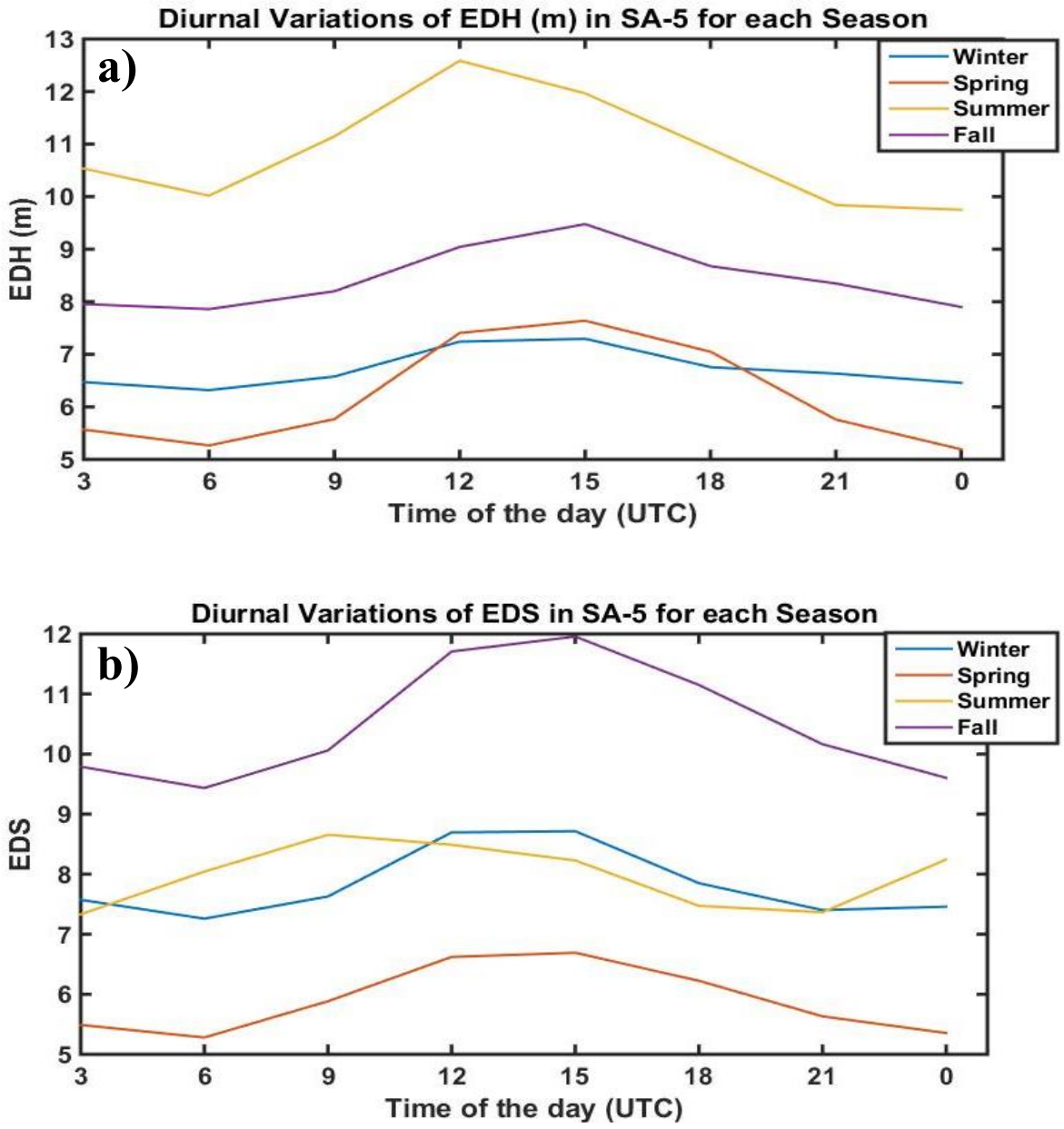

Diurnal variation of EDH in SA-5 is highest in the summer. EDHs are also highest in magnitude in the summer. The maximum EDH in SA-5 is about 12.8 m at 15

UTC in the summer. Diurnal variation of EDH is also strong (about 2 m) in the spring although EDHs are smaller in magnitude than they are in the summer. Diurnal variation of EDH is smallest in the winter (less than a meter). Diurnal variation of EDS is strongest in the fall. It is the second strongest diurnal variation of EDS (slightly weaker than the one in SA-4) for the entire Eastern Mediterranean Sea. EDSs are also higher in magnitude in the fall than they are in other seasons. Diurnal variation of EDS in the summer is different from that in other seasons. EDSs in the summer are at a minimum at 3 UTC and a maximum at 9 UTC while EDSs in other seasons are at a minimum at 6 UTC and a maximum at 15 UTC.

To summarize, the diurnal variation of EDH in summer is stronger than it is in other seasons. The strongest diurnal variation of EDH in the entire Mediterranean Sea occurs in SA-1 in the summer. Similarly, the diurnal variation of EDS is strongest in the fall and the strongest diurnal variation of EDS in the entire Mediterranean Sea occurs in SA-4 in the fall. Figure 20 and Figure 21, respectively, illustrate plots of the strongest diurnal variations of EDH (in the summer) and EDS (in the fall) so that we can see the spatial and diurnal variations of EDH and EDS together throughout the entire Eastern Mediterranean Sea.

As seen in Figure 20, the spatial variation of EDH in summer is very high throughout the entire Eastern Mediterranean Sea. Highest EDHs occur in the Aegean Sea (SA-1) in the summer between 15 and 21 UTC. EDHs are getting lower towards the south from the Aegean Sea. They are remarkably lower in the west part of the Eastern Mediterranean Sea than they are in the east part of the Eastern Mediterranean Sea.

Figure 20. 1990–2015 Three-hour Means of EDH in Summer for: a) 00 UTC; b) 03 UTC, c) 06 UTC, d) 09 UTC, e) 12 UTC, f) 15 UTC, g) 18 UTC, and h) 21 UTC. (x axis: Longitude (ºE), y axis: Latitude (ºN). Colors Represent EDH in Meters).

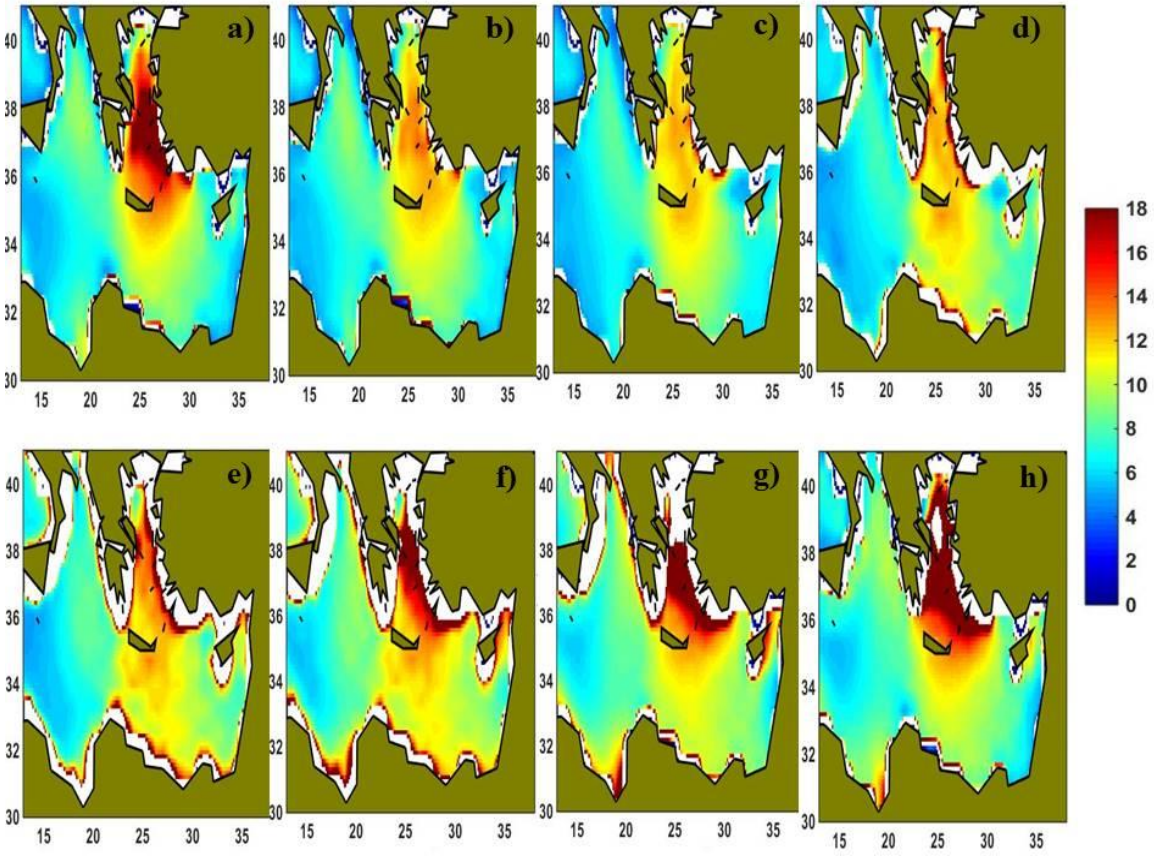

Figure 21 clearly shows that EDSs in the fall are higher in the east part of the Eastern Mediterranean Sea than they are in the west part of it. EDSs increase as we go south in the east part of the Eastern Mediterranean Sea. They are highest between 12 and 15 UTC. Effects of atmospheric factors on spatial and diurnal variations of EDH and EDS are analyzed in Sections D and E of this chapter.

Figure 21. 1990–2015 Three-hour Means of EDS in Fall for: a) 00 UTC, b) 03 UTC, c) 06 UTC, d) 09 UTC, e) 12 UTC, f) 15 UTC, g) 18 UTC, and h) 21 UTC. (x axis: Longitude(ºE), y axis: Latitude(ºN). (Colors Represent EDS (No Units)).

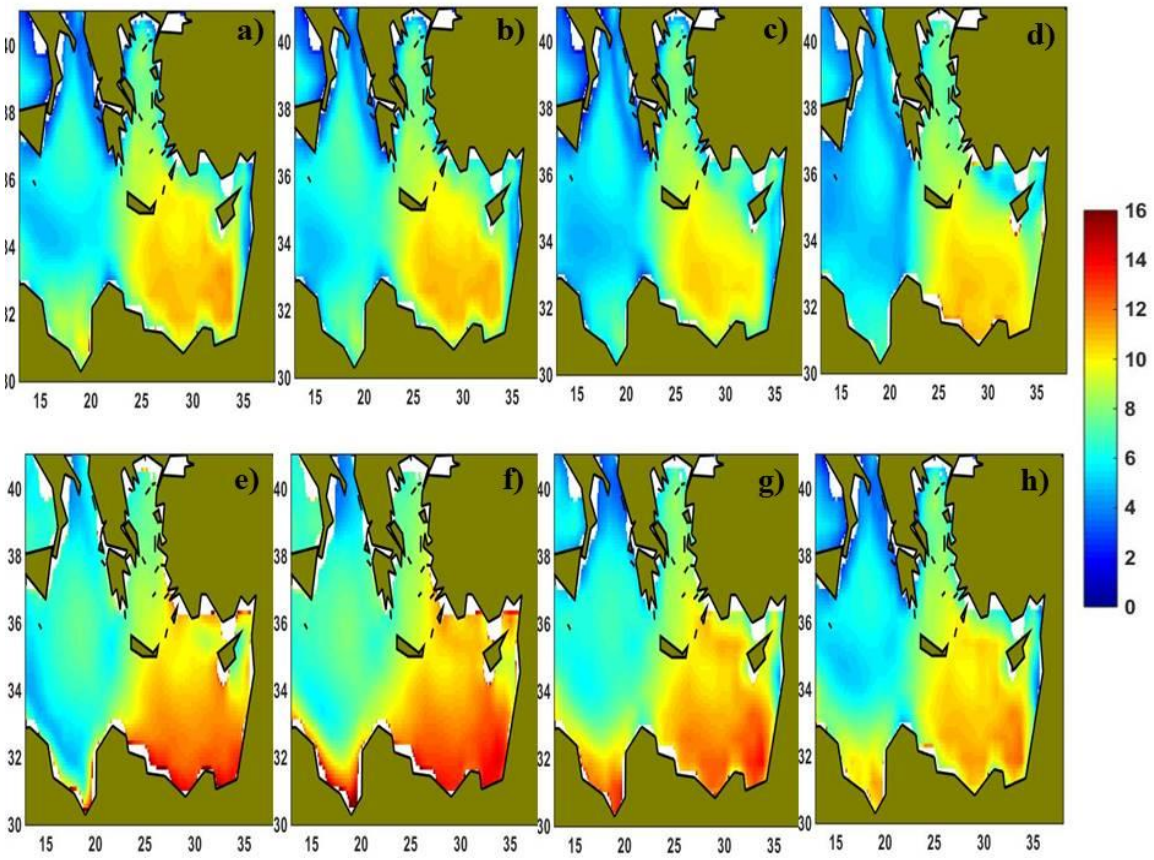

D. SEASONAL VARIATIONS IN ATMOSPHERIC FACTORS

In this section, seasonal and spatial variations in four atmospheric variables (ASTD, WS, *Dq*, *Rb*) are analyzed in order to understand the cause of the variabilities in EDH and EDS that were discussed in Sections A, B, and C.

1. Air-Sea Temperature Difference (ASTD)

Seasonal means of ASTD throughout the Eastern Mediterranean Sea are seen in Figures 22a, 22b, 22c, and 22d.

Figure 22. 1990–2015 Seasonal Means of ASTD in K for a) Winter, b) Spring, c) Summer, and d) Fall.

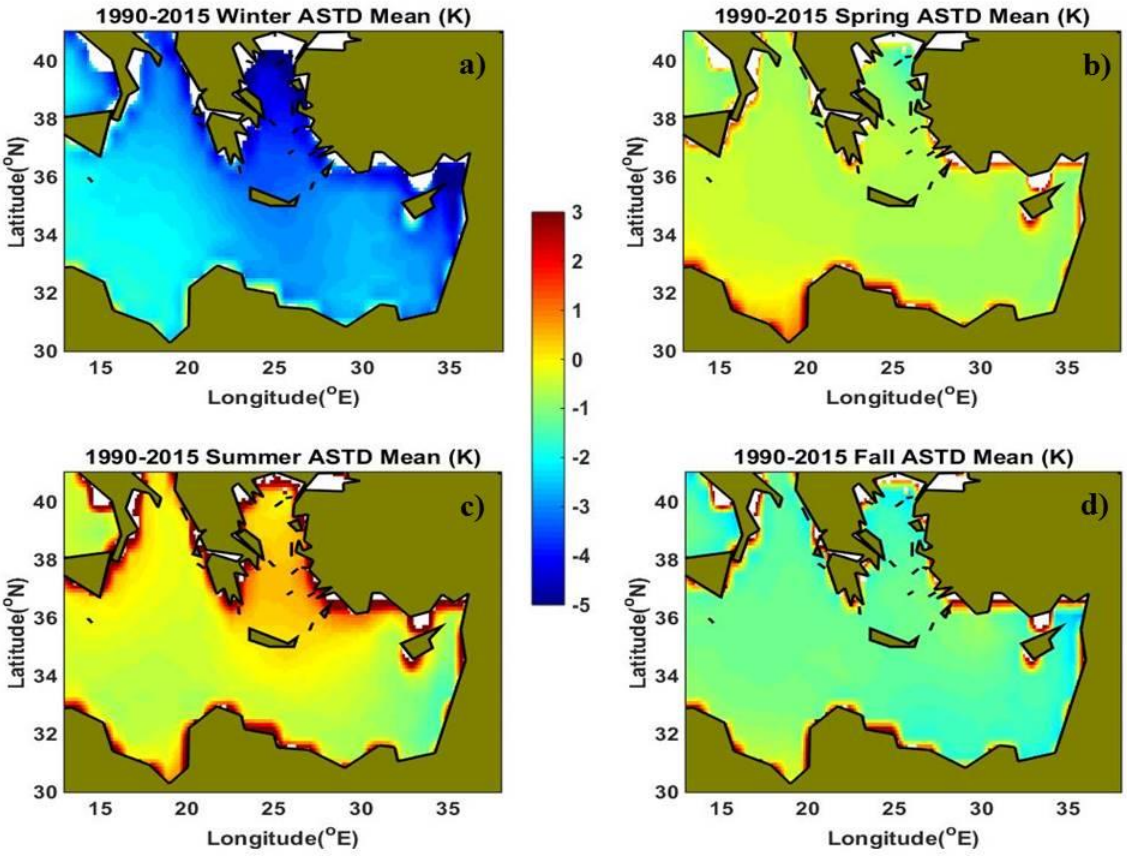

Figure 22 shows that ASTD is mostly positive in the summer and almost exclusively negative in winter. ASTD in the spring and fall seasons is close to neutral, though slightly negative in the fall and slightly positive in the spring. The Aegean Sea (SA-1) and south of it (SA-2) have the highest ASTD in the summer and the lowest ASTD in the winter, suggesting strongly stable and unstable thermal stability in the spring and fall seasons, respectively.

In comparing with the EDH seasonal variabilities in Figure 12 with those of the ASTD in Figure 22, we found the high EDHs often occur in the region with the strongest thermal stratification in the summer of Aegean Sea (SA-1). In all other seasons or regions, EDHs are in general rather low, with a magnitude of less than 8 m, although ASTD varies over a large range between near neutral to strongly unstable. Figure 23a and

Figure 23b, respectively, show a direct comparison of the EDH and the ASTD in the SA-1 region in two extreme stability seasons (winter and summer).

Figure 23. Diurnal Variations of EDH (m) (left y axis) and ASTD (K) (right y axis) in SA-1 for a) Summer and b) Winter.

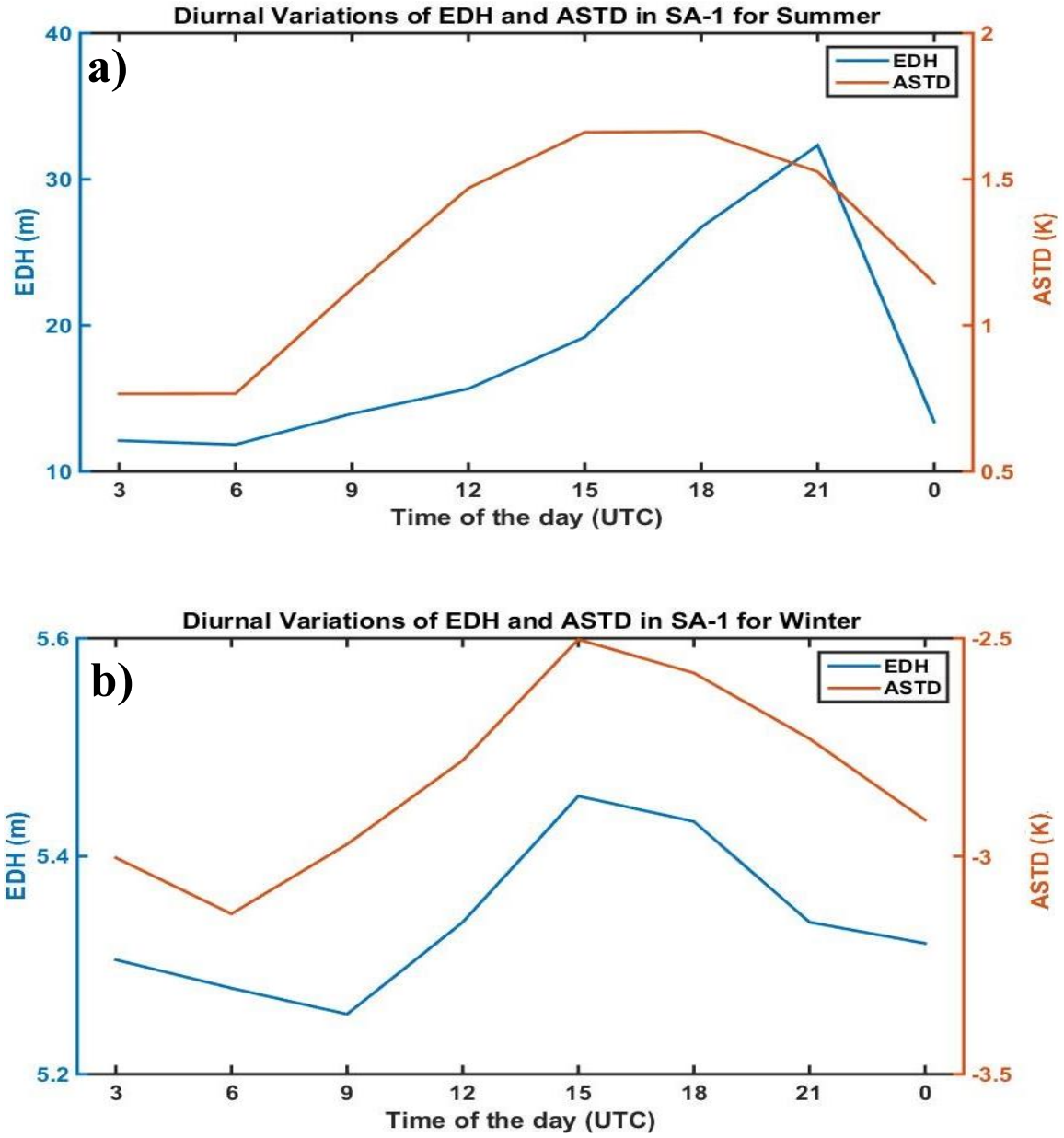

In Figure 23, EDH is shown in blue and ASTD is shown in red. The SA-1 region is in stable thermal stratification (positive ASTD) in the summer and unstable

stratification in the winter season (negative ASTD). We found that the trends of EDH and ASTD variation are loosely correlated in the summer, but strongly correlated in the winter. It should also be noted that EDHs are much higher in stable conditions than they are in unstable conditions.

2. Wind Speed (WS)

Seasonal means of 10 m height wind speeds and wind directions (white arrows) throughout the Eastern Mediterranean Sea are shown in Figures 24a, 24b, 24c, and 24d.

Figure 24. 1990–2015 Seasonal Means of Wind Speed in m/s for a) Winter, b) Spring, c) Summer, and d) Fall.

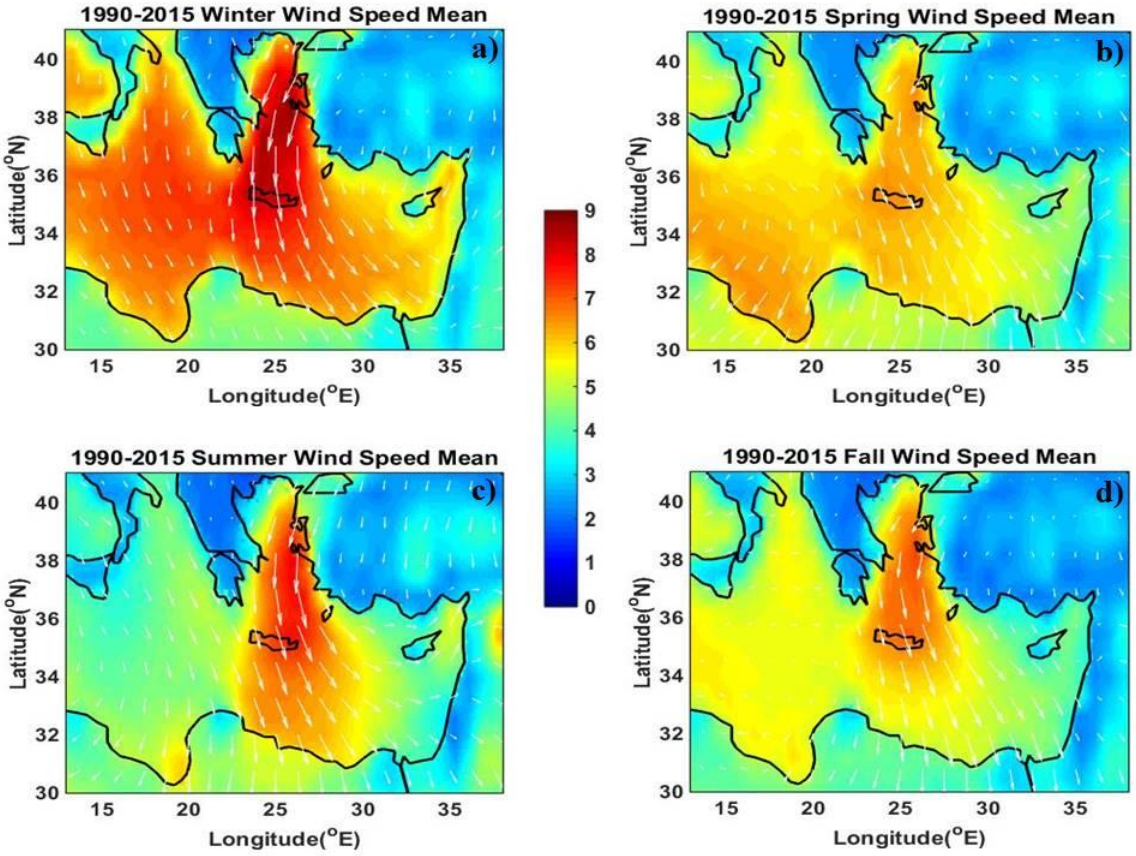

It can be seen from Figure 24 that winds are not very strong over the Eastern Mediterranean Sea, although wind speed is remarkably higher in the winter than it is in

other seasons. Wind speed is also higher over the Aegean Sea compared to other regions. Average wind speed in the winter is 8–9 m/s over the Aegean Sea and 6–7 m/s over the west part of the Eastern Mediterranean Sea.

Mean winds at 10 m height are mostly northerly and northwesterly throughout the year. Strong northerly winds bring cold air from land to the Mediterranean Sea in the winter, generating a strongly unstable surface layer as seen in the large magnitude of the negative ASTD in winter. Similarly, strong northerly winds over the Aegean Sea in the summer might contribute to high EDHs by bringing warm air from land (except at night when the air is colder over land than it is over the Aegean Sea) and decreasing SST (by creating mixing in the sea). Thus, this results in large and positive ASTD.

The correlation between diurnal variations of EDH and wind speed in SA-1 for the summer and winter are shown in Figure 25. In both seasons, the variation in wind speed and EDH are nearly out of phase, suggesting that low EDH in the case of higher wind is seen and vice versa. As seen in Figure 23a, the summertime ASTD in SA-1 reaches its maximum between 15 and 18 UTC; this is the period when the mean wind reaches its minimum (Figure 25a). Hence, this time period (15–18 UTC) has the weakest mechanical forcing and the maximum buoyancy consumption for turbulence kinetic energy. The EDH in this weak turbulence condition reaches its maximum of over 30 m. In the winter (Figure 25b), mean wind speeds are slightly higher than they are in the summer, with very similar diurnal variations. The largest difference is seen in EDH, which averages 5.4 m as compared to 11–30 m in the summer. Although there is still observable diurnal variation in both wind speed and EDH with apparent negative correlation, the magnitude of such variation is extremely small (less than 0.3 m for EDH and less than 0.2 m/s for wind speed).

Figure 25. Diurnal Variations of EDH (m) (left y axis) and Wind Speed (m/s) (right y axis) in SA-1 for a) Summer and b) Winter.

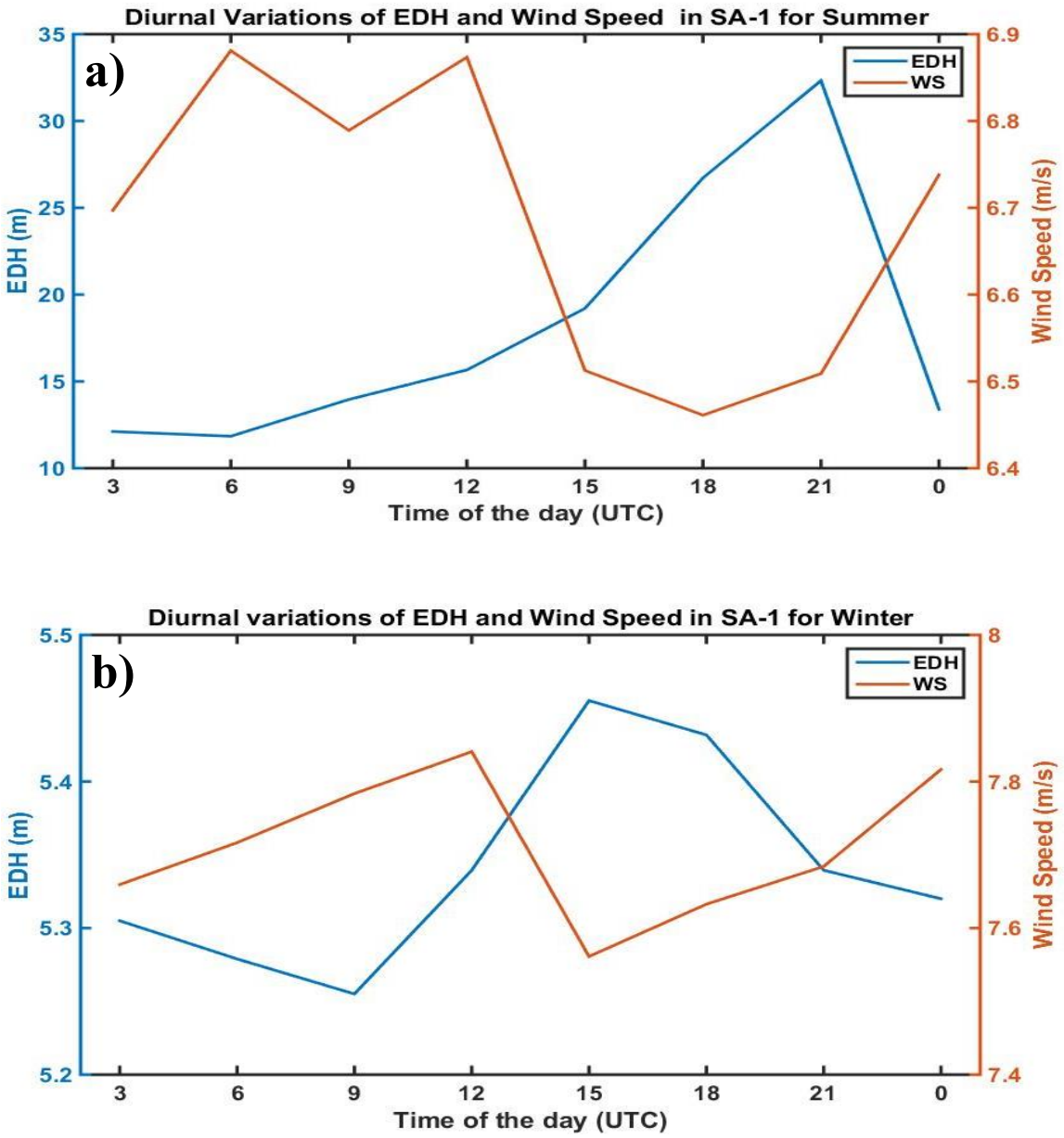

3. Specific Humidity Depression

Humidity variations in the surface layer are represented by specific humidity depression, which is the specific humidity difference between 2 m height and surface calculated using sea surface temperature and assuming 98 percent saturation. A large

surface layer moisture gradient should result in negative *Dq* with large magnitude. Seasonal variations of *Dq* throughout the Eastern Mediterranean Sea are depicted in Figure 26.

Figure 26. 1990–2015 Seasonal Means of *Dq* in g/kg for a) Winter, b) Spring, c) Summer, and d) Fall.

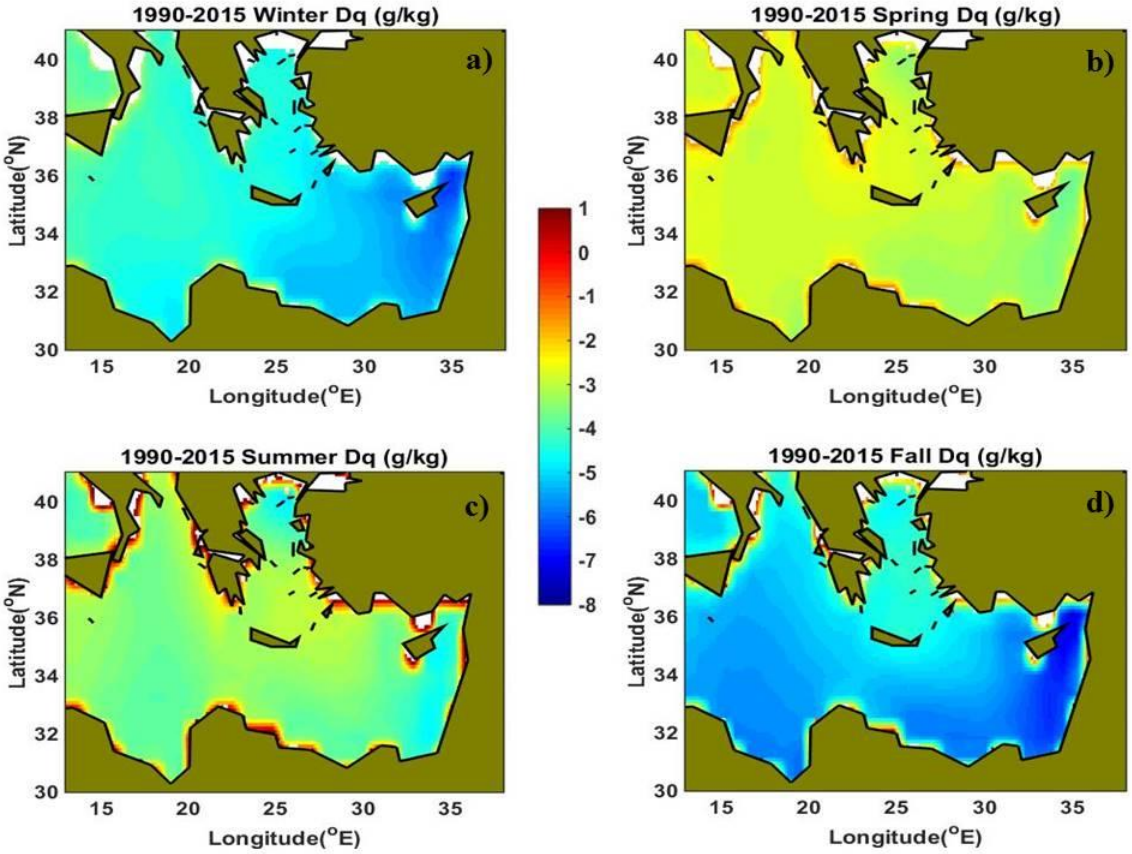

Figure 26 shows that *Dq* values are never positive throughout the Eastern Mediterranean Sea. That means the specific humidity at the sea surface is always higher than the specific humidity at 2 m height. The most negative specific humidity depression (-5 to -8 g/kg) occurs in fall. This shows that the largest vertical gradient occurs in fall. The smallest specific humidity depression occurs in spring, when the *Dq* is least negative. It is also noted that the difference between the east and west parts of the Eastern

Mediterranean is not significant. The sensitivity of EDH and EDS to specific humidity depression, together with other atmospheric factors, is analyzed in Section E.

4. Bulk Richardson Number

Seasonal variations of *Rb* throughout the Eastern Mediterranean Sea are depicted in Figures 27a, 27b, 27c, and 27d.

Figure 27. 1990-2015 Seasonal Means of *Rb* for
a) Winter, b) Spring, c) Summer, and d) Fall.

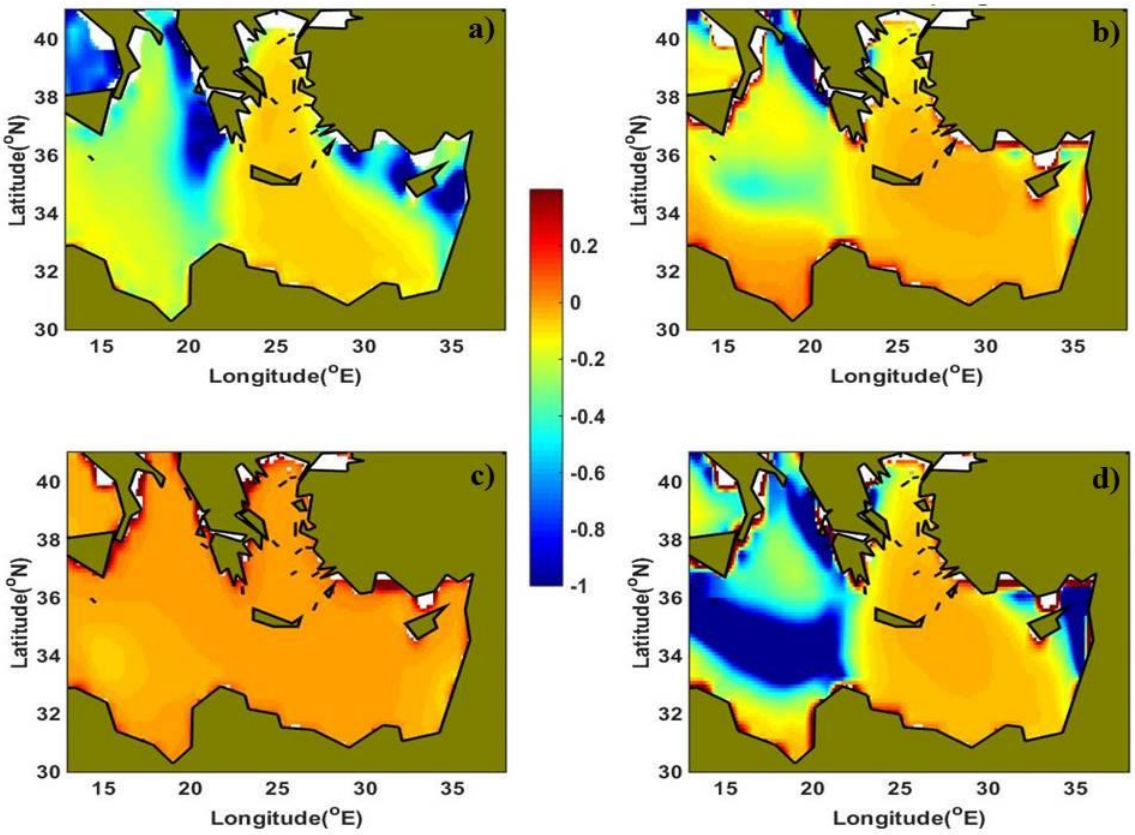

The bulk Richardson number represents the turbulent thermal and dynamic stability in the atmosphere, where a large positive *Rb* denotes strong dynamic stability, and in the high *Rb* cases, laminar flow. Meanwhile, positive *Rb* denotes stable thermal stability and negative *Rb* denotes unstable thermal stability. In the case of strong winds,

the boundary layer tends to experience small magnitude of *Rb*, a condition close to neutral stratification. This is the case shown in Figure 27 where the regions of relative strong wind speed tend to have small magnitude of *Rb* (light orange-yellow color). The summer months over the Eastern Mediterranean Sea have a stable surface layer corresponding to the largest EDHs. Turbulent stability is lowest over some part of the northern Eastern Mediterranean Sea in the winter and to the west in the fall. These regions are generally weak in wind speed, and the turbulence mixing is mainly caused by positive buoyancy force. It should also be noted that the spatial distribution of *Rb* is similar to the spatial distribution of EDS in the fall. EDSs in the fall over the west part of the Eastern Mediterranean Sea, where there is buoyancy generated turbulence, are lower than the EDSs over the east part. The dependence of EDH and EDS on wind speed and humidity depression under different stability conditions is analyzed further in Section E.

E. THE SENSITIVITY OF EDH AND EDS TO ATMOSPHERIC FACTORS

To assess the sensitivity of EDH and EDS to atmospheric factors, EDH and EDS were plotted and analyzed under different turbulence stability (represented by *Rb*), specific humidity (represented by *Dq*), and wind conditions. Summer means of EDH in SA-1 were analyzed separately in order to better understand cases with extremely high EDHs.

1. Sensitivity of EDH to Atmospheric Factors

Figure 28 shows mean EDH as a function of the bulk Richardson number and specific humidity depression from all seasons between 1990 and 2015 in regions consisting of SA-2, SA-3, SA-4, and SA-5 for all wind conditions. As seen in Figure 28, the unstable surface layer (Rb < 0) shows a clear relationship of EDH relative to Rb and Dq. Here, EDH increases with greater magnitude of Dq at a given Rb, suggesting that a dryer atmospheric surface layer relative to the surface tends to result in deeper EDH. For any given Dq value, we also find that the EDH increases rapidly as Rb decreases in magnitude towards neutral conditions when Rb is close to 0. However, in the very unstable conditions (Rb less than -0.2), the dependence of EDH on Rb is weaker and EDH is mostly dependent on Dq. When Rb is between -0.2 and -0.05, EDH is sensitive to both Rb and Dq.

Figure 28. 1990–2015 EDH Means in SA-2, SA-3, SA-4, and SA-5 (Color Bar in m) as a Function of the Bulk Richardson Number and Specific Humidity Depression (g/kg) for all Wind Conditions and All Seasons.

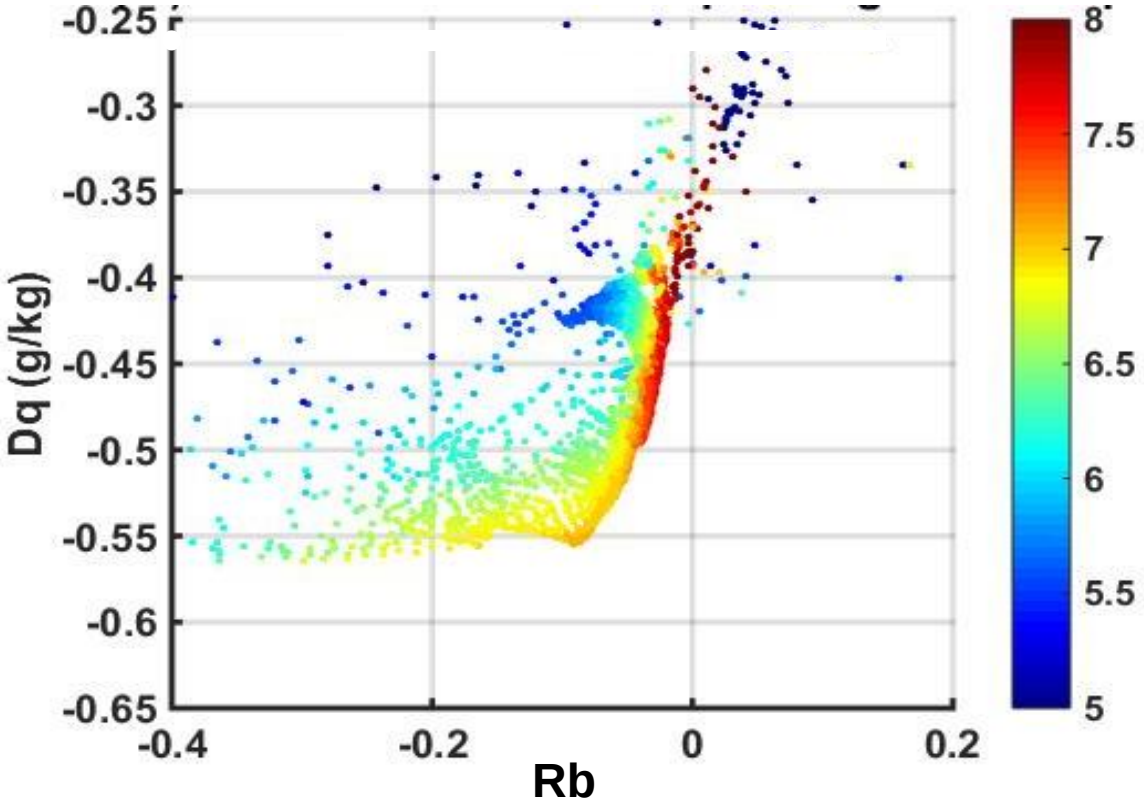

The conditions when *Rb* is between -0.05 and 0 are the near neutral and unstable. In these conditions, EDH is extremely dependent on the bulk Richardson number and increases as stability increases towards the neutral condition. The maximum EDH occurs when *Rb* is between -0.05 and 0 and *Dq* is between -0.5 and -0.4, indicated by the red colored symbols. It should be noted that in unstable thermal conditions, maximum EDHs do not occur when the specific humidity gradient is strongest (most negative *Dq* values). In stable conditions (*Rb* > 0), the relationship of EDH with *Rb* and *Dq* is not apparent. And, the EDHs are either very large (dark red) or very small (dark blue). More stable cases are needed to allow clear identification of the relationship.

Wind speed also has an important effect on EDH, since it determines dynamic mixing. For this reason, it also needs to be analyzed to ensure a better understanding of

atmospheric effects on EDH. Figure 29 shows the same results as in Figure 28, except they are grouped by different ranges of wind speed. The wind speed in the Mediterranean region is generally low and the variation of the wind speed is also small. Hence, there are only two categories of wind speed ranges: low wind (3–6 m/s) and moderate wind (6–9 m/s).

Figure 29. Comparison of Results from Figure 28 Grouped by Wind Speeds for a) 3 to 6 m/s and b) 6 to 9 m/s.

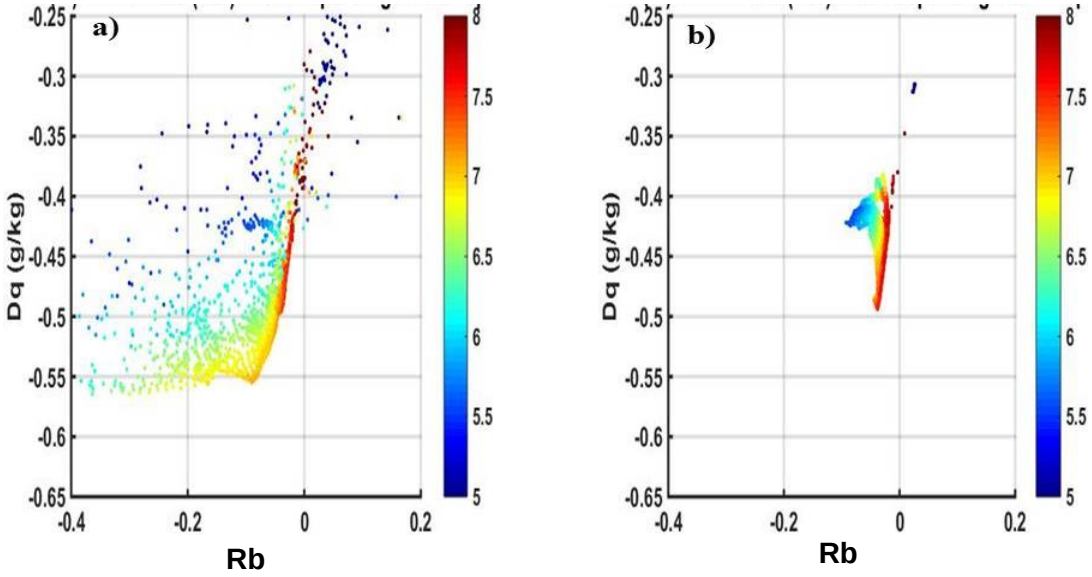

As seen in Figure 29, wind speeds are between 3 and 9 m/s. Turbulent stability is higher (indicated by greater *Rb* values) when wind speed is higher since wind speed is in the denominator of the *Rb* equation. Additionally, variability in *Dq* is also reduced in higher wind conditions than it is in lower wind conditions.

In lower wind conditions (Figure 29a), *Dq* and *Rb* vary over a relatively wide range. The general variation of EDH follows that of Figure 28. Figure 29b shows that moderate wind conditions often see a very narrow range of *Dq* and *Rb*. On the unstable side, *Dq* varies -0.38 and -0.5 g/kg. There are only a few cases of moderate wind in stable conditions to allow any meaningful discussions. The bulk Richardson number in Figure 29b also shows the near neutral stability that is consistent with stronger mechanical forcing. When the specific humidity depression has a magnitude larger than 0.44 g/kg,

EDH variation is very small, between 7 m and 8 m. For the relatively dry surface layer, EDH becomes very sensitive to small changes in the bulk Richardson number and shows nearly no sensitivity to *Dq*.

Figure 30. 1990–2015 Summer EDH Means in SA-1 (Color Bar in m) as a Function of Bulk Richardson Number and Specific Humidity Depression (g/kg) for all Wind Conditions.

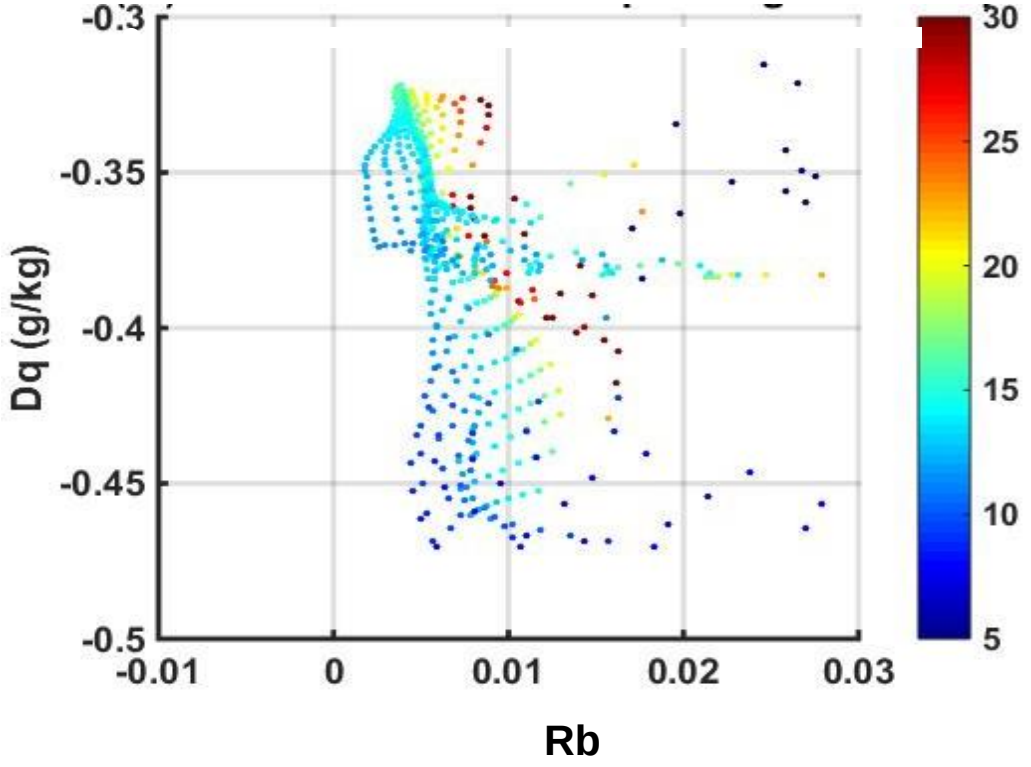

Since maximum EDHs occur in the summer in the Aegean Sea (SA-1), special emphasis is put on this case in order to better understand the effects of atmospheric factors on EDH. Figure 30 shows the same plot as Figure 28 for the SA-1 region and the summer seasons.

When we compare the values of Dq and *Rb* in Figure 30 with those in Figure 28, we see that the *Rb* values are higher in summer, indicating more stability. We also see that specific humidity depression values are lower in the summer compared to the means of all seasons. Most of the *Dq* values are between -0.35 and -0.45 in summer, while they

are between -0.45 and -0.55 in the means for all seasons. Less specific humidity depression (between surface and 2 m height) in the summer is an expected result because of the small ASTD seen in Figure 22.

As seen from Figure 30, EDHs change extremely with small changes in *Rb* and *Dq*. EDHs tend to be higher at smaller magnitudes of specific humidity depressions (less negative *Dq* values) for a given *Rb*. EDHs also tend to be higher in higher stability conditions (increasing *Rb* values) at a given *Dq*. Sensitivity of EDH to stability is greater at lower *Dq* values in most cases. Maximum sensitivity occurs when *Dq* is between -0.32 and -0.35, where we also see maximum EDHs.

Figure 31 was created to analyze wind effects on EDH in the summer. As seen in the figure, EDHs are higher at higher wind speeds (6–9 m/s). Although *Rb* values at higher wind speeds are close to those at lower wind speeds, the sensitivity of EDH to *Rb* is remarkably higher at higher wind speeds.

Figure 31. Comparison of Results from Figure 30 Grouped by Wind Speeds for a) 3 to 6 m/s and b) 6 to 9 m/s.

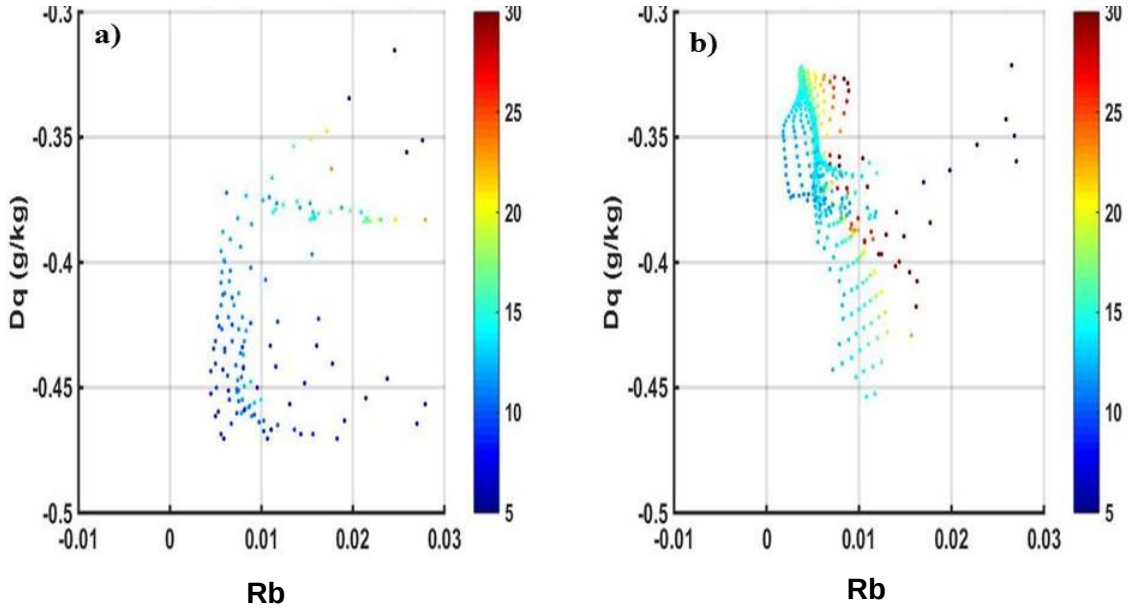

In summary, the stable stratification and small specific humidity depression in the summer (compared to the mean values of all seasons) are the most important factors that cause greater EDHs. The effects of these factors are stronger at higher wind speeds. The sensitivity of EDH to these factors is affected by many other factors and should be analyzed carefully.

2. Sensitivity of EDS to Atmospheric Factors

EDS was also analyzed to understand its sensitivity to turbulence stability (*Rb*), specific humidity depression (*Dq*), and wind speed. Figure 32 shows the mean EDSs in SA-2, SA-3, SA-4, and SA-5 for all seasons.

The behavior of EDS under different *Rb* and *Dq* conditions is very similar to the behavior of EDH under these conditions. EDS is very sensitive to stability under slightly unstable conditions ($-0.15 < Rb < 0$), and the EDH increases with increasing *Rb* toward neutral stability. The sensitivity of EDS to specific humidity depression is very small under slightly unstable conditions. Under less stable conditions ($Rb < -0.15$), EDS is more sensitive to specific humidity depression than it is to turbulence dynamic stability, where EDS increases with increasing *Dq*.

Another point to note is that maximum EDS occurs in a slightly unstable regime ($-0.15 < Rb < 0$) and under the highest specific humidity depression conditions, when *Dq* is between -0.55 and -0.45. This is different from the maximum EDH case in that the maximum EDH occurs in moderate values of the specific humidity depression (below the maximum *Dq).* Similar to EDH, a high stability and low specific humidity gradient (upper right part of the plot where *Rb* is greater than 0 and *Dq* is between -0.32 and -0.25) leads to minimum EDS as indicated by the dark blue symbols in the plot.

Figure 32. Mean EDSs from SA-2, SA-3, SA-4, and SA-5 Averaged between 1990-2015 as a Function of Bulk Richardson Number and Specific Humidity Depression (g/kg) for all Wind Conditions and All Seasons.

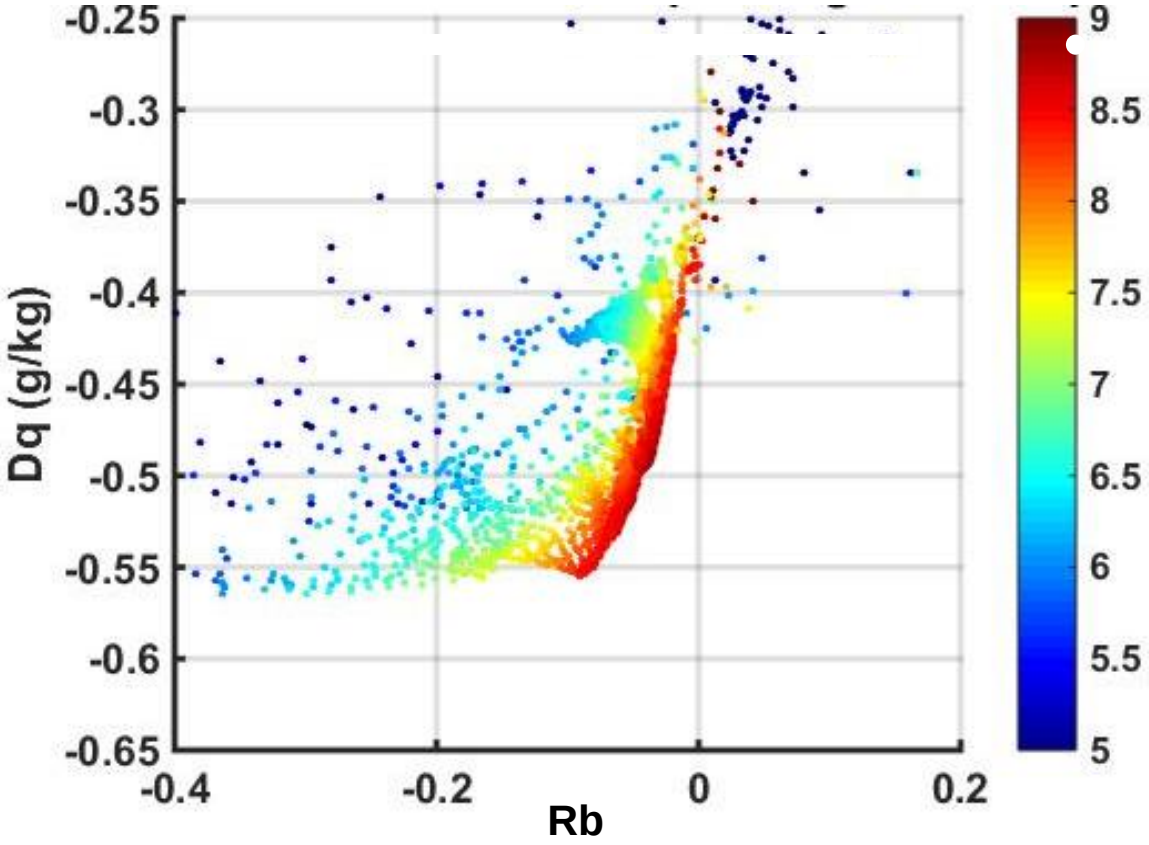

Figure 33 shows EDS values under low (3 to 6 m/s) and moderate (6 to 9 m/s) wind speed conditions to assess the effects of wind speed on EDS. Such effects are found to be very similar to the effects of wind speeds on EDH.

Figure 33. Same as Figure 32 Except for Wind Speeds between a) 3 to 6 m/s and b) 6 to 9 m/s.

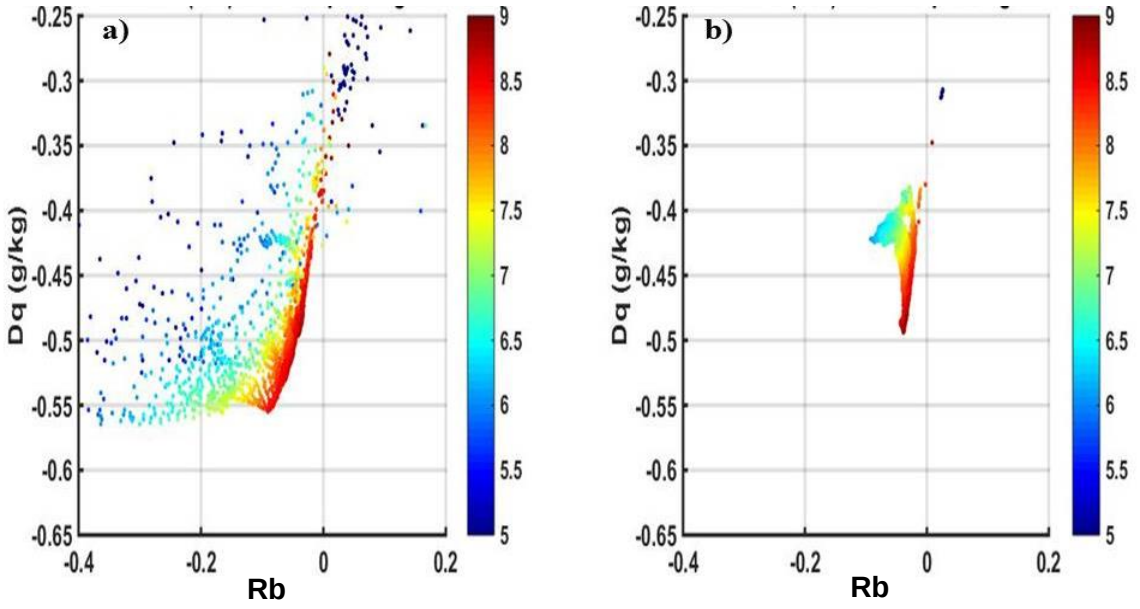

In summary, EDSs and EDHs increase with increasing magnitude of *Dq* (at a given *Rb*) under both low and moderate wind conditions. But the sensitivity of EDS to *Dq* in lower wind conditions is much stronger than it is in higher wind conditions.

The sensitivity of EDS to stability is also different in different stability conditions. EDS is highly sensitive to the bulk Richardson number when *Rb* values are between -0.1 and 0. Since stability is closer to neutral in higher wind conditions, it is a more important factor for EDS than specific humidity depression in moderate wind conditions.

THIS PAGE INTENTIONALLY LEFT BLANK

V. CONCLUSIONS AND RECOMMENDATIONS

A. CONCLUSIONS

Understanding and exploiting atmospheric effects on EM propagation are very important for the efficiency and success of systems and sensors in the EM spectrum. For EM frequencies, the atmospheric refractive effects significantly affect EM propagation by bending and attenuating the EM energy in the atmosphere.

In this study, I chose to study evaporation ducts to address atmospheric effects on EM propagation for three reasons. First, evaporation ducts are present over the oceans most of the time. They are the most frequently occurring EM ducts in the atmosphere. Second, since they occur in the surface layer, they have important effects on the EM systems and sensors on naval ships. Last, they are very sensitive to changes in the lower atmosphere and the surface. Small changes in humidity, temperature, and pressure can cause important variations in evaporation ducts, and those variations can have significant effects on EM propagation conditions. For this reason, we should analyze evaporation ducts precisely in order to fully understand and operationally exploit them.

This study utilized ECMWF surface reanalysis data from 1990 to 2015 and from the COARE evaporation duct model to calculate 3-hour EDHs and EDSs in the Eastern Mediterranean Sea. These calculations enabled us to examine spatial, diurnal, and seasonal variations of evaporative ducts in the region. After presenting the long term means and variations in the EDH and EDS, we analyzed their sensitivity to atmospheric factors (specific humidity depression, Bulk Richardson number, wind speed, and air-sea temperature difference) to assess and characterize the effects of those factors on EDH and EDS.

It was found that EDHs were highest in the summer and between 12 and 15 UTC. It was also found that spatial and diurnal variations of EDH were remarkably stronger in summer. The highest EDHs occurred in the Aegean Sea in the summer, with a mean EDH of about 18 m, whereas the highest EDHs were between 6 and 8 m in other parts of

the Eastern Mediterranean Sea. The identification of the extremely high summer mean of EDH in the Aegean Sea is one of the most important results of this study.

It was also discovered that EDSs were highest in the fall and between 12 and 15 UTC. Spatial and diurnal variations of EDS were strongest in the fall. In other seasons, they were not so important as to have operationally significant impacts on EM propagation. The peak EDS (about 11 M units) occurred in the east part of the Eastern Mediterranean Sea in the fall.

In some cases, EDH was not defined. Those cases showed up as white regions on the maps and were not taken into account in the calculations. They occurred in stable regions where air-sea temperature difference is positive and in low wind conditions. Those conditions occurred most commonly in the summer, especially in the coastal Aegean Sea and other coastal regions surrounding the studied area. Under those conditions, the COARE evaporation duct model did not result in a vertical M profile from which EDH and EDS below 50 m can be defined.

Different sets of atmospheric variables were considered to represent the atmospheric effects on EDH and EDS. After some initial testing, it was decided that bulk Richardson number (representing turbulence stability) and specific humidity depression are the atmospheric factors that best represent those effects (Cherrett 2015). The correlation between those factors and EDH and EDS were consistent and provided us with insightful sensitivity analyses.

In sensitivity analyses, it was found that EDH is very sensitive to stability in slightly unstable cases when *Rb* is between -0.05 and 0 and increases with increasing stability. In lower stability cases (when *Rb* is smaller than -0.05), EDH is more sensitive to the specific humidity gradient rather than stability and increases with an increasing specific humidity gradient (with greater magnitudes of *Dq*). Sensitivity analyses of EDS also showed very similar results.

Sensitivity analyses of EDH and EDS were also conducted in different wind conditions to assess the sensitivity of EDH and EDS to wind speed. Those analyses revealed that the sensitivity of EDH and EDS to stability is higher in moderate wind

conditions. The specific humidity gradient effect on EDH and EDS was very limited in the moderate wind category. This result is consistent with stronger wind resulting in a smaller bulk Richardson number, where EDH and EDS show larger sensitivities to *Rb*.

EDH and EDS should be examined correctly in order to predict and exploit trapping effects of evaporation ducts. As stated in Chapter II, the maximum wavelength that can be trapped by ducts is proportional to EDH and the square root of EDS. In this regard, evaporation ducts in the Eastern Mediterranean Sea can trap EM waves between frequencies of 3,000 MHz and 30,000 MHz (from Equation (4) and Table 2). But these frequency limits are not hard boundaries, and frequencies slightly above and below these limits can also be trapped.

When EM waves are trapped by evaporation ducts, they can propagate to longer distances. This might increase detection ranges of surface radars for low flyers compared to cases with no ducts. Additionally, ducting can also lead to enhanced detection capabilities by causing increased signal strength resulting from higher intensity of EM waves within the duct. However, increased signal strength might also increase clutter, which degrades systems and sensors performance. For this reason, operators should be careful and tune the sensitivity of systems and sensors to compensate for this possible clutter effect of evaporation ducts.

B. RECOMMENDATIONS FOR FUTURE WORK

Although some useful results were obtained in this study, there are ways these results can be evaluated and improved. ECMWF surface reanalysis data were used with horizontal resolution of 0.125º x 0.125º for the purposes of this study. My results can be improved with higher horizontal resolution reanalysis data. This will be useful to improve the accuracy of this study, especially in the areas close to shore. Additionally, it will be useful to validate the reanalysis data using observational data or data from forecast models.

In addition to improvement and testing of the input data, future research could assess the COARE evaporation duct model using an alternative evaporation duct model. This additional work would provide an insight into the uncertainties of our results due to

model deficiencies. More importantly, a thorough evaluation of the evaporation duct model using in situ observations is much needed, especially to improve the area where the models have difficulties. One such difficulty area is the stable stratification and light wind conditions. We were not able to obtain EDH and EDS in these conditions, especially near the coast. It is not clear whether this is the case or it is a result of model problems.

EDH is a very useful parameter to represent atmospheric effects on EM propagation in the surface layer. But surface ducts and elevated ducts might also have considerable impact on propagation conditions in the surface layer and above. For this reason, including other types of ducts in future studies will help not only to obtain results that are more accurate for the surface layer, but also assess propagation conditions above the surface layer. Furthermore, future studies might also benefit from atmospheric propagation prediction models (e.g., the Advanced Refractive Effects Prediction System, AREPS) to acquire more precise and operationally useful predictions on the propagation conditions.

APPENDIX. PLOTS OF MONTHLY MEANS OF EDH AND EDS VALUES

Figure 34. 1990–2015 January Mean of a) EDH (m) and b) EDS.

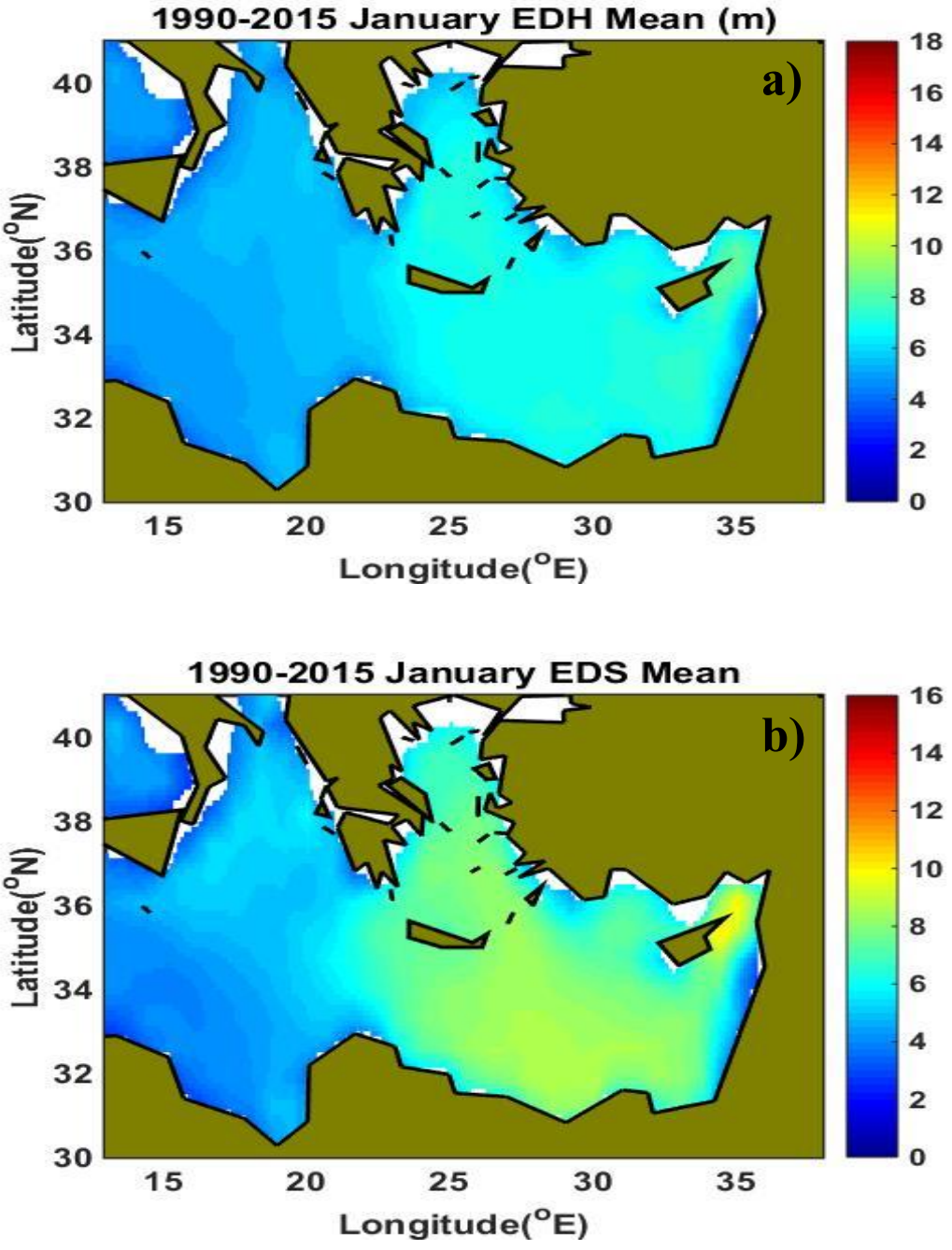

Figure 35. 1990–2015 February Mean of a) EDH (m) and b) EDS.

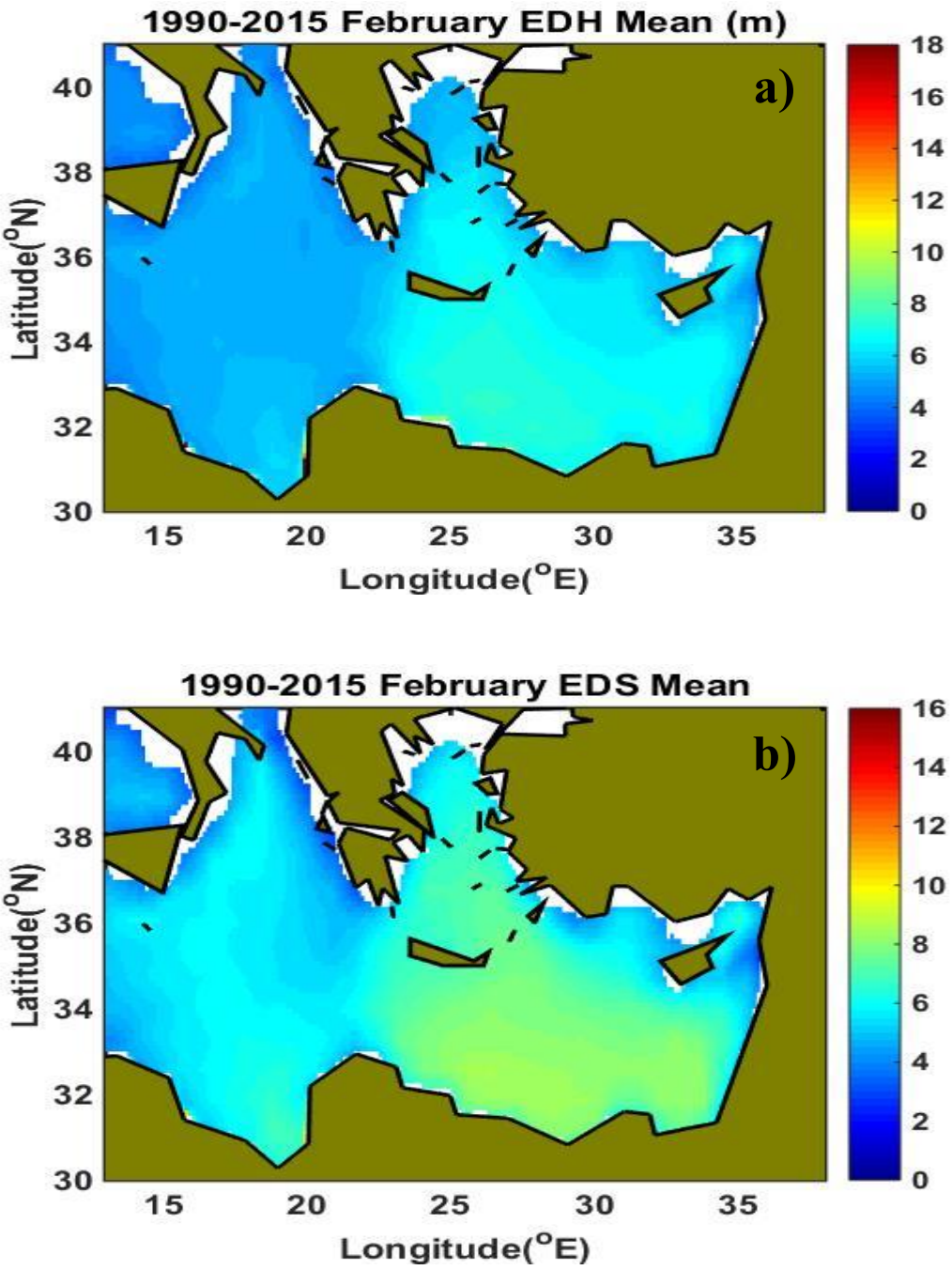

Figure 36. 1990–2015 March Mean of a) EDH (m) and b) EDS.

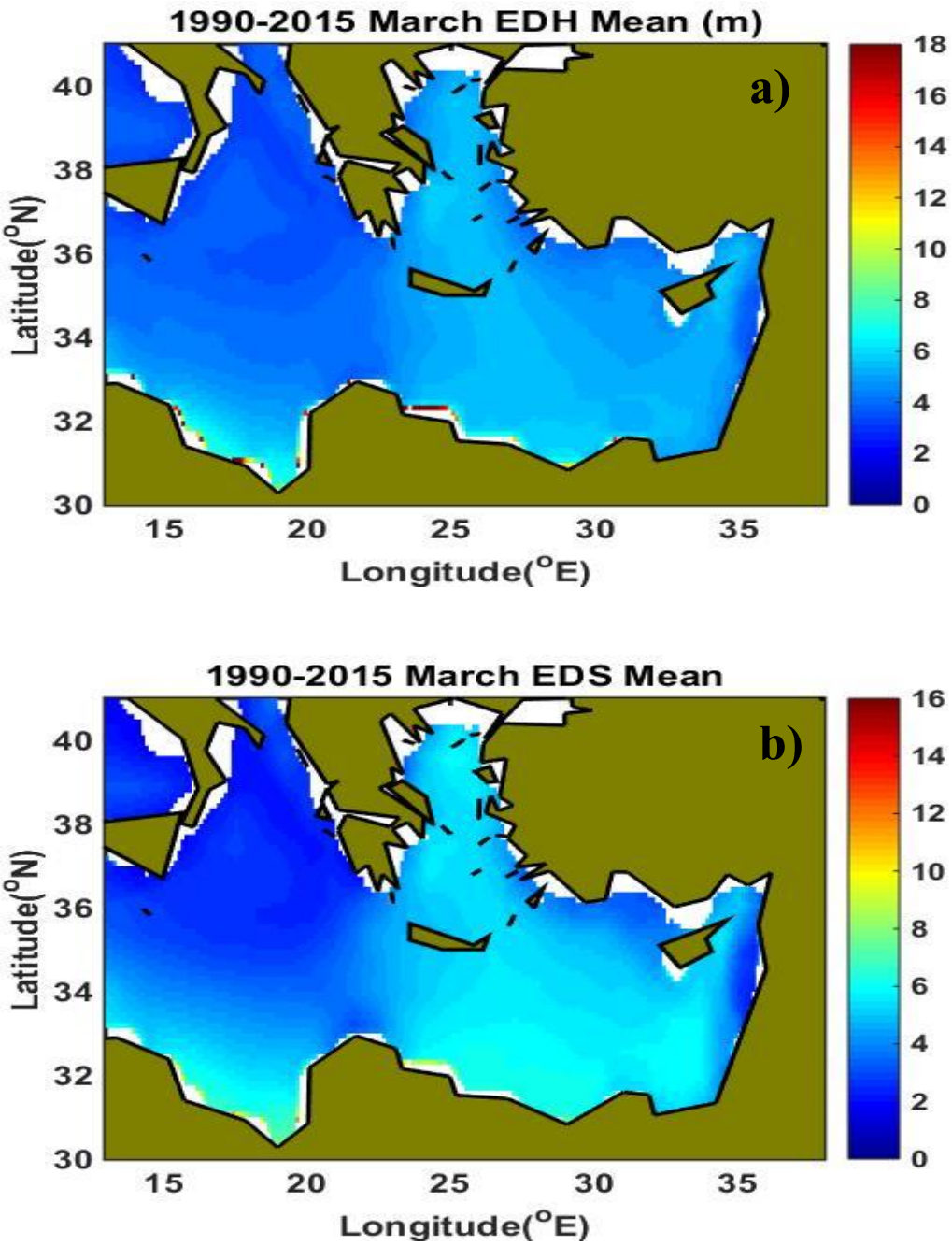

Figure 37. 1990–2015 April Mean of a) EDH (m) and b) EDS.

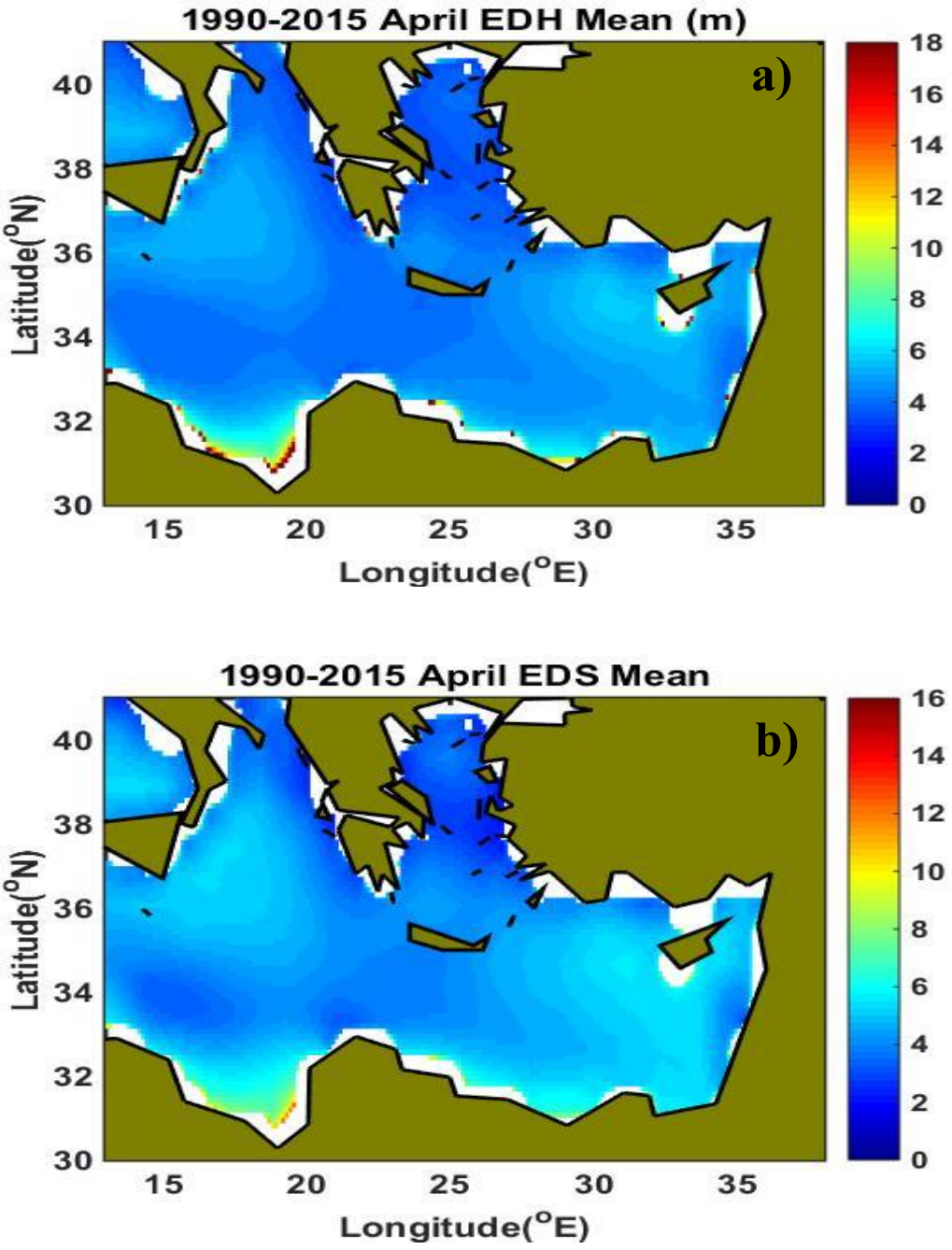

Figure 38. 1990–2015 May Mean of a) EDH (m) and b) EDS.

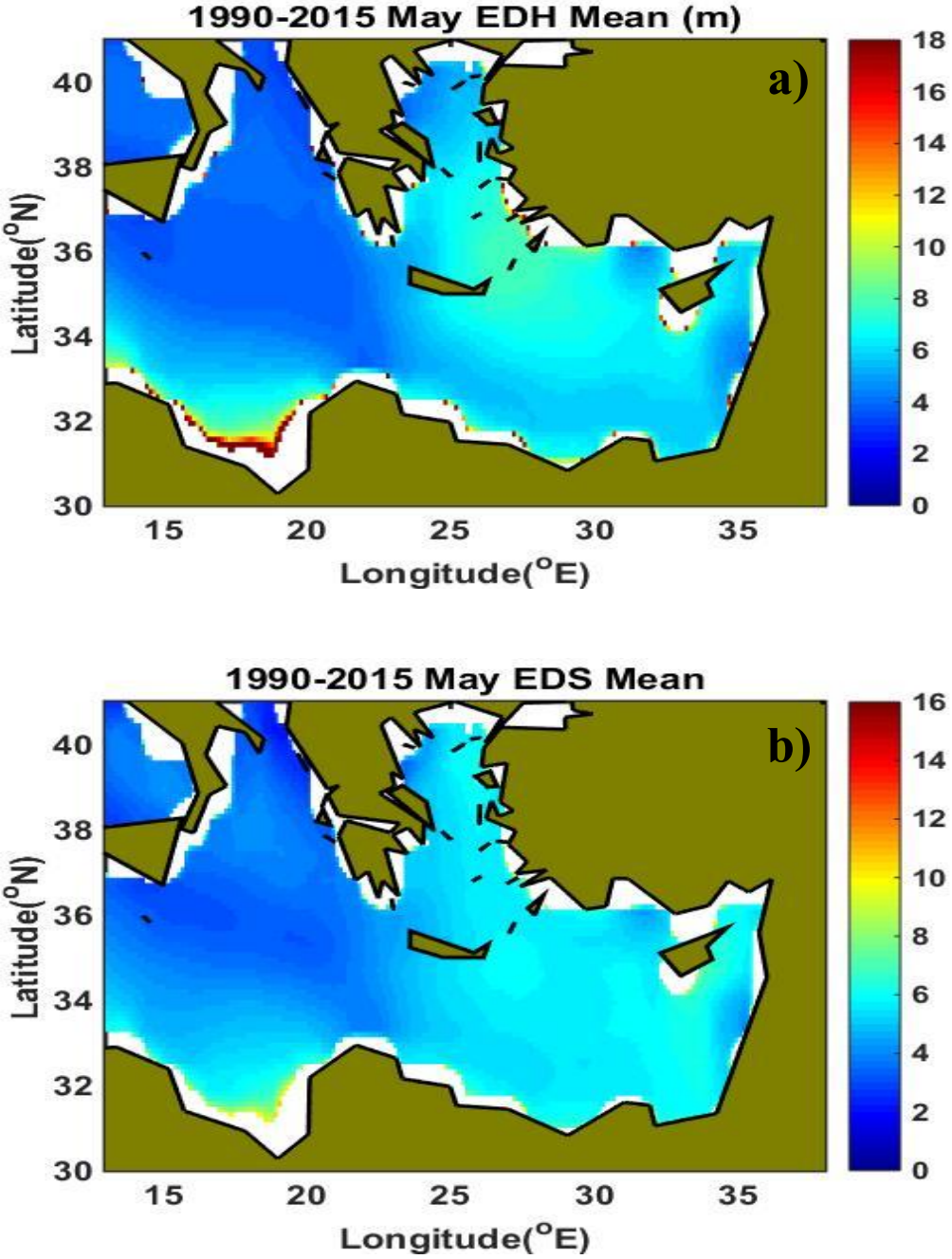

Figure 39. 1990–2015 June Mean of a) EDH (m) and b) EDS.

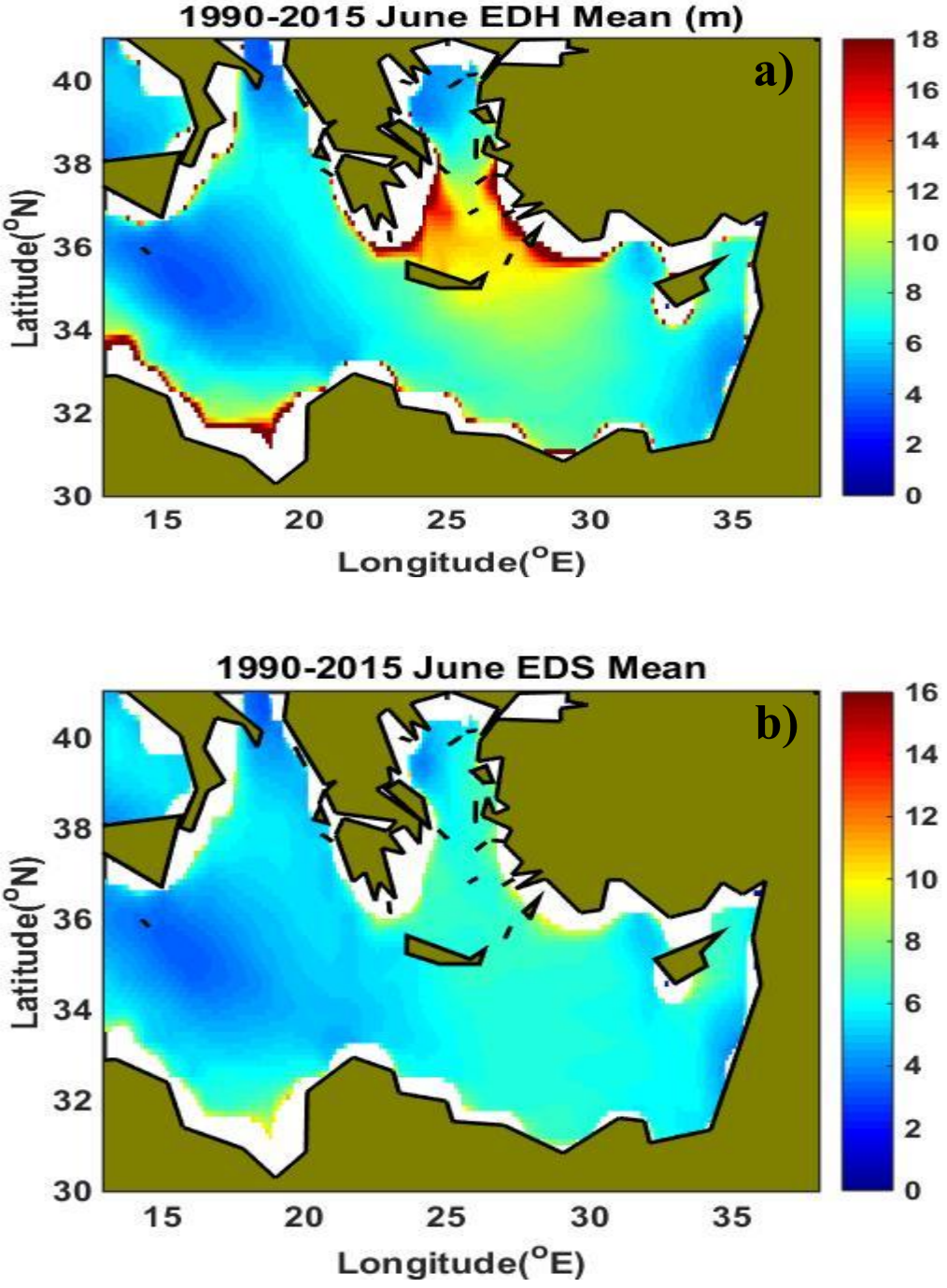

Figure 40. 1990–2015 July Mean of a) EDH (m) and b) EDS.

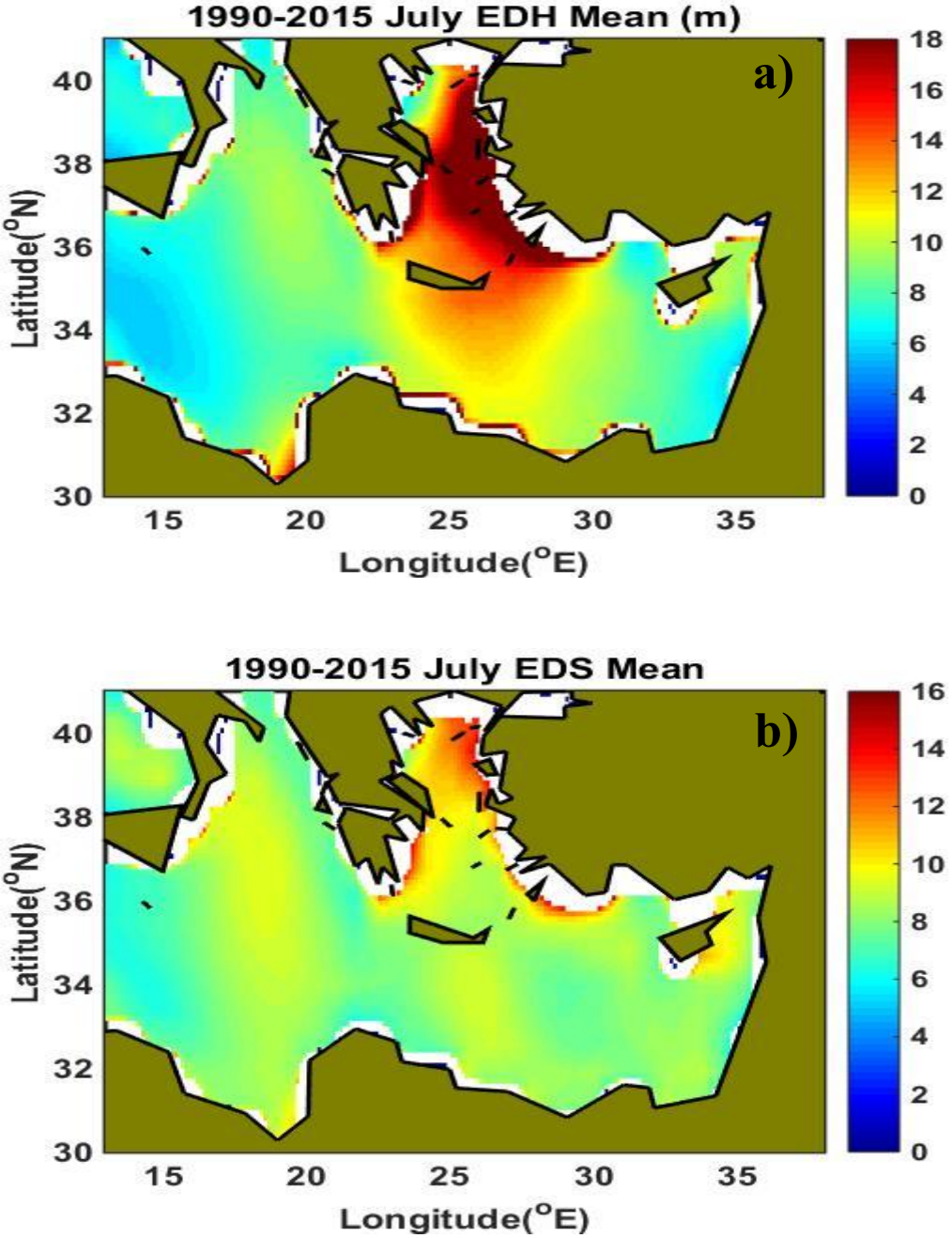

Figure 41. 1990–2015 August Mean of a) EDH (m) and b) EDS.

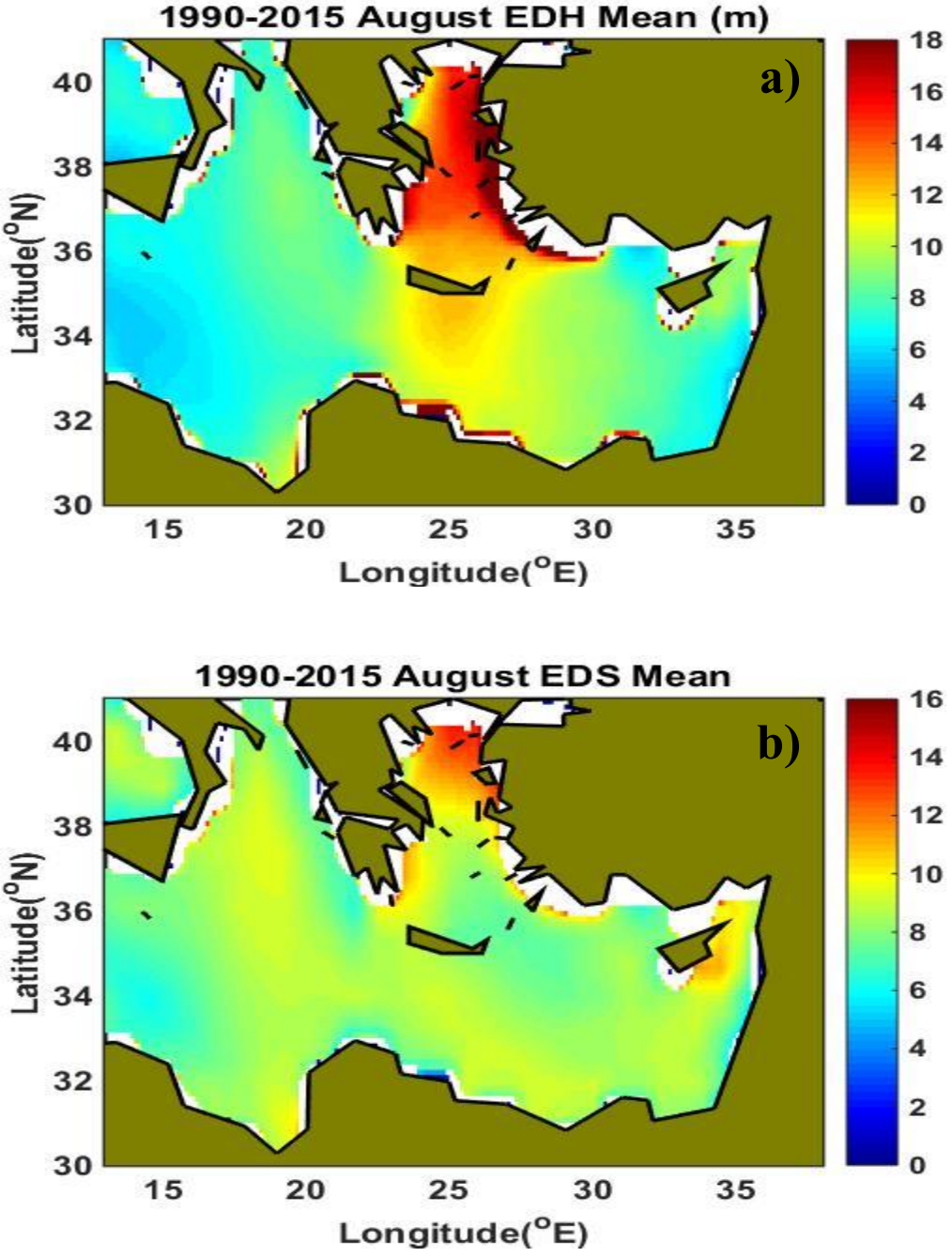

Figure 42. 1990–2015 September Mean of a) EDH (m) and b) EDS.

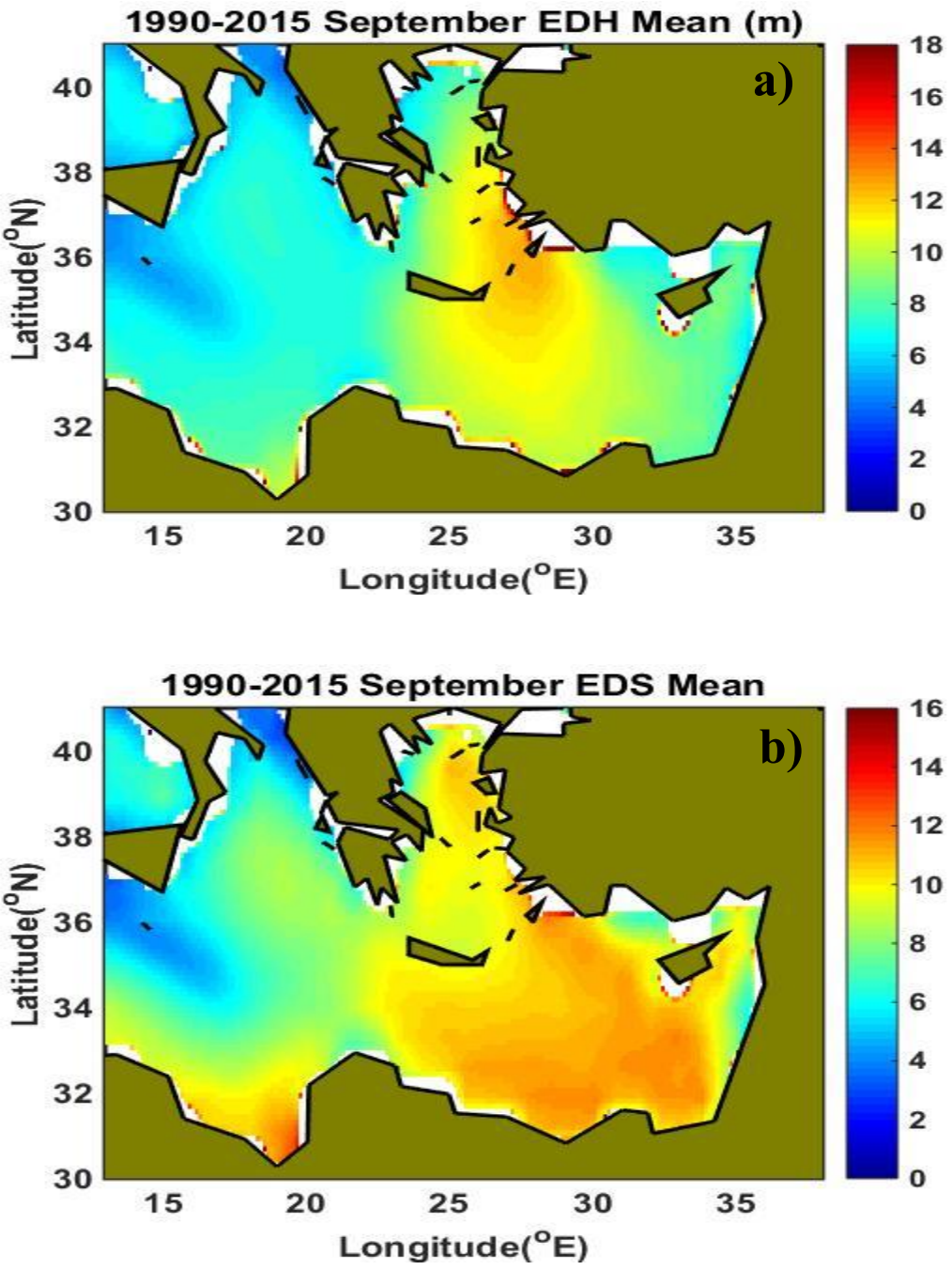

\

Figure 43. 1990–2015 October Mean of a) EDH (m) and b) EDS.

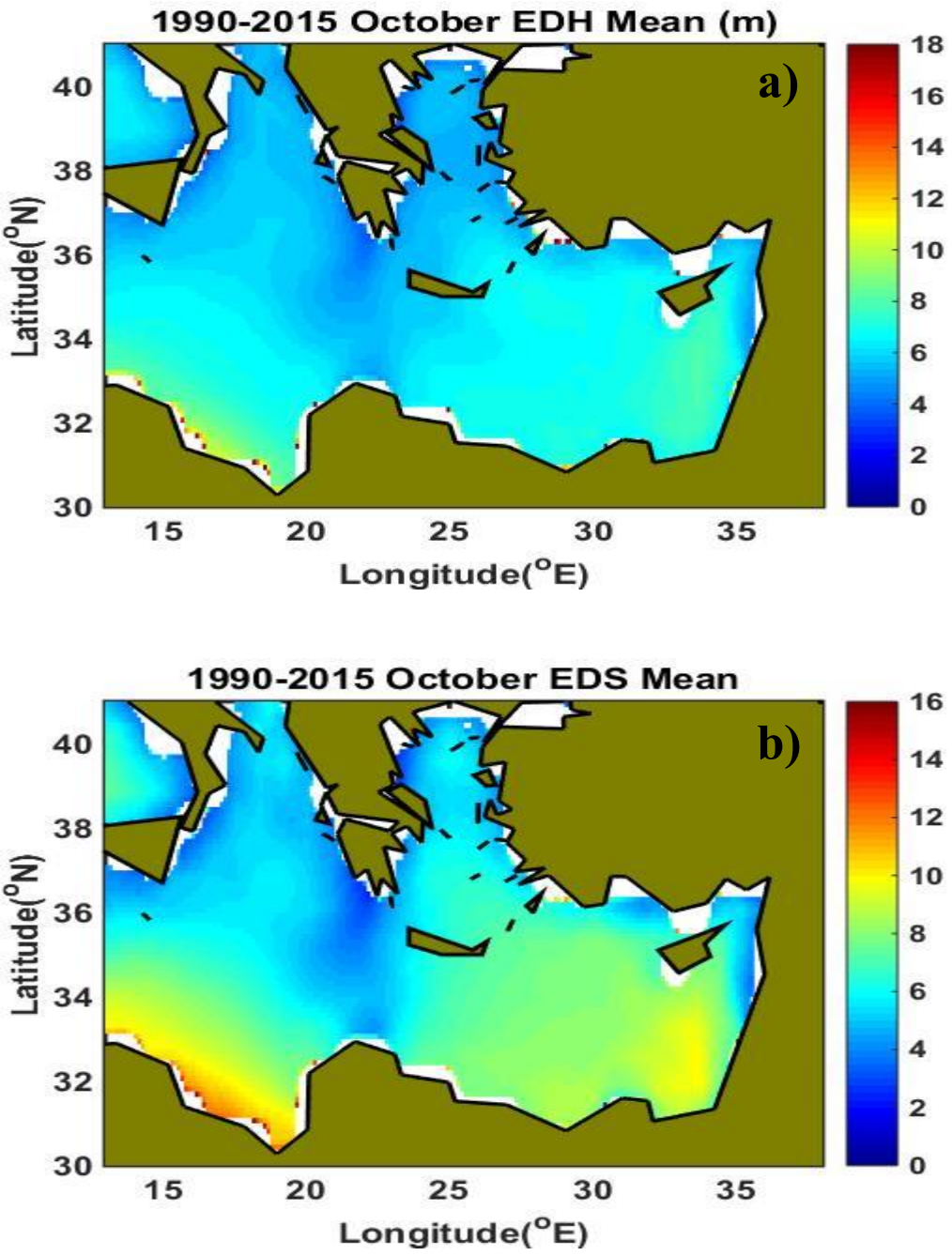

Figure 44. 1990–2015 November Mean of a) EDH (m) and b) EDS.

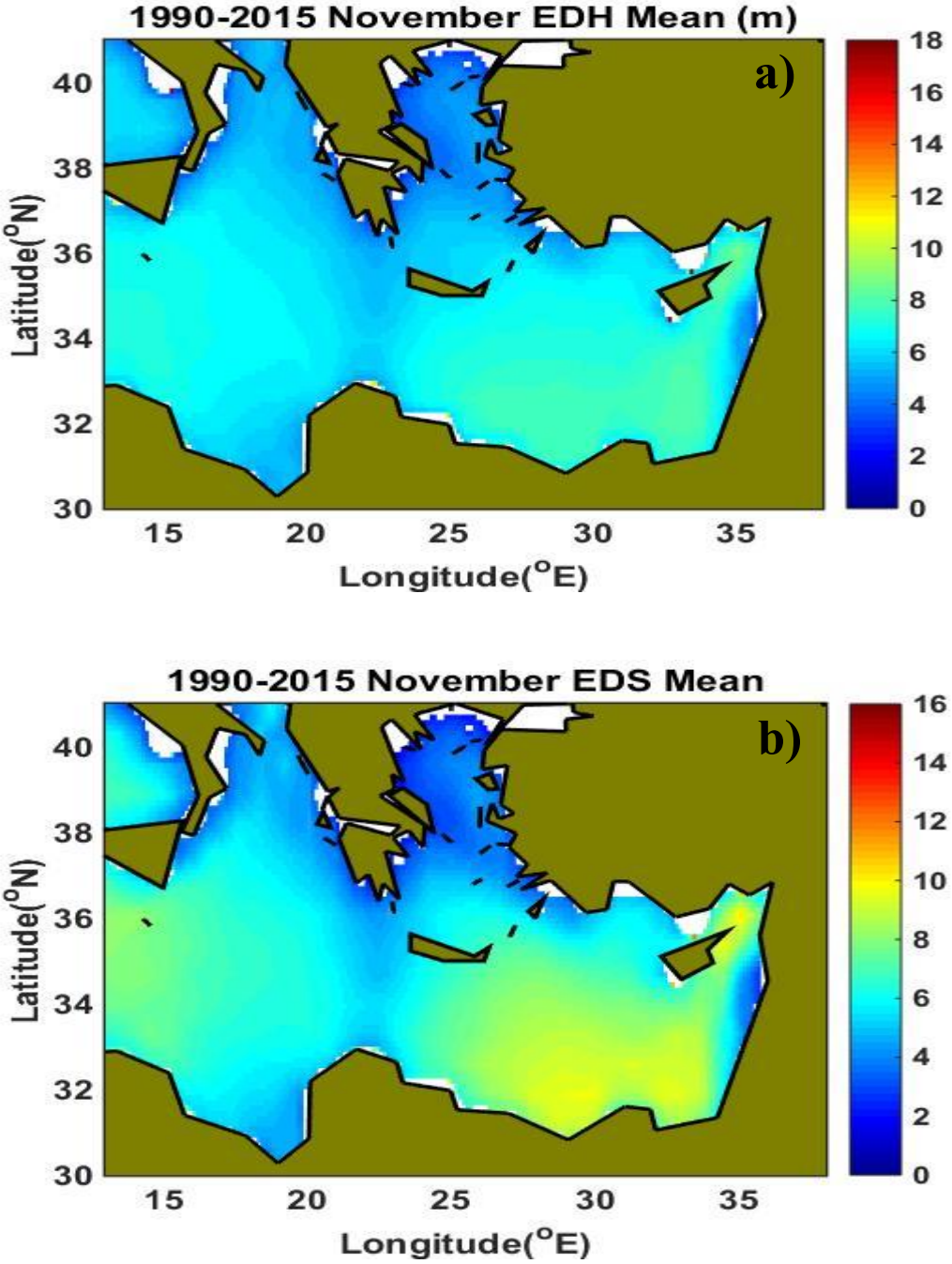

Figure 45. 1990–2015 December Mean of a) EDH (m) and b) EDS.

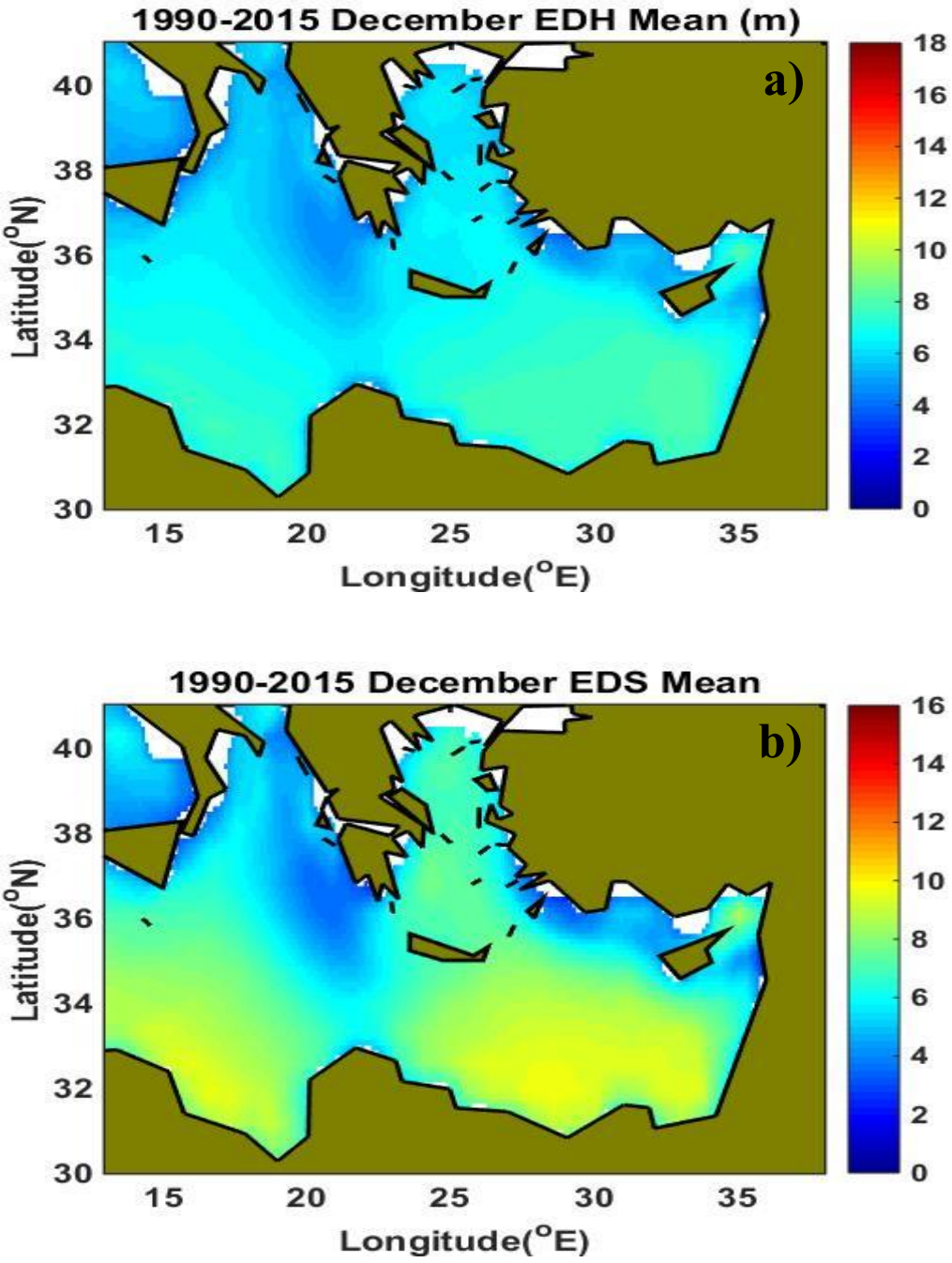

LIST OF REFERENCES

Anderson, L. J., 1944: Atmospheric Refraction - A Preliminary Quantitative Investigation. NRSL Report : WP-17, Dec 28,1944.

Aviation Meteorology, 2016: Climate in Europe. Accessed 30 August 2016. [Available online at http://www.aviamet.gr/cms.jsp?moduleId=022&extLang=LG.]

Babin, S. M., 1996: Surface duct height distributions for Wallops Island, Virginia, 1995–1996. *J. Appl. Meteor*., **35**, 86–93.

Babin, S. M., G. S. Young, and J. A. Carton, 1997: A new model of the oceanic evaporation duct. *J. Appl. Meteor.*, **36(3)**, 193–204.

Bean, B. B., and E. J. Dutton, 1968: *Radio Meteorology.* Dover Publications, 435 pp.

Berrisford, P. and Coauthors, 2011: The ERA-Interim archive version 2.0. European Centre for Medium-Range Weather Forecasts ERA Tech. Rep., **1**, 23.

Cherrett, R. C., 2015: Capturing characteristics of atmospheric refractivity using observations and modeling approaches. Dissertation, Naval Postgraduate School, 62 pp.

Davidson, K. L., 2003: Assessment of atmospheric factors in EM/EO propagation. Course material, Dept. of Meteorology, Naval Postgraduate School.

Dee, D. P. and Coauthors, 2011: The ERA-Interim reanalysis: Configuration and performance of the data assimilation system. *Quart. J. Roy. Meteor. Society*, **137(656)**, 553–597.

Encyclopedia Britannica, 2010: Mediterranean Sea. Accessed 07 February 2015. [Available online at https://www.britannica.com/place/Mediterranean-Sea.]

EIU, 2016: Eastern Illinois University, Department of Geology/Geography website. Accessed 15 July 2016. [Available online at http://www.ux1.eiu.edu/~cfjps/1400/circulation.html].

Fairall, C. W., E. F. Bradley, D. P. Rogers, J. B. Edson, and G. S. Young, 1996: Bulk parameterization of air-sea fluxes for tropical ocean-global atmosphere coupled-ocean atmosphere response experiment. *J. Geophys. Res.: Oceans*, **101(C2)**, 3747–3764.

Fairall, C., E. F. Bradley, J. Hare, A. Grachev, and J. Edson, 2003: Bulk parameterization of air-sea fluxes: Updates and verification for the COARE algorithm. *J. Clim*. **16**, 571–591.

Frederickson, P. A., K. L. Davidson, and A. K. Goroch, 2000: Operational bulk evaporation duct model for MORIAH. Draft Version 1.2 (May), Naval Postgraduate School, 70 pp.

Guest, P., 2016: Atmospheric effects on electromagnetic systems. Online course material, Dept. of. Meteorology, Naval Postgraduate School. Accessed 11 June 2016. [Available online at https://cle.nps.edu/portal/site/14649221-7ace-4a46-b12e-c2fe55a28c8c/page/080a4646-46a5-488a-a9ba-1c6e69f41db9.]

Hermann, J. A., A. S. Kulessa, C. Lucas, R. A. Vincent, J. M. Hacker, and C. M. Ewenz, 2002: Impact of elevated atmospheric structures upon radio-refractivity and propagation. *Conf. Proc. Workshop on the Applications of Radio Science: Commission F*, 4 pp.

HMSO, 1962: Weather in the Mediterranean I: General Meteorology. Her Majesty's Stationery Office, 362 pp.

Jeske, H., 1973: State and limits of prediction methods of radar wave propagation conditions over the sea. Modern Topics in Microwave Propagation and Air–Sea Interaction, A. Zancla, Ed., D. Reidel Publishing, 130–148.

Liu, W. T., K. B. Katsaros, and J. A. Businger, 1979: Bulk parameterization of the air–sea exchange of heat and water vapor including the molecular constraints at the interface. J. *Atmos. Sci.*, **36**, 1722–1735.

Martin, A. L., 2007: VHF and microwave propagation characteristics of ducts. Accessed 29 August 2016. [Available online at http://www.df5ai.net/ArticlesDL/VK3KAQDucts2007V3.5.pdf.]

Mason, S. P., 2010: Atmospheric effects on radio frequency (RF) wave propagation in a humid, near-surface environment. M.S. thesis, Dept. of Meteorology, Naval Postgraduate School, 69 pp.

Mentes, S. and Z. Kaymaz, 2007: Investigation of surface duct conditions over Istanbul, Turkey, *J. Appl. Meteor. Clim.*, **46**, 318–337, doi:10.1175/JAM2452.1.

Monin, A. S., and A. M. Obukhov, 1954: Basic laws of turbulent mixing in the surface layer of the atmosphere. Trudy Geofiz. Inst. Aca. Nauk SSSR, **24**, 163–187.

Murphy, R.M., 2005: Analysis of high-resolution COAMPS with observed METOC data to demonstrate atmospheric impact on EM propagation. M.S. thesis, Dept. of. Meteorology, Naval Postgraduate School, 78 pp.

National Geographic Society, 2009: Eastern Mediterranean Sea. Accessed 12 February 2015. [Available online at http://nationalgeographic.org/media/eastern-mediterranean/.]

Newton, D.A., 2003: COAMPS ™ modeled surface layer refractivity in the roughness and evaporation duct experiment. M.S. thesis, Dept. of. Meteorology, Naval Postgraduate School, 185 pp.

NOAA, 2016: Physical sciences division website. Accessed 7 March 2016. [Available online at http://www.esrl.noaa.gov/psd/].

OCA/CNES, 2015: The Mediterranean Sea. Accessed 12 June 2016. [Available online at http://www-g.oca.eu/cerga/gmc/kids/cd/pdfus/Med.pdf].

Paulus, R. 1985: Practical application of an evaporation duct model, *Radio Sci.* **20**, 887–896.

Paulus, R. A., 1989: Specification for environmental measurements to assess radar sensors. NOSC Tech. Doc. 1685, 43 pp. [Available from National Technical Information Service, U.S. Department of Commerce, Springfield, VA.]

Petty, G. W., 2006: *A First Course in Atmospheric Radiation*. 2nd ed. Sundog Publishing, 458 pp.

Raptis, K., 2012: Climatological factors affecting electromagnetic surface ducting in the Aegean Sea region. M.S. thesis, Dept. of. Meteorology, Naval Postgraduate School, 165 pp.

Rogers, L. T., 1998: Demonstration of an efficient boundary layer parameterization for unbiased propagation estimation. *Radio Sci*. **33**, 599–1608.

Rizzoli, M. P. and A. Hecht, 1988: Large-scale properties of the Eastern Mediterranean: A review, *Oceanologica Acta*, **11**, 4.

Sensoy, S., 2004: The mountains influence on Turkey climate. *Balwois Conference on Water Observation and Information System for Decision Support*, Ohrid, Republic of Macedonia.

Skliris, N., S. S. Sofianos, A. Gkanasos, P. Axaopoulos, A. Mantziafou, and V. Vervatis, 2011: Long-term sea surface temperature. *Advances in Oceanography and Limnology*, **2:2**, 125–139.

Soto-Navarro, F. J. and F. Criado-Aldeanueva, 2012: Model thermohaline trends in the Mediterranean Sea during the last years: A change with respect to the last decades? *The Scientific World Journal*, **2012**.

Turk, S., 2010: Atmospheric effects on communication and electronic warfare systems within Turkey and surrounding areas. M.S. thesis, Dept. of. Information Sciences, Naval Postgraduate School, 75 pp.

Turton, J. D., D. A. Bennets, and S. F. G. Farmer, 1988: An introduction to radio ducting. *Meteor. Mag*., **117**, 245–254.

INITIAL DISTRIBUTION LIST

1. Defense Technical Information Center
   Ft. Belvoir, Virginia

2. Dudley Knox Library
   Naval Postgraduate School
   Monterey, California